1-1-2016

Control of Gortler Vortices by Means of Wall Deformations and Blowing/Suction

Lamiae Taoudi

Control of Görtler vortices by means of wall deformations and blowing/suction

By

Lamiae Taoudi

A Thesis
Submitted to the Faculty of
Mississippi State University
in Partial Fulfillment of the Requirements
for the Degree of Master of Science
in Aerospace Engineering
in the Department of Aerospace Engineering

Mississippi State, Mississippi

August 2016

Control of Görtler vortices by means of wall deformations and blowing/suction

By

Lamiae Taoudi

Approved:

_____

Adrian Sescu
(Major Professor)

_____

J. Mark Janus
(Committee Member/Graduate Coordinator)

_____

David S. Thompson
(Committee Member)

_____

Jason M. Keith
Dean
Bagley College of Engineering

Name:Lamiae Taoudi

Date of Degree: August 12, 2016

Institution: Mississippi State University

Major Field: Aerospace Engineering

Major Professor: Adrian Sescu

Title of Study: Control of Görtler vortices by means of wall deformations and blowing/suction

Pages in Study:102

Candidate for Degree of Master of Science

Görtler vortices evolve in boundary layers over concave surfaces as a result of the imbalance between centrifugal forces and radial pressure gradients. Depending on various geometrical and free-stream flow conditions, these instabilities may lead to secondary instabilities and early transition to turbulence. In this thesis, a control algorithm based on the boundary region equations is applied to reduce the strength of the Görtler instabilities by controlling the energy of the fully developed vortices, using either local wall deformations or blowing/suction at the wall. A proportional-integral control scheme is utilized to deform the wall or to provide transpiration velocity, where the inputs are either the wall-normal or streamwise velocity components in a plane that is parallel to the wall. The results show that the control based on wall deformation using wall-normal velocity components is more effective in tempering the vortex during its streamwise growth by almost one or two orders of magnitude.

ACKNOWLEDGEMENTS

I would like to seize this opportunity to thank my advisor, Dr. Adrian Sescu, for his excellent guidance, his infinite patience and his great support for me during my research work. I truly appreciated his advice and encouragement from day one. My thanks are also extended to all of the committee members, Dr. Mark Janus and Dr. David Thompson, for their valuable involvement to improve my work. I am also grateful to my classmates John Haywood, Vasileos Sassaniss and Prabhat Jha for their continuous support.

I want to thank everyone from the International University of Rabat and the Aerospace department in the Bagley College of Engineering as well as the academic staff and faculty for the partnership between the two universities, which presents a fruitful and successful experience for the students and the development in research for both Morocco and the United States. I would also like to give my sincere and deeply felt thanks to Dr Jason Keith for his continuous support and Mrs Tamra Swan for everything she has been doing since I arrived to Starkville.

Lastly and most importantly, I would like to express my profound gratitude to my parents, my brother and my sister for their unconditional love, moral support and encouragement throughout this project period. I would therefore like to dedicate this thesis to my parents Lalla Zineb Lamraoui and Abdelmajid Taoudi.

TABLE OF CONTENTS

APPENDIX

LIST OF TABLES

LIST OF FIGURES

CHAPTER I

INTRODUCTION

1.1 Introduction

Prandtl was the first to introduce the concept of boundary layer in a fluid flow over a surface [1-2]. He assumed that the fluid inside the boundary layer, a thin viscous region near the surface, sticks to the surface due to friction effects. Therefore the flow over a surface comprises two parts; a viscous region inside the boundary layer and an inviscid flow outside the boundary layer (figure1.1).

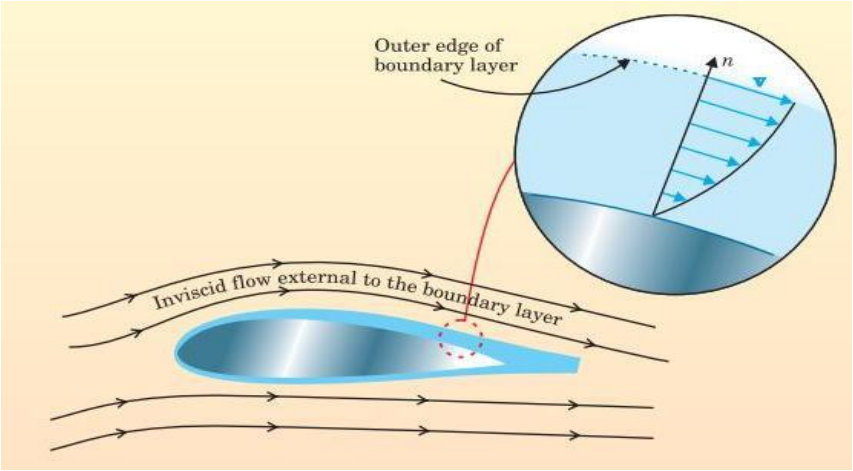

Figure 1.1 Flow over an airfoil [2].

The fluid flow over an airfoil comprises two parts. The thin boundary layer (blue) near the surface experiences high friction. The velocity, v, changes as a function of normal distance, n, from zero at the surface (no slip condition) to the full inviscid-flow value at the outer edge.

In his work, Prandtl also described flow separation. At the separation point, the momentum of the fluid particles in the boundary layer is no longer sufficient to allow the flow to proceed into regions of high pressure. This can be seen in the velocity profile illustrated in figure 1.2. At the separation point (B), the velocity profile has an inflection point and the boundary layer detaches from the surface [1-2]. The flow is then reversed and vortices are formed. Hence, the smooth laminar flow breaks down and separates from the wall.

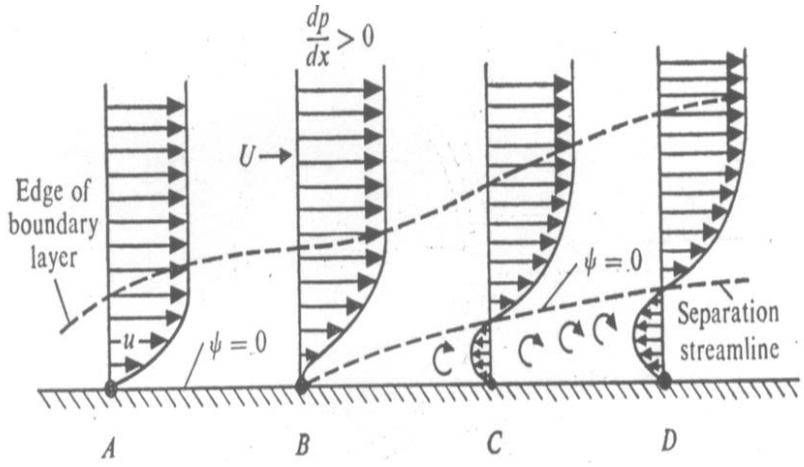

Figure 1.2 Boundary layer separation initiated by local flow reversal [3]

Focused studies on transition in boundary layers from laminar to turbulent flow are motivated by a need to fully understand this physical process and to predict and control the transition of boundary layers over flat or concave surfaces [4]. Concave surface boundary layer flows are subjected to centrifugal instability due to the imbalance between the radial pressure gradient and centrifugal force of the fluid particles. Laminar-turbulent transition in these boundary layers, which is influenced by free-stream

turbulence or surface imperfections, is preceded by the growth of elongated streaky structures. These streaks are the result of three-dimensional disturbances growing transiently in the boundary layer or the existence of roughness elements on the surface. They are the result of the acceleration (high speed streaks) or deceleration (low speed streaks) of the fluid particles. These two types of streaks may be correlated with counter-rotating vortices moving downward inside the boundary layer. These vortices are named after Görtler [5] who first analytically predicted their occurrence. Depending on various geometrical and free-stream flow conditions, these instabilities may lead to secondary instabilities, breakdown and eventually burst into turbulence [6-12].

From a drag reduction standpoint, it is desirable to delay transition. The main approach for reducing the drag (especially skin friction drag) is delaying the transition to turbulence in boundary layers. This can be achieved by removing or controlling the streaks and vortices that are excited by either free stream disturbances or surface imperfections. Various laminar flow control strategies have been proposed during the last few decades.

It has been found that, among numerous turbulence control strategies investigated so far that, the application of steady wall suction and blowing to attenuate the boundary layer disturbances is one of the most practical control methods for reducing skin friction drag. It significantly weakens the strength of the streamwise vortices near the wall responsible for the production of turbulence, leading to drag-reduction [13-14]. Researchers also focused on using surface effects to control the boundary layer. The basic idea is to suppress boundary layer streaks that break down into turbulences using

streamwise elongated surface streaks. It was shown that these surface streaks reduce the vortices energy and thus the disturbances amplitude [15-18].

The research in this thesis is focused on the control of Görtler vortices using surface deformations in the form of streamwise elongated surface streaks and blowing/suction. The objective is to use active control of the boundary layer by wall deformation and blowing/suction in order to achieve a reduction of the energy associated with the disturbances. The basic idea is to use the surface streaks and the blowing/suction to reduce the energy of Görtler vortices that may experience secondary instabilities and eventually contribute to the transition into turbulence. The analysis is performed using a high Reynolds number asymptotic framework where the boundary layer growth is described by the boundary region equations (BRE) [19]. The BRE are parabolic in the streamwise coordinate and the wall deformation is incorporated using a Prandtl transformation. Görtler vortices are excited using an array of roughness elements that are introduced via a previously derived asymptotic solution [19] and the BRE are solved numerically. The secondary instabilities are then determined by solving the generalized Rayleigh pressure equation, which is an eigenvalue problem for the growth rate of a small perturbation about the Görtler vortex [20]. Results will show that surface streaks can significantly reduce the energy of Görtler vortices.

1.2 Thesis organization

This thesis is structured as follows. Following the introduction in this chapter, a literature review about transition from laminar to turbulence in boundary layers, Görtler vortices and their instabilities, secondary instabilities and proposed flow control techniques especially blowing/suction method and the wall deformation method is

presented in CHAPTER II. After presenting the relevant background, the method is developed along with the proportional control scheme in CHAPTER III. The descriptions of the test problems and a discussion of the results are given in CHAPTER IV. Finally, conclusions are discussed in CHAPTER V.

CHAPTER II

LITERATURE REVIEW

2.1 Transition in boundary layers

The problem of transition from laminar flow to turbulent flow in boundary layers is of great practical interest. For example, the low skin friction coefficient of laminar boundary layer flow is very attractive to those who design high performance automobiles and aircraft. On the other hand, there are many cases in which the high mixing and heat-transfer rates of turbulent boundary layer are desirable. There are also occasions in which the transition zone itself needs to be understood, for instance in a turbine blade channel. Transition studies are motivated by a need to understand fully this physical process, and to apply the knowledge to the prediction and control of transition in practice.

Reynolds and, later, Rayleigh were the first to develop a hypothesis on the mechanism of transition from laminar to turbulent flow; they assumed the transition as a consequence of evolving instabilities in laminar boundary layers. This hypothesis triggered many theoretical and experimental works to further understand this process. Years later, Schlichting presented a theoretical approach to the transition phenomenon through the stability theory [1]. This theory explains the behavior of small disturbances in the laminar boundary layer; if they will amplify or damp out as they travel downstream. If these disturbances, named Tollmein-Schlichting (T-S) waves, amplify as they travel downstream, the study reveals that they ultimately break up into turbulent spots which

grow in size and finally merge to form a turbulent region [21] (see figure 2.1).According to the stationary-wave-dominated transition experiments, the breakdown to turbulence occurs very rapidly along a jagged front [22]. This behavior is illustrated in flow-visualization studies such as that by Dagenhart and Saric [23]. These studies suggest that the final stage of transition occurs over a very short streamwise distance and is the result of a secondary instability initially described experimentally by Kohama et al. [24] and Kawakami et al. [25] and analytically and computationally by Malik et al. [26] and Janke and Balakumar [27].

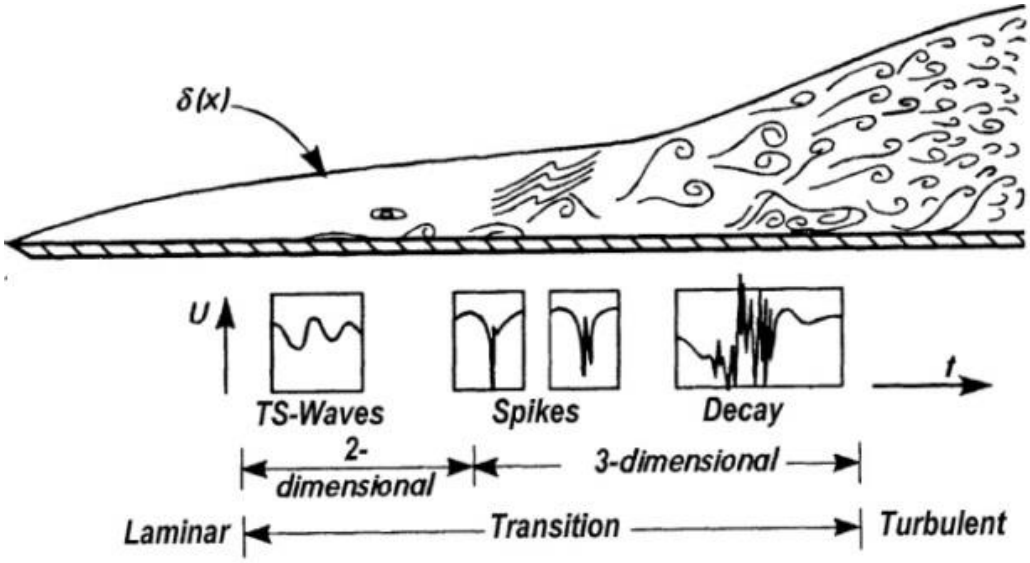

Figure 2.1 Transition process on a flat plate: spatial development [28]

In boundary-layer flows, transition can proceed in two different ways, depending on the level of external disturbances. The first type of transition, natural transition, occurs when the environmental perturbations, in the form of surface roughness, free streamwise turbulence, acoustic waves, model vibration, etc., are low. In this case, the transition

process undergoes these following stages: instability, secondary instability, nonlinear interaction and final laminar breakdown. Natural transition occurs in most controlled transition experiments [1-4-29-30]. If the external perturbations are strong enough, however, the transition will go into the nonlinear interaction stage directly. The T-S wave's instability is not directly involved and the initial linear instability stage is bypassed. This phenomena was named bypass transition by Morkovin [31]. In both natural and bypass transition, vortices are generated inside the flow. Therefore, many studies have been conducted to understand and study the vortices inside boundary layers.

2.2 Görtler vortices

Görtler vortices are generated due to the imbalance between pressure and centrifugal forces of fluid particles in laminar boundary layers that develop along concave walls (see Figure 2.2). These counter-rotating streamwise vortices are one of the main instabilities that lead to boundary layer transition. These vortices were first predicted and theoretically analyzed by Görtler [5] after whom the non dimensional stability parameter G is named.

$$G = \frac{U_\infty \delta_t}{v}(\delta, K)^{1/2} = Re_\theta \sqrt{\frac{\theta}{R}} \tag{2.1}$$

where U_∞ is the freestream velocity, δ_t is the boundary layer thickness, v is the kinematic viscosity,$K = \frac{1}{R}$ is the curvature of the wall, Re_θ is the Reynolds number,θ is the boundary layer momentum thickness and R is radius of the curvature.

His analysis of boundary layer instabilities along a concave wall was conducted by assuming a parallel flow, which was similar to Taylor's analysis of the Couette flow

between concentric rotating cylinders [33]. Görtler found a critical value for the stability parameter *G* above which disturbances to the basic state are amplified.

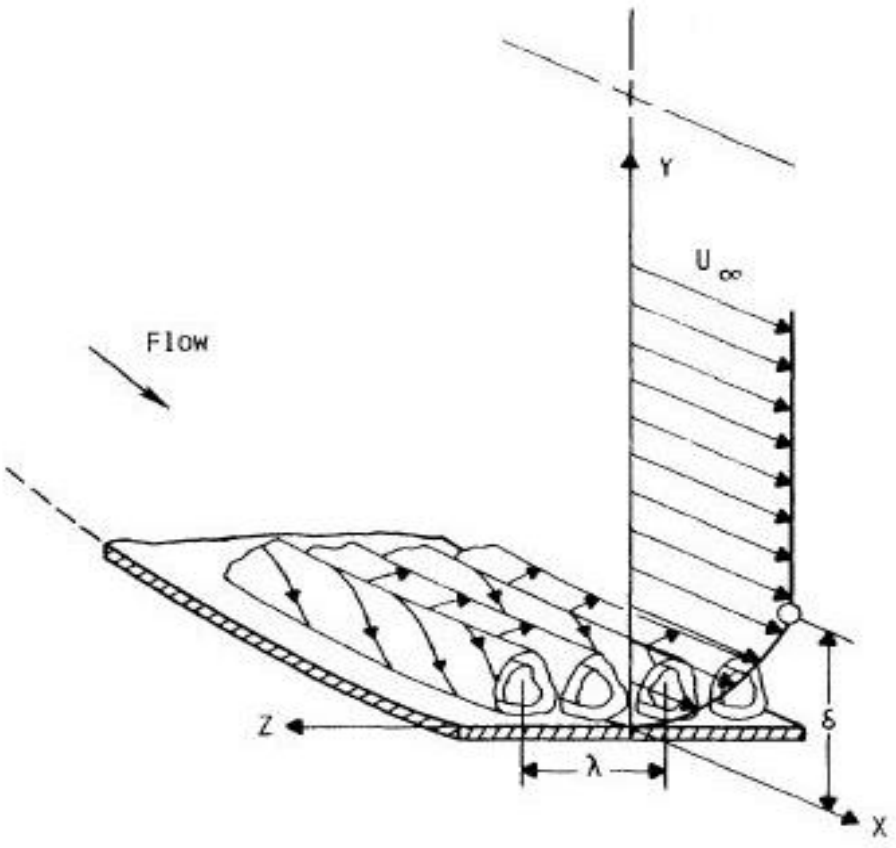

Figure 2.2 Schematic of Görtler vortices in the boundary layer over a concave surface [32].

Liepmann [34] was the first to experimentally confirm that the boundary layer instability along concave walls is governed by the Görtler parameter. Later, Smith [35] derived a set of modified equations including higher-order curvature terms and terms accounting for the non-parallel nature of the boundary layer. Moreover, unlike Görtler who investigated the temporal growth of these disturbances, Smith formulated the

problem to study their spatial growth. Since then, a number of theoretical [36-38] and experimental [39] studies have been devoted to the investigation of Görtler instability.

2.3 Görtler stability analysis

Görtler's original numerical analysis [5] is similar to a stability analysis for boundary layer flows over a flat plate with a few simple modifications taking into account the curvature of the wall. His analysis provides a good foundation for understanding work related to stability that has been done for flow over concave surfaces. In his stability analysis, Görtler formulated the Navier-Stokes equations in curvilinear coordinates for a constant radius of curvature, R, and assumed that R is much larger than δ. He used a two-dimensional perturbation of the form:

$$\psi(x, y, t) = \phi(y)e^{i(\alpha x - \beta t)} \tag{2.2}$$

where β is a complex number and indicates whether or not there is amplification or damping with increasing time. The results of the linearization and non-dimensionalization are grouped in three dimensionless characteristics of the flow. The first one is Görtler number, G in equation (2.1), which expresses the ratio of centrifugal effects to viscous effects. The second is a dimensionless wave number given by:

$$\alpha\theta = \frac{2\pi}{\lambda}\theta \tag{2.3}$$

where α is disturbance wavenumber, θ is boundary layer momentum thickness and λ is disturbance wavelength that has been non-dimensionalized to become the boundary layer thickness, δ. Görtler found that θ had smaller effects in his final results than δ. So he found a third dimensionless parameter τ,

$$\tau = \sqrt{\alpha^2\delta^2\frac{\beta\delta^2}{v}} \tag{2.4}$$

that he called the amplification factor, where β is the amplification coefficient. The case when β= 0 is called neutral stability because there is no amplification or damping of the disturbances at this point. In other words, along this curve the only amplification that occurs is due to boundary layer growth; therefore, the Görtler number is at its smallest value.

Görtler solved these equations for 3-D, laminar, incompressible flow with the Blasius boundary layer as the basic boundary layer profile. He imposed small perturbations, in the form of two-dimensional vortices, on the basic boundary layer profile and examined the response of the flow field to these disturbances. He observed that as Görtler number increases, the flow becomes more susceptible toboth larger and smaller disturbances in the flow. The minimum Görtler number at whichthe flow can become unstable is the critical Görtler number, $G_{c,}$, $G_c = \frac{U_0\theta}{\nu}\sqrt{\frac{\theta}{R}} = 0.58$ and is shown as aminimum on the neutral stability curve. It is. Below this point the flow is always stable.

Many improvements have been incorporated into Görtler's original analysis. Some researchers focused on using more accurate coordinate systems. Floryan and Saric [9] used a general orthogonal curvilinear system to formulate the Görtler problem. The results from their stability study of Görtler vortex flow over a convex curved wall showed the stabilizing effect of convex curvature on the Görtler vortex boundary layer flow.

In a series of studies on Görtler instability, Hall [36-38] has shown that the linear stability equations governing the Görtler instability cannot be reduced to ordinary differential equations, but instead must be solved by a set of partial differential equations, which is parabolic in the streamwise direction. He argues that the effect of the non-

parallel nature of the basic flow in which the Görtler vortices develop is not negligible, and the approximations that reduce the governing equations to in ordinary differential equations cannot be justified; and that the parallel flow theories are mathematically valid only at large wavelengths. He also showed that the main problem associated with the parallel flow theories arises from their inability to describe appropriately the decay of the vortices at the edge of the boundary layer. Hall concludes this to be the cause of the wide variation in the neutral curves predicted by parallel flow theories. Hall [8] then solved the governing partial differential equations as an initial value problem using a finite difference marching scheme. The main result of this study was that the growth (and thus the position of neutral stability) of the Görtler vortices depends crucially on how and where the boundary layer was perturbed.

Day, Herbet and Saric [44] compared the growth rates of the parallel and non-parallel marching scheme for stability analysis. They first performed a parallel flow analysis to determine the most unstable modes and then used these results as initial conditions to the non-parallel flow numerical scheme. They found that the parallel flow analysis predicts higher growth rates of the vortices than the non-parallel technique.

2.4 Secondary instabilities analysis

According to the linear stability theory, if the initial environmentally-generated disturbance is small enough, the primary mode growth stage is observed in the transition process [45]. These primary modes do not directly burst into breakdown, but instead lead to the generation of secondary instabilities. When the primary modes grow, they distort the mean flow, which creates inflection points in the velocity profile. They thereafter

begin to exhibit nonlinearities and the linear theory no longer applies. These secondary instabilities lead rapidly to breakdown due to their higher frequencies [24-26-27].

Many researchers have attempted a non-linear analysis about the flow over concave surfaces. Sabry et al.[46] solved computationally the fully non-linear equations to examine the breakdown of the fully developed Görtler vortices. They found that a sinuous secondary instability would destabilize the Görtler vortices and eventually leads to breakdown and fully turbulent flow. Hall and Horsman investigated the inviscid instability of a longitudinal vortex structure within a steady boundary layer. They solved a general Rayleigh equation and solved it for the case when the vortices are generated by curvature. They found that the instability has a wavelength of the same order of the boundary layer thickness, which justifies the use of the quasi-parallel technique to the instability problem of Görtler vortices [47].

2.5 Flow control techniques

Various laminar flow control strategies have been proposed during the last two decades to reduce the skin friction drag, especially in the aeronautics field. These methods are classified into passive and active control. Passive control techniques involve geometrical modifications of the surface whereas the active control approach involves adding energy or momentum to the flow.

Several researchers focused on avoiding separation by using the motion of the solid wall. Hack and Zaki [48] modeled the growth of boundary-layer streaks generated over a spanwise oscillating flat plate. Galionis and Hall [49] found a reduction in the growth rate of Görtler vortices by considering the growth above a spanwise oscillating surface that is concave in the streamwise direction. Other experimental

(Laadharietal.[50]), numerical (Quadrio and Ricco[51]) and modeling (Dhanak and Si[52]) studies were conducted using spanwise wall oscillations. They have all shown to attenuate effectively the turbulence intensity in wall bounded flows and produce a reduction of turbulent wall friction.

Another popular technique is the use of compliant coatings to reduce the energy of the boundary layer streaks. The main challenge is to find an appropriate coating with the optimum physical properties to achieve the desired target. After early observations by Kramer [53] on exceptional swimming capabilities of dolphins, there was a long series of experimental attempts to verify the effectiveness of compliant wall technology. This work is described in Bushnell et al.[54]. Results from numerical studies of laminar-to-turbulent flow transition delay (involving compliant walls) were reported by Carpenter and Morris[55] and by Davies and Carpenter[56].

Other studies focused on controlling a supersonic boundary layer by injecting a gas different from the external stream through a porous surface into the boundary layer. This method reduces the heat exchange between the wall and the stream and provides thermal protection at high supersonic velocities [1]. Another method is cooling the wall. It was shown that in a specific range of high Mach numbers, the boundary layer can be stabilized by cooling the surface and that this method can preserve the vehicle itself [57].

2.6 Blowing/ Suction control technique

In order to reduce the skin friction drag, many studies were conducted to minimize the energy associated with disturbances inside both laminar and turbulent boundary layers. Regardinglaminar boundary layer flow control, most studies have focused on controlling T-S waves by a periodic suction, removal of decelerated fluid

particles from the boundary layer before they cause separation shown in figure 2.3c, or a periodic blowing that adds energy to those particles near the wall shown in figure 2.3a,b.

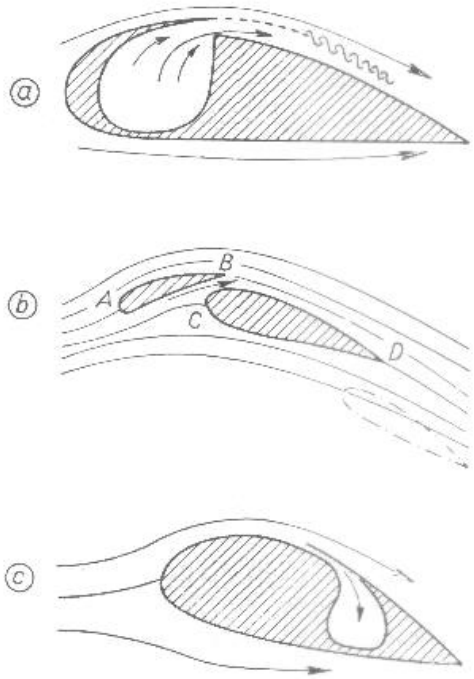

Figure 2.3 Different arrangements for boundary layer control.
a) Discharge of fluid, b) slotted wing, c) suction [1].

When trying to control bypass transition or fully-developed turbulent boundary layer flows, the streamwise-oriented structures of high and low-velocity streaks in the near wall region, which are assumed to be the starting points for the bursting sequence, are the primary focus. Usually the strategy employed is to decrease the spanwise variation of streamwise velocity and thereby decrease the number or strength of the bursting sequences. This can be achieved by placing localized suction regions below low-velocity streaks and blowing regions below high-velocity streaks. An attractive

technique(termed opposition control) to reduce the skin friction drag in a turbulent channel flow was introduced by Choi et al. [58]. They performed direct numerical simulations with active wall control based on blowing and suction by placing various indicators inside the flow, and found that a detection plane close to the wall (approximately 10 wall units) can provide a drag reduction of approximately 25%. From a practical standpoint, it is difficult to place sensors in the flow because they may interfere with the disturbances. In this study, they also investigated the same control algorithm but with sensors placed at the wall and achieved a reduction of approximately only 6%. Koumoutsakos [59] introduced a feedback control algorithm using wall information that was applied in simulations of turbulent channel flow at low Reynolds number. By using the vorticity flux components that can be obtained as a function of tim eby measuring the instantaneous pressure at the wall and calculating its gradient, he claimed a skin friction reduction of 40%.

2.7 Wall deformation method

Controlled wall deformations to counteract boundary layer streaks have been used in the context of turbulent boundary layers to reduce the skin friction at the wall. One important characteristic of streaks generated by roughness elements in boundary layers is the associated steadiness. According to the upstream steadiness, these streaks from the surface by setting appropriate surface streaks can possibly be controlled as wall conditions [16]. These results show that the surface streaks with a maximum amplitude 10-15% higher than the spanwise separation can reduce significantly the amplitude of the disturbances. Endo et al. [17] performed DNS studies with feedback control of deformable walls to reduce the skin friction in a turbulent channel flow. The control

scheme was based on physical arguments pertaining to the near-wall coherent structures. A 10% friction drag reduction was obtained. Endo et al. [16] also pointed out that the energy input required to deform the wall is much smaller than the pumping power involved in blowing/suction. Kang and Choi [60] investigated the potential of reducing the skin-friction drag in a turbulent channel flow via active wall motions. They noticed that the instantaneous shapes at the wall took the form of elongated streaks. A reduction of the friction drag by the order of 13-17% was realized. Koberg [61] experimentally developed an approach for the reduction of skin friction in turbulent flow via active wall deformation. The method aimed to match the velocity sensed away from the wall by imposing a velocity of the opposite direction at the wall; a skin friction reduction of 15% was obtained.

CHAPTER III

COMPUTATIONAL METHODOLOGY

3.1 Mathematical model

This study considers an incompressible boundary layer flow over a concave surface. The spanwise length scale of the roughness row, Λ, is of the same order of magnitude as the local boundary-layer thickness $\delta* \equiv x_0^*/\sqrt{R} = x_0^*\delta$ at the roughness location $x = x_0^*$, where $R = x_0^* U_\infty/\nu^*$ is the Reynolds number based on $x_0^*$and U_∞ is the free stream velocity, with ν^* being the kinematic viscosity, and $\delta \equiv R^{-1/2} = \varepsilon^3$ being the scaled boundary layer thickness.

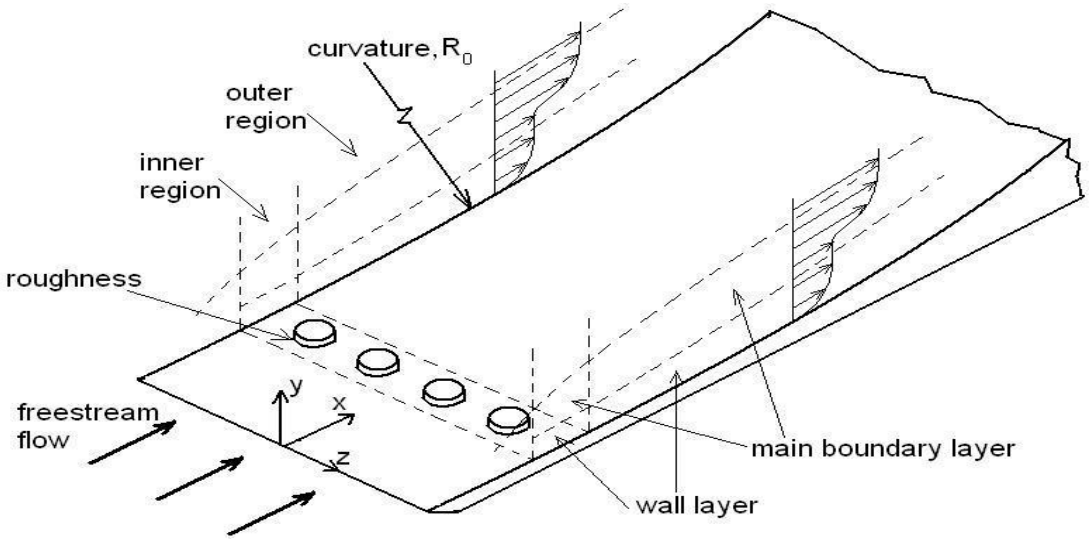

Figure 3.1 Sketch of the boundary layer over concave surface with distributed roughness elements [63].

The three-dimensional Navier-Stokes equations with the origin located at the leading edge of the plate, the x-axis aligned with the wall in the streamwise direction, y-axis perpendicular to the wall, and z-axis aligned with the spanwise direction, are considered. The spatial coordinates are scaled by the spanwise length scale, Λ, as $(x, y, z) = (x^*, y^*, z^*)/\Lambda$. For the curved surface case, the streamwise streaks are expected to develop when $x \sim 2\pi/k_1 \sim \Lambda R_\Lambda$ which suggests the introduction of the slow streamwise variable $X = x/R_\Lambda$, based on the Reynolds number $R_\Lambda = U_\infty \Lambda/\nu$ ($k_1$is the wavenumber corresponding to the streamwise direction). The dimensionless velocity components and pressure are

$$u = \frac{u^*}{U_\infty}, v = \frac{R_\Lambda u^*}{U_\infty}, p = \frac{R^2{}_\Lambda p^*}{(\rho U_\infty)u} \tag{3.1}$$

where (u^*, v^*, w^*) is the dimensional velocity vector, and ρ is the density. The flow variables will become

$$\{u^*, v^*, w^*, p^*\} = \{u(X,y,z), \varepsilon v(X,y,z), \varepsilon w(X,y,z), \varepsilon^2 p(X,y,z)\} + \ldots \tag{3.2}$$

where $\varepsilon = 1/R_\Lambda$. Substituting the dimensionless independent and dependent variables into the Navier- Stokes equations, and using the appropriate Lamé coefficients, $h_1 = (R_0 - y)/R_0$, $h_2 = 1$ in the assumption that the curvature is much larger than the spanwise separation (Wu et al.41), and $h_3 = 1$, the nonlinear boundary region equation (BRE) are obtained as

$$u_X + v_y + w_z = 0, \tag{3.3}$$

$$uu_X + vu_y + wu_z = u_{YY} + u_{zz}, \tag{3.4}$$

$$uv_X + vv_y + wv_z + G_\Lambda u^2 = -p_y + v_{yy} + v_{zz}, \tag{3.5}$$

$$uw_X + vw_y + ww_z = -p_z + w_{YY} + w_{zz} \tag{3.6}$$

where the subscripts(*X, y, z*) represent partial derivatives and the effect of the curvature is contained in the fourth term of the left hand side of equation (3.5), $G_\Lambda = R^2_\Lambda / R_0$ being the global Görtler number. Since the streamwise second order derivatives were eliminated from the original Navier-Stokes equations, the BRE set of equations (3.3-3.6) is parabolic in the streamwise direction. The surface deformations are considered on the surface starting at a location upstream of the initiation of the streamwise streak (such a location can be determined from the solution to the BRE for a boundary layer flow over a smooth surface, with appropriate disturbances imposed through initial/upstream conditions). It was found that the way the surface deformations are initiated in the upstream is important because these deformations can generate streamwise pressure gradients that may impact the development of downstream instabilities. This issue was not addressed in the previous studies involving turbulent boundary layer control via wall deformations since periodic boundary conditions were imposed in the streamwise direction for both the flow and the wall deformations. Here we employ a ramping function in the form

$Fr(x) = 0.5[1 - cos\,(\frac{\pi(x - x1)}{(x2 - x1)})]$ applied between x_1 and x_2.

The boundary conditions at the wall are given as

$$u(X, y_r, z) = w(X, y_r, z) = 0, \quad v(X, y_r, z) = v_w \tag{3.7}$$

where the surface of the wall is described by the function $y_r = G(X, z)$, and v_w is the vertical velocity at the wall in the case of blowing/suction control. The Prandtl transformation can be used to incorporate the surface streaks into the BRE equations, by defining the new independent and dependent variables,

$$Y = y - h_s G \tag{3.8}$$

$$\hat{v} = v - h_s(uG_X + vG_z), \tag{3.9}$$

respectively. Working out the transformations of derivatives in equations (3-6) using the chain-rule, a new set of equations in Cartesian coordinates is obtained as

$$u_X + \hat{v}_Y + w_z = 0, \tag{3.10}$$

$$uu_X + \hat{v}u_Y + wu_z = u_{YY} + (\partial_z - h_s G_z \partial_Y)^2 u, \tag{3.11}$$

$$uv_X + \hat{v}v_Y + wv_z + G_\Lambda u^2 = -p_Y + v_{YY} + (\partial_z - h_s G_z \partial_Y)^2 v, \tag{3.12}$$

$$uw_X + \hat{v}w_Y + ww_z = -(\partial_z - h_s G_z \partial_Y)\, p + w_{YY} + (\partial_z - h_s G_z \partial_Y)^2 w \tag{3.13}$$

Since equations (3.10-3.13) are parabolic in the X -direction, the receptivity of the boundary layer flow to surface roughness elements will enter the problem through initial (or upstream) conditions. Under the assumption that a generic roughness element is much smaller than the local radius of curvature R_0, the local asymptotic high Reynolds number solution in the vicinity of the roughness element as derived previously for the flat plate case in Goldstein et al.[19] (hereafter referred to as GSDC), is used. As in GSDC, the boundary layer flow is divided into an inner region in the vicinity of the roughness elements and an outer region that extends further downstream shown in figure (3.1). The amplitudes of the surface streaks are magnified by a factor of three, and the streamwise length is decreased by a factor of two (see figure3.2).

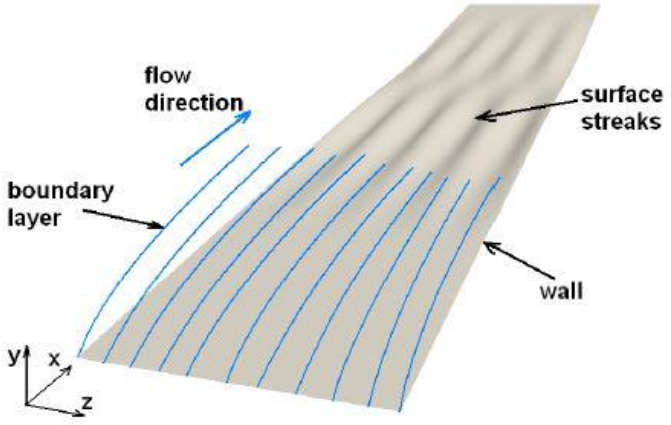

Figure 3.2 Sketch of the boundary layer and the surface streaks in the downstream.

Goldstein et al. [61] have performed a detailed analysis of the inner region in GSDC, however, the focus of this paper is on the latter region, where Görtler vortices are expected to develop as a result of receptivity to the roughness elements located in the upstream region.

We consider an asymptotic expansion of the velocity and pressure in the proximity of the roughness element, as in GSDC, in the form

$$\{u, \frac{v}{R_\Lambda}, \frac{w}{R_\Lambda}, \frac{p}{R_\Lambda{}^2}\} = \{U_B(\eta_B), \delta V_B(X, \eta_B), 0, 0\} + \varepsilon^3\{\tilde{u}(X, \bar{y}), \delta\tilde{v}(X, \bar{y}), 0, \tilde{p}(X, \bar{y})\} + \ldots$$

$$\varepsilon^3\alpha - 4\{\tilde{u}(X, \bar{y}, \bar{z}), \delta\tilde{v}(X, \bar{y}, \bar{z}), \delta\tilde{w}(X, \bar{y}, \bar{z}), \delta^2\tilde{p}(X, \bar{y}, \bar{z})\} + \ldots \quad (3.14)$$

where $\bar{X} = \left(\frac{\Lambda}{x_0^*}\right) R_\Lambda X$, $\bar{y} = \left(\frac{\Lambda}{\delta^*}\right) y$, $\bar{z} = \left(\frac{\Lambda}{\delta^*}\right) z$ since the slow variable $\bar{X}$ and the transverse coordinates, $\bar{y}$ and $\bar{z}$, are defined differently in GSDC, $\alpha = 8/3$, and the denominators on the left hand side were introduced to link the dependent variables in equation (A.25) of GSDC to the dependent variables in the nonlinear BRE (3.10)-(3.13). The base flow is just the solution to the Blasius equation in terms of the function $F(\eta_B)$, $F'''(\eta_B) + 1/2\, F(\eta_B)\, F''(\eta_B) = 0$, with boundary conditions, $F(0) = F'(0) = 0$, $F'(\infty) = 1$, where $\lambda \equiv F''(0) \approx 0.33206$, $\eta_B \equiv \bar{y}/\sqrt{\bar{X}}$. The second term on the right hand side of the expansion (3.14) is the spanwise-uniform component, which is separated out from the spanwise-dependent component because of the difference in order of magnitude. It is determined from the two-dimensional constant pressure linearized boundary layer equations and has the form given in Appendix A.

The spanwise variable perturbations $\{\tilde{u}, \tilde{v}, \tilde{w}, \tilde{p}\}$ are found from the linearized boundary region (LBR) equations

$$\tilde{u}_X + \tilde{v}_{\bar{y}} + \tilde{w}_{\bar{z}} = 0, \tag{3.15}$$

$$U_B\tilde{u}_X + V_B\tilde{u}_{\bar{y}} + \tilde{u}U_{B,X} + \tilde{v}U_{B,\bar{y}} = \tilde{u}_{\bar{y}\bar{y}} + \tilde{u}_{\bar{z}\bar{z}}, \tag{3.16}$$

$$U_B\tilde{v}_X + V_B\tilde{v}_{\bar{y}} + \tilde{u}V_{B,X} + \tilde{v}V_{B,\bar{y}} = -\tilde{p}_y + \tilde{v}_{\bar{y}\bar{y}} + \tilde{v}_{\bar{z}\bar{z}}, \tag{3.17}$$

$$U_B\tilde{w}_X + V_B\tilde{w}_{\bar{y}} = -\tilde{p}_z + \tilde{w}_{\bar{y}\bar{y}} + \tilde{w}_{\bar{z}\bar{z}}, \tag{3.18}$$

applied in the vicinity of the roughness elements, where the curvature term has been neglected, subject to the transverse boundary conditions

$$\tilde{u}, \tilde{v}, \tilde{w} = 0;\ for\ \bar{y} = 0;\ and\ \tilde{u}, \tilde{v}, \tilde{w}, \tilde{p} \rightarrow 0, as\ \bar{y} \rightarrow \infty \tag{3.19}$$

and appropriate upstream matching conditions represented by the uniformly valid composite expansion of the upstream matching conditions as $\bar{X} \rightarrow 1$ for the LBR equations, as derived in GSDC (Appendix A). To avoid numerical instabilities, a linear buffer region that connects the upstream conditions with the solution to the nonlinear equations is considered, where the linear BRE (3.15-3.18) starting with the upstream conditions (34-37) are solved see Sescu and Thompson [62]. Then, the numerical solution to the linear equations is used as an upstream condition to the nonlinear BRE via the expansion (3.14). As an example, figure 2 shows the energy associated with the first mode as a function of the streamwise coordinate in the downstream of the roughness element for four numerical solutions: a) the linear BRE solution for the entire range of X, without curvature effect; b) the linear BRE solution in the buffer region (enclosed by the vertical dashed lines) and the nonlinear BRE solution in the downstream, without curvature effect; c) and iv) the linear BRE solution in the buffer region and the nonlinear BRE solution in the downstream, respectively, with curvature effect and for two different Görtler numbers (5,2 and 7,3, respectively) based on the momentum displacement thickness, θ. All four solutions match in the buffer region, while the solutions to the

nonlinear BRE with curvature effect do show an increase in energy in the outer region due to the Görtler term on the left side of the second momentum equation.

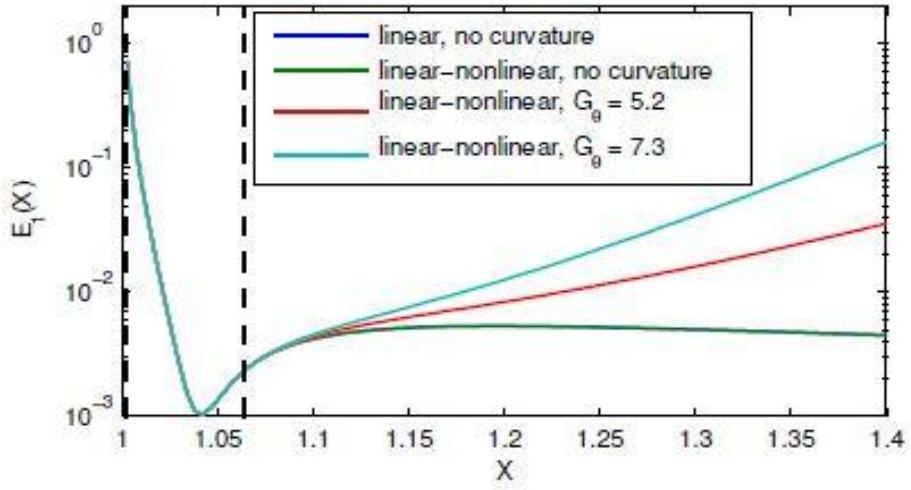

Figure 3.3 Energy associated with the first mode for four cases.

i) the linear BRE solution for the entire range of *X*, without curvature effect; ii) the linear BRE solution in the buffer region and the nonlinear BRE solution in the downstream, without curvature effect; iii) and iv) the linear BRE solution in the buffer region and the nonlinear BRE solution in the downstream.[18]respectively, with curvature effect. The buffer region is located between the two vertical dashed lines on the left.

At $y = 0$, Dirichlet conditions are imposed for u, v and $w$in equations (3.10-3.13) in the form

$$u(X, y = 0, z) = v(X, y = 0, z) = w(X, y = 0, z) = 0, \qquad (3.20)$$

while, at the upper boundary, the flow matches the free stream conditions. Equations (3.10-3.13) and the corresponding initial and boundary conditions will be solved numerically using a marching technique in the streamwise direction, taking advantage of the parabolic character of the equations. A staggered grid was used to avoid decoupling between the velocity and pressure, and second order accurate difference schemes were

employed along both *y* and *z* directions. Since the equations are nonlinear, convergence is achieved by a relaxation method; this was done by including time derivative terms in the equations that were converged to zero, using an appropriate preconditioning technique applied to the continuity equation.

Hall and Horseman [47] showed that the leading order secondary instability modes whose amplitude are of the same order as the local boundary layer thickness are governed by the two-dimensional Rayleigh stability equation,

$$(\partial_{yy} + \partial_{zz} - \alpha^2)\tilde{p} - \frac{2}{(u-c)}(\partial_y u \partial_y + \partial_z u \partial_z)\tilde{p} = 0 \tag{3.21}$$

on a streamwise flow $u(y, z; x)$, where $\tilde{p}$ is the normal mode subject to the associated boundary conditions $\tilde{p}(y, z;\ x) \rightarrow 0\ as\ y \rightarrow \infty;\ \partial_y \tilde{p}(0, z;\ x) = 0, \partial_y \tilde{p}(y, z;\ x) = \partial_y \tilde{p}(y, z + \Lambda;\ x)$, and Λ is the wavelength along the spanwise direction which is in this case the spanwise separation of roughness elements. Equation (3.21) can be regarded as an eigenvalue problem. For temporal stability, α is real, and the phase speed c is sought as a complex eigenvalue, while the eigensolution is $\tilde{p}(y, z)$. Velocity modes can be obtained by considering a velocity perturbation of the form $(u', v', w') = (\tilde{u}, \tilde{v}, \tilde{w})e^{i(\alpha x - \omega t)}$, which, together with the pressure mode substituted into the perturbation equations, leads to the equations (Hall and Horseman [47], Li and Malik [26])

$$i\alpha U + \partial_y \tilde{v} + \partial_z \tilde{w} = 0 \tag{3.22}$$

$$i\alpha(U - c)\tilde{u} + \tilde{v}\partial_y U = -i\alpha\tilde{p} \tag{3.23}$$

$$i\alpha(U - c)\tilde{v} = -\partial_y \tilde{p} \tag{3.24}$$

$$i\alpha(U - c)\,\tilde{w} + \tilde{w}\partial_z U = -\partial_z \tilde{p} \tag{3.25}$$

Using a finite difference to discretize the Rayleigh pressure equation (3.21, a generalized eigenvalue problem can be obtained in the form $Ar = \omega Br$, which is solved using a QR method that yields all eigenvalues and eigenfunctions.

3.2 Feedback control algorithm

A control algorithm is utilized here to determine the optimum shape of the wall deformations that provides the lowest growth rate of energy associated with the boundary layer streaks. The input to the control loop is the streamwise velocity disturbance distribution in a $y = const$ plane, at a specified distance from the wall. Alternatively, an integral over the wall-normal direction (from 0 to 1 or to a specified $y = const$) of the streamwise velocity disturbance can be used to determine the control input.

A typical proportional-integral (PI) controller is used here of the form

$$A(X,z) = K_p * e(X,z) + K_i \int_0^t e(X,z,t')dt' \tag{3.26}$$

where *t* is a variable defining the iterative direction of the controller. $e(X,z)$is the error signal which is definedhere as the difference between the streamwise velocity solution as obtained from BRE and the Blasius streamwise velocity component at a specified y_c distance from the wall, $e(X,z) = u(X,y_c,z) - U_B(X,y_c)$.

An alternative is to consider the integrated streamwise velocity disturbance along the wall-normal direction,

$$e(X,z) = \int_0^t [u(X,y',z) - U_B(X,y')]\, dy' \tag{3.27}$$

However, this is only effective if the boundary layer disturbances are close to the wall, and there is no sign change in the streamwise velocity disturbance along the vertical direction (in such cases replacing the upper limit of the integral with a finite number may

provide a better solution). The amplitude and the shape of the wall deformations can be updated at each iteration based on the control signal as $G(X,z) = G(X,z) + A(X,z)$. The proportional and the integral gains, K_p and K_i, respectively, are determined here using the popular frequency response method of Ziegler [63].

Briefly, the control algorithm steps are:

- **First step:** numerically solve the BRE for the initial flat wall surface;
- **Second step:** deform the wall surface using the streamwise velocity disturbance distribution on a control plane;
- **Third step**: solve the BRE with the new deformed wall surface;
- **Fourth step:** repeat the previous two steps until convergence is achieved (e.g., when the boundary layer streak energy or amplitude does not change significantly from one step to the other).

CHAPTER IV

RESULTS AND DISCUSSION

In this chapter, the results of various numerical simulations are presented and discussed. First, contour plots of the streamwise velocity and the corresponding velocity profiles for each case are plotted. Then, results from the stability analysis are provided including plots of the energy disturbance and the growth rates from the secondary instability analysis.

4.1 Procedures

In this work, a row of roughness elements located at a distance of 0.5 m from the leading edge, with three different spanwise separations of 1.2, 1.8 and 2.4 cm and two different curvature radii 0.5 m and 1 m, is considered. The functional form describing the roughness element is given by the localized function

$$\tilde{F}(x,z) = e^{-\frac{x^2+(z-\pi l)^2}{(d/2)^2}} \tag{4.1}$$

where d is small enough (in the calculations included in this work) to diminish potential discontinuities in the first derivative with respect to z (at the midpoint between two adjacent roughness elements) to negligible levels. The Görtler number based on the momentum displacement thickness is 10.8, and the freestream velocity is 5 m/s, which gives a Blasius boundary layer thickness of 0.7 cm (note that the spanwise separation is on the order of the boundary layer thickness). Either the streamwise velocity disturbance

u' or the wall-normal velocity disturbance v' is used as input to the feedback control algorithm. The input velocities are taken from a sectional plane $y = y_c$ inside the boundary layer, where three elevations are considered: y_c = 0.1 cm, y_c = 0.2 cm and y_c= 0.3 cm. The control is performed using both wall deformations and blowing/suction, and the results in terms of streamwise velocity contours, energy of the vortices and growth rates from the secondary instability analysis are compared.

The 72 run cases performed in this work are given in the three tables 4.1, 4.2 and 4.3.

Table 4.1 Run cases for spanwise separation 1.2 cm.

Case number	Method	Radius (m)	Plane elevation (cm)	Control inputs
1	Wall deformations	0.5	0.1	u'
2				v'
3			0.2	u'
4				v'
5			0.3	u'
6				v'
7		1	0.1	u'
8				v'
9			0.2	u'
10				v'
11			0.3	u'
12				v'
13	Blowing/suction	0.5	0.1	u'
14				v'
15			0.2	u'
16				v'
17			0.3	u'
18				v'
19		1	0.1	u'
20				v'
21			0.2	u'
22				v'
23			0.3	u'
24				v'

Table 4.2 Run cases for spanwise separation 1.2 cm.

Case number	Method	Radius (m)	Plane elevation (cm)	Control inputs
25	Wall deformations	0.5	0.1	u'
26				v'
27			0.2	u'
28				v'
29			0.3	u'
30				v'
31		1	0.1	u'
32				v'
33			0.2	u'
34				v'
35			0.3	u'
36				v'
37	Blowing/suction	0.5	0.1	u'
38				v'
39			0.2	u'
40				v'
41			0.3	u'
42				v'
43		1	0.1	u'
44				v'
45			0.2	u'
46				v'
47			0.3	u'
48				v'

Table 4.3 Run cases for spanwise separation 1.8 cm.

Case number	Method	Radius (m)	Plane elevation (cm)	Control inputs
49	Wall deformations	0.5	0.1	u'
50				v'
51			0.2	u'
52				v'
Case number	Method	Radius (m)	Plane elevation (cm)	Control inputs
53	Wall deformations	0.5	0.3	u'
54				v'
55		1	0.1	u'
56				v'
57			0.2	u'
58				v'
59			0.3	u'
60				v'
61	Blowing/suction	0.5	0.1	u'
62				v'
63			0.2	u'
64				v'
65			0.3	u'
66				v'
67		1	0.1	u'
68				v'
69			0.2	u'
70				v'
71			0.3	u'
72				v'

4.2 Streamwise velocity

The following figures show contours of streamwise velocity at a cross-section through the Görtler vortex after the energy of the vortex reached its maximum, and

streamwise velocity profiles at a spanwise location corresponding to the center of the "mushroom" shape.

The contour plots and velocity profiles for two different curvature radii, R=0.5 m and R=1 m for both wall deformation and blowing/ suction using both u and v control are presented. Figure 4.1 shows contour plots for control based on wall deformations for curvature radius of0.5 m. At the top (4.1a), the original vortices developing over the undeformed surface reveal fully-developed 'mushroom' shapes with alternating low-speed streaks(in blue) and high-speed streaks (in red) in the spanwise direction. Within the control algorithm, the wall surface is gradually moved downward at the spanwise location corresponding to the low-speed streak, while at the same time it is moved upward at the spanwise location where there are high-speed streaks. This change in the geometry of the wall surface enhances or decreases the momentum of the flow, thus reducing the energy associated with the Görtler vortices, and eventually delaying breakdown into turbulence. This is shown in the next parts of the figures, corresponding to different geometrical and flow conditions. Figure 4.1b shows a controlled boundary layer using u' as the input "measured" from a control plane located at y_c = 0.1 cm from the wall, while figure 4.1c shows the same result, the input is v' taken from control planes at y_c = 0.1 cm. Similar results are shown in figures 4.1d and 4.1e, where the control plane is taken at y_c = 0.2 cm for u' and v' control respectively. And similarly figures 4.1f and 4.1g show results for both u' and v' control taken at y_c = 0.3 cm. It can be noted that the best results (the contours are closest to the Blasius solution) are obtained when the control is performed based on v'. On the left side of figures 4.1b, 4.1c, 4.1d, 4.1e, 4.1f,

4.1g, streamwise velocity profiles are included to show that the inflection point vanishes when control is applied.

Figure 4.2 shows contours of streamwise velocity at a cross-section through the Görtler vortex and streamwise velocity profiles for wall deformation for a surface with curvature radius equal to 1 m. As in figure 4.1, contour plots of the streamwise velocity are on the left and their velocity profiles are on the right. Following the same order for figures 4.2b, 4.2c, 4.2d, 4.2e, 4.2f, 4.2g, as in figure 4.1, it can be observed that the curvature radius affects the vortices and that the best control is given by *v'* control.

Figure 4.3 and 4.4 show contour plots and velocity profiles for blowing and suction control methods for a curvature radius of 0.5 m and 1 m, respectively, with a roughness spanwise separation of 1.2 cm. The two figures show a reduction in the energy of the Görtler vortices that does not differ significantly for the two cases. However, control based on wall deformations is much more effective than the control based on blowing and suction, especially in the case where *v'* is used as the control input.

Similarly, the results corresponding to a roughness spanwise separation of 1.8cm, illustrated in figures 4.5, 4.6, 4.7 and 4.8 show that similar conclusions hold: the control based on wall deformations and using *v'* as the input are the most effective. An even larger spanwise separation 2.4 cm is considered in figures 4.9, 4.10, 4.11 and 4.12, where the control is based again in wall deformations and blowing/suction for radius curvature values 0.5 m and 1 m.

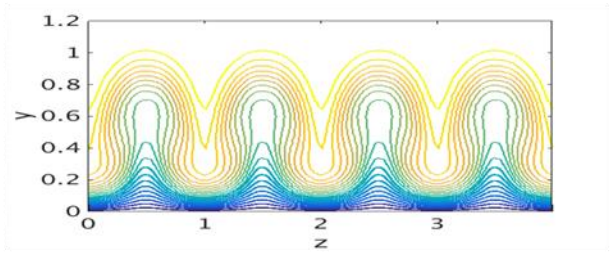

a)

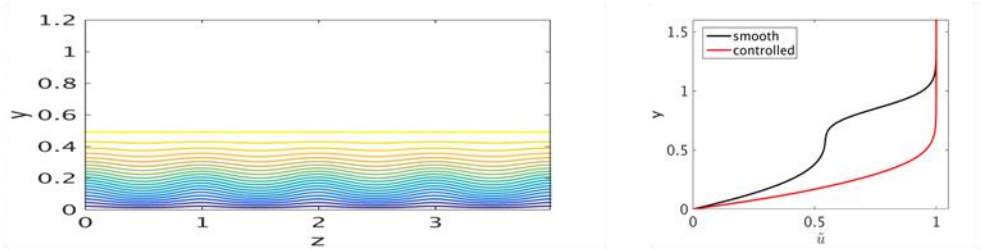

b)

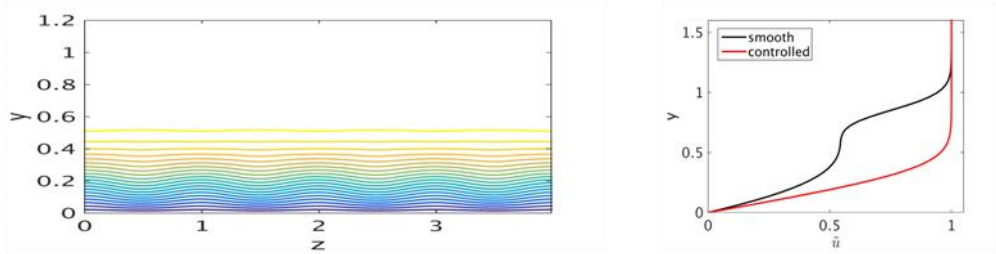

c)

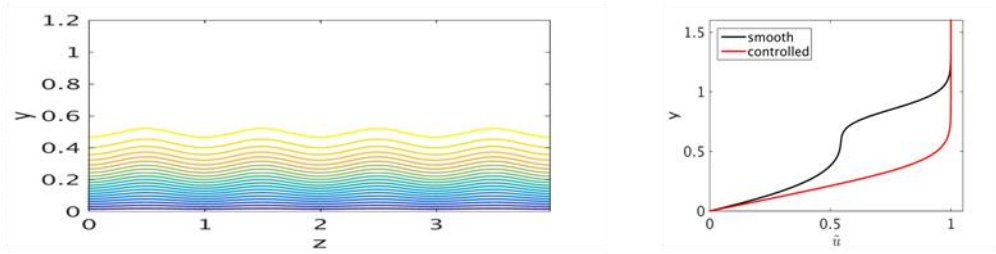

d)

Figure 4.1 Stream wise velocity contours (left column) and profiles (right) for control based on wall deformations for radius 0.5 m; spanwise separation is 1.2 cm.

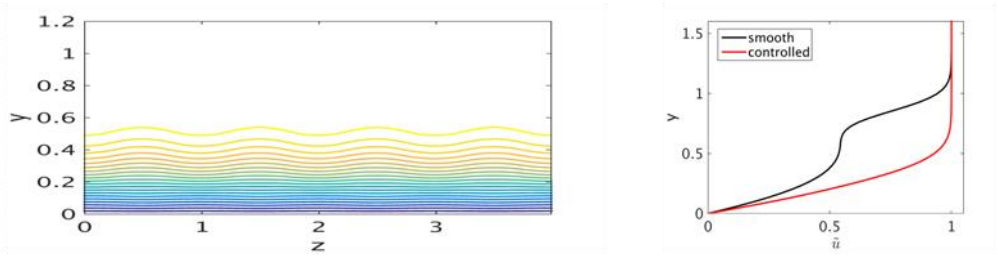

e)

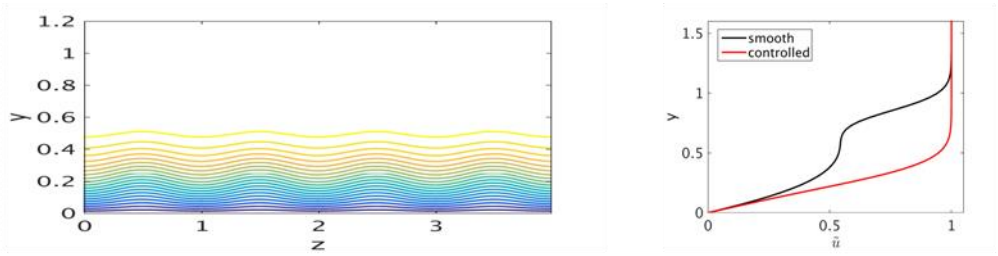

f)

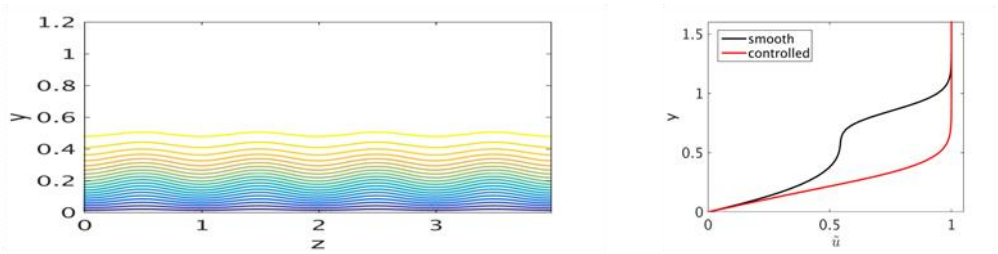

g)

Figure 4.1 (continued).

a) smooth surface; b) control based on u and control plane at y = 0.1; c) control based on v and control plane at y = 0.1; d) control based on u and control plane at y = 0.2; e) control based on v and control plane at y = 0.2; f) control based on u and control plane at y = 0.3; g) control based on v and control plane at y = 0.3.

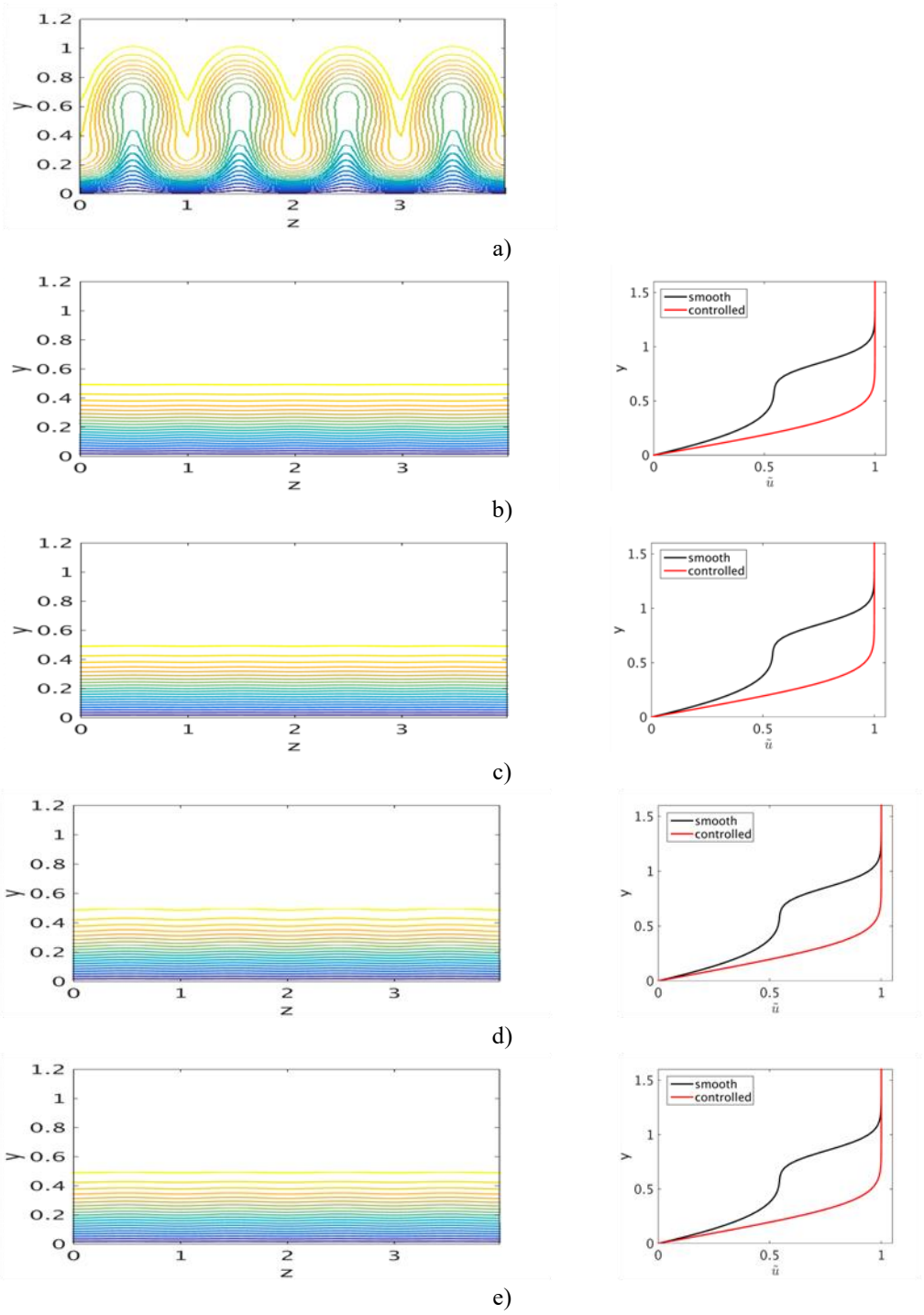

Figure 4.2 Stream wise velocity contours (left column) and profiles (right) for control based on wall deformations for radius 1 m; spanwise separation is 1.2 cm.

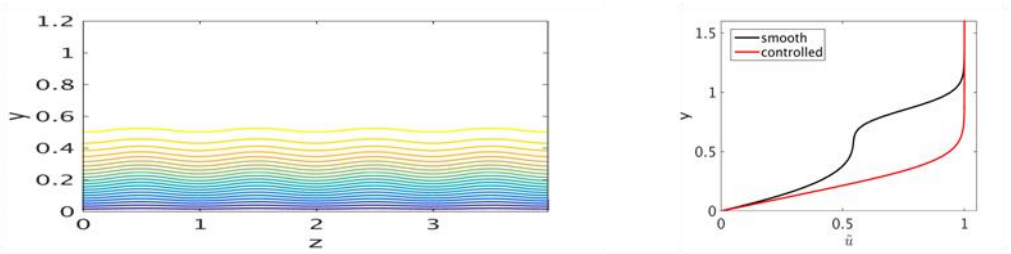

f)

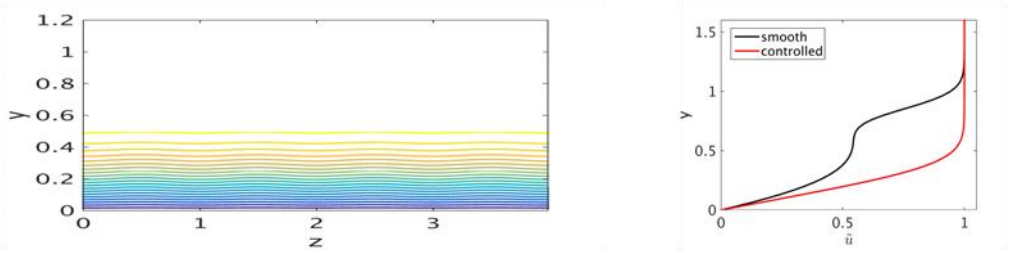

g)

Figure 4.2 (continued).

a) smooth surface; b) control based on u and control plane at y = 0.1; c) control based on v and control plane at y = 0.1; d) control based on u and control plane at y = 0.2; e) control based on v and control plane at y = 0.2; f) control based on u and control plane at y = 0.3; g) control based on v and control plane at y = 0.3.

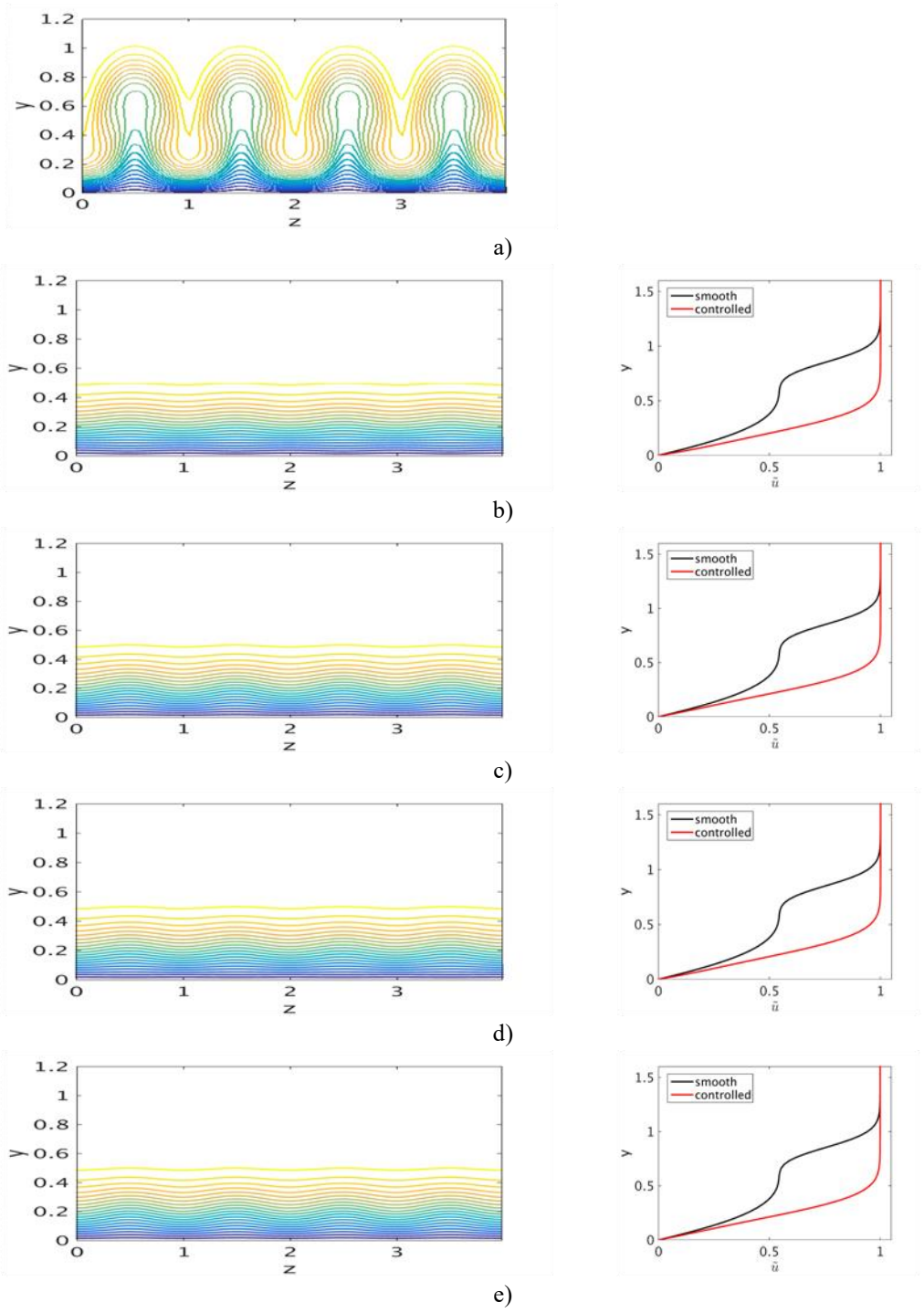

Figure 4.3 Stream wise velocity contours (left column) and profiles (right) for control based on blowing and suction for radius 0.5 m; spanwise separation is 1.2 cm.

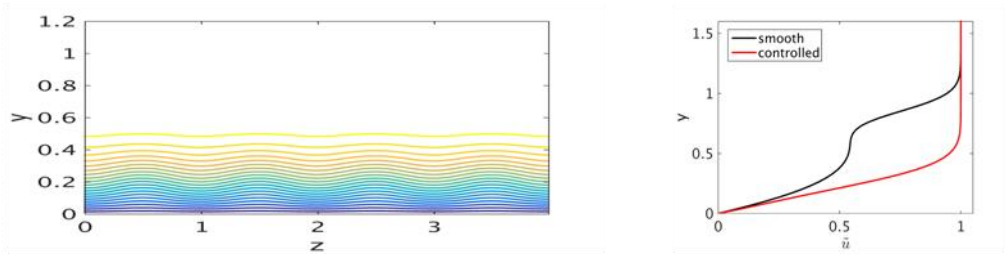

f)

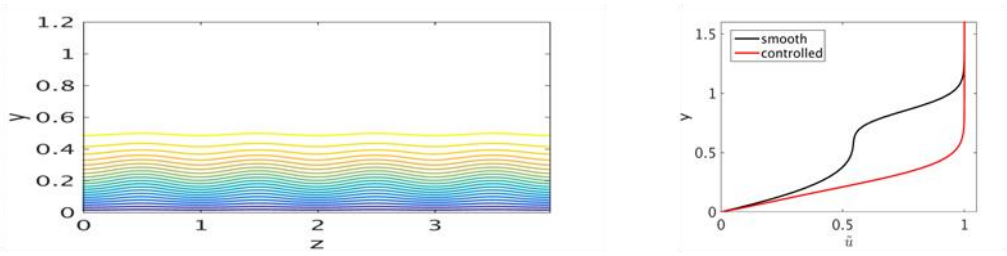

g)

Figure 4.3 (continued).

a) smooth surface; b) control based on u and control plane at y = 0.1; c) control based on v and control plane at y = 0.1; d) control based on u and control plane at y = 0.2; e) control based on v and control plane at y = 0.2; f) control based on u and control plane at y = 0.3; g) control based on v and control plane at y = 0.3.

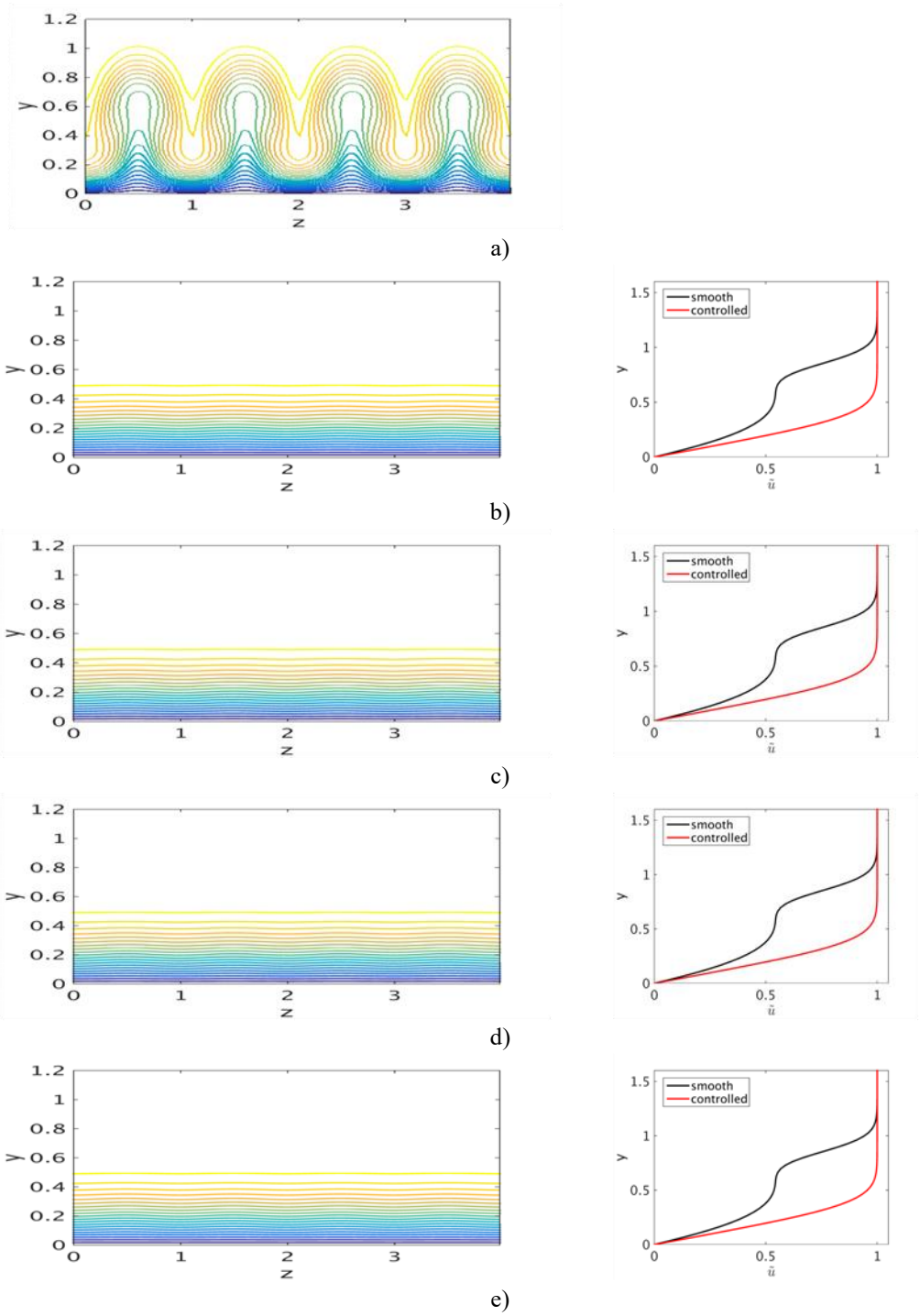

Figure 4.4 Stream wise velocity contours (left column) and profiles (right) for control based on blowing and suction for radius 1 m; spanwise separation is 1.2 cm.

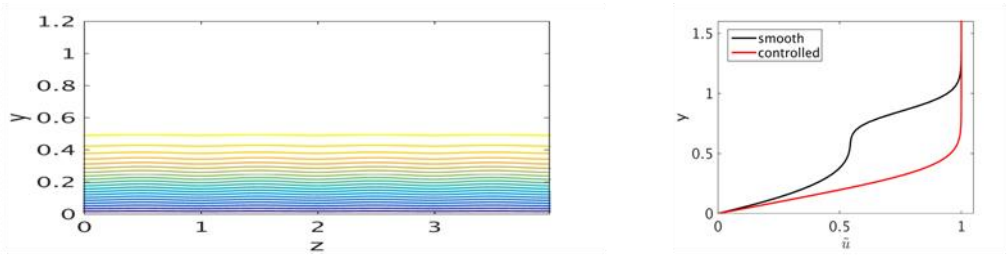

f)

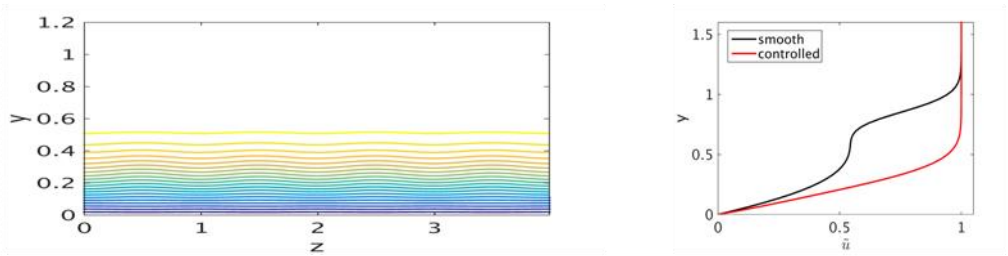

g)

Figure 4.4 (continued).

a) smooth surface; b) control based on u and control plane at y = 0.1; c) control based on v and control plane at y = 0.1; d) control based on u and control plane at y = 0.2; e) control based on v and control plane at y = 0.2; f) control based on u and control plane at y = 0.3; g) control based on v and control plane at y = 0.3.

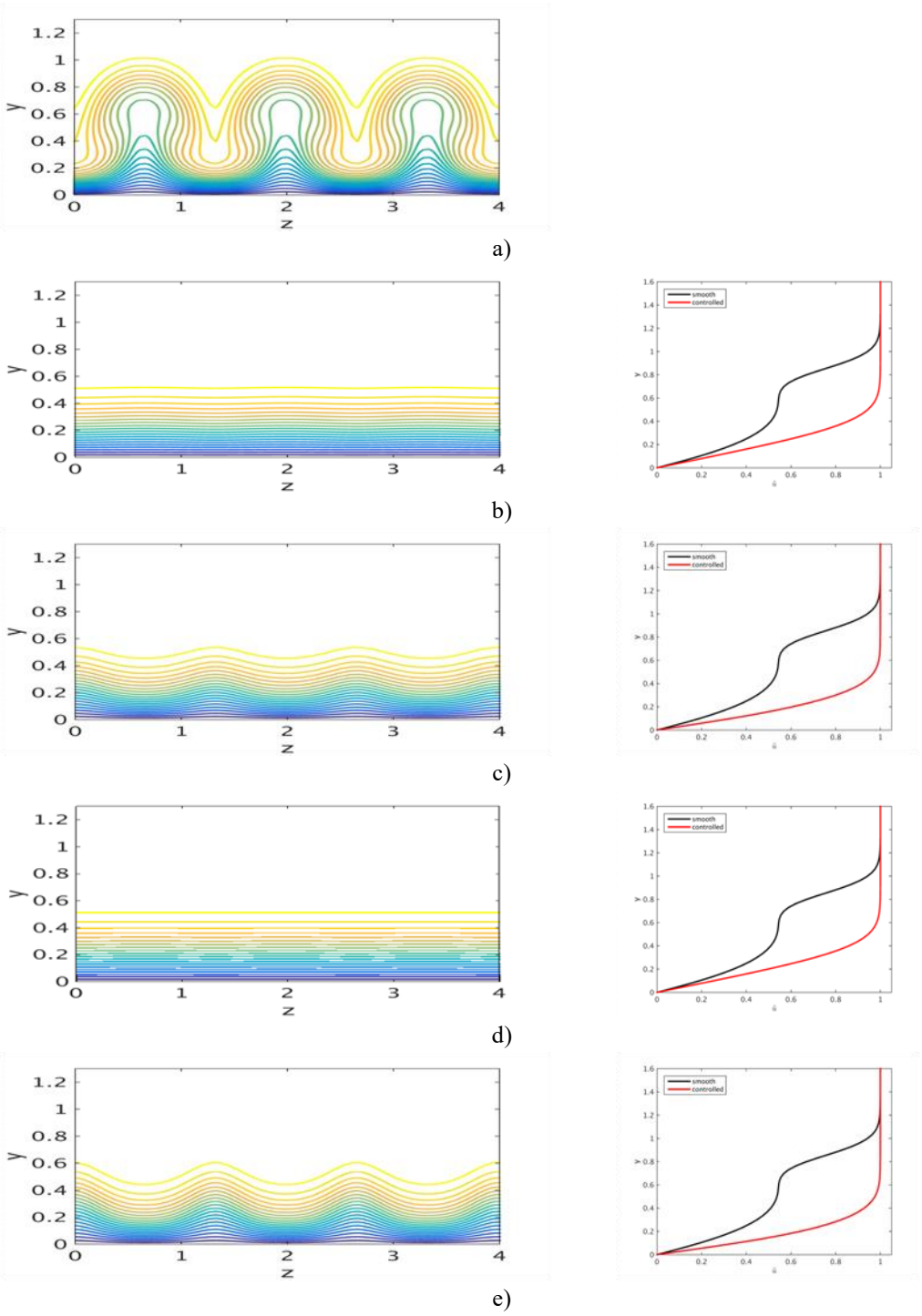

Figure 4.5 Stream wise velocity contours (left column) and profiles (right) for control based on wall deformation for radius 0.5 m; spanwise separation is 1.8 cm.

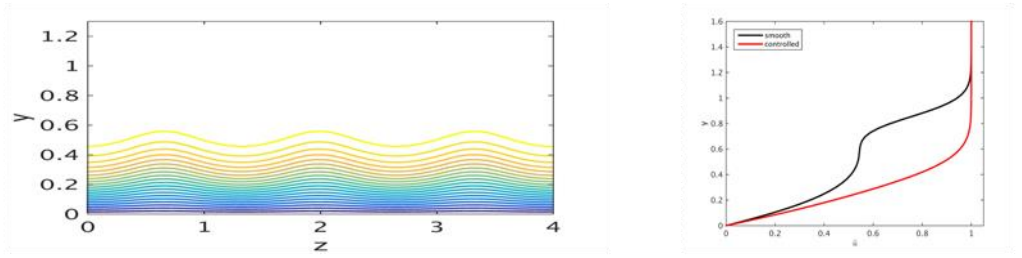

f)

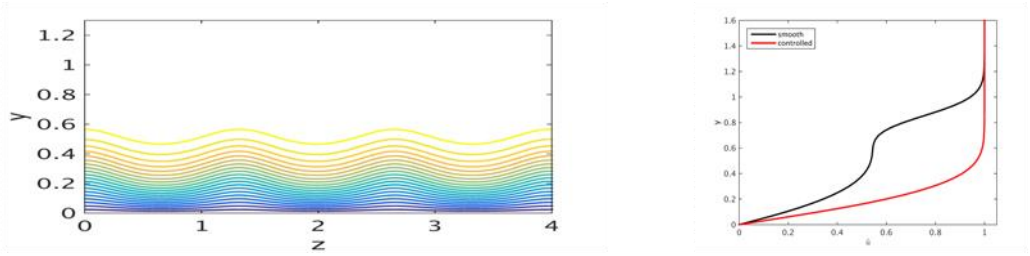

g)

Figure 4.5 (continued).

a) smooth surface; b) control based on u and control plane at y = 0.1; c) control based on v and control plane at y = 0.1; d) control based on u and control plane at y = 0.2; e) control based on v and control plane at y = 0.2; f) control based on u and control plane at y = 0.3; g) control based on v and control plane at y = 0.3.

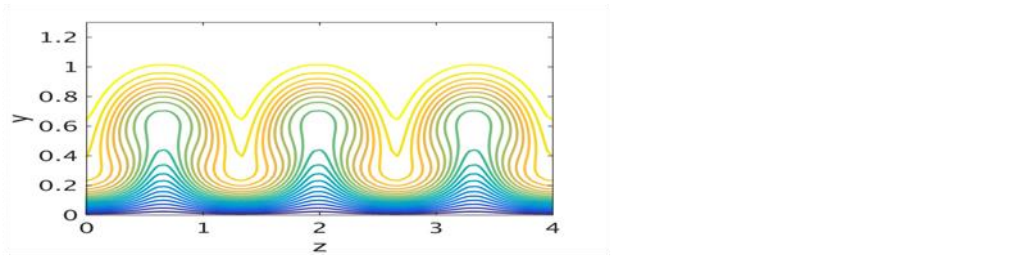

a)

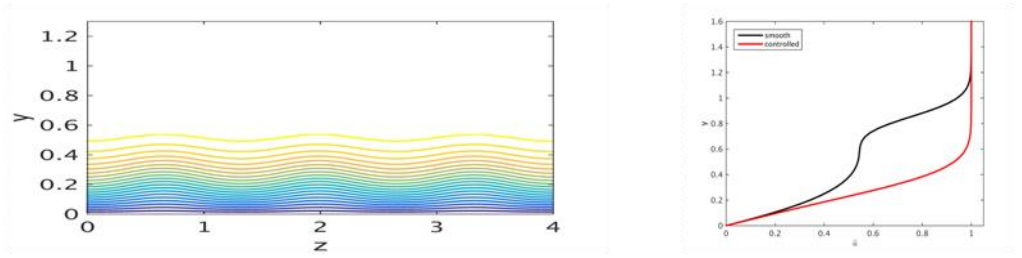

b)

Figure 4.6 Stream wise velocity contours (left column) and profiles (right) for control based on wall deformation for radius 1 m; spanwise separation is 1.8 cm.

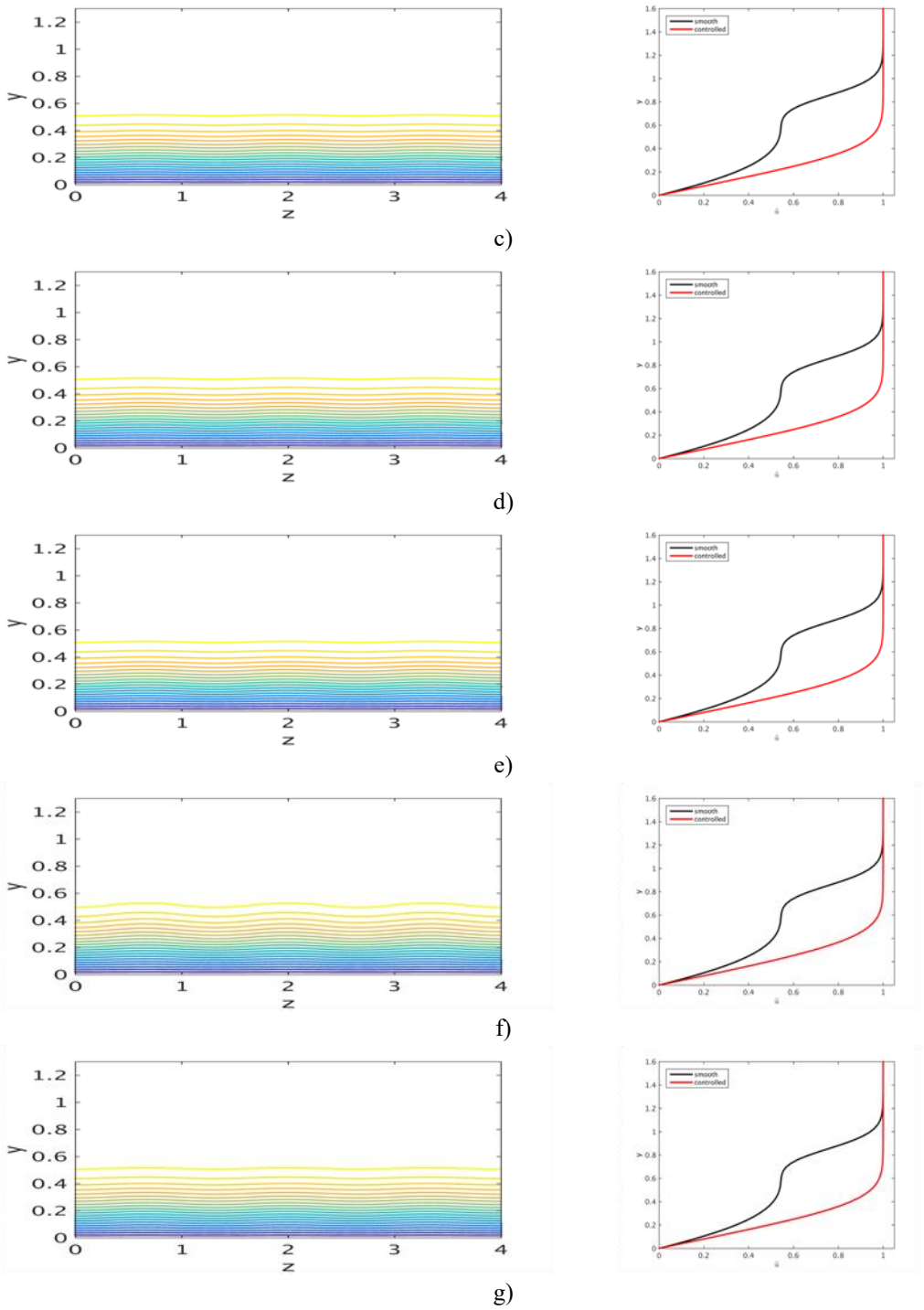

Figure 4.6 (continued).

a) smooth surface; b) control based on u and control plane at y = 0.1; c) control based on v and control plane at y = 0.1; d) control based on u and control plane at y = 0.2; e) control based on v and control plane at y = 0.2; f) control based on u and control plane at y = 0.3; g) control based on v and control plane at y = 0.3.

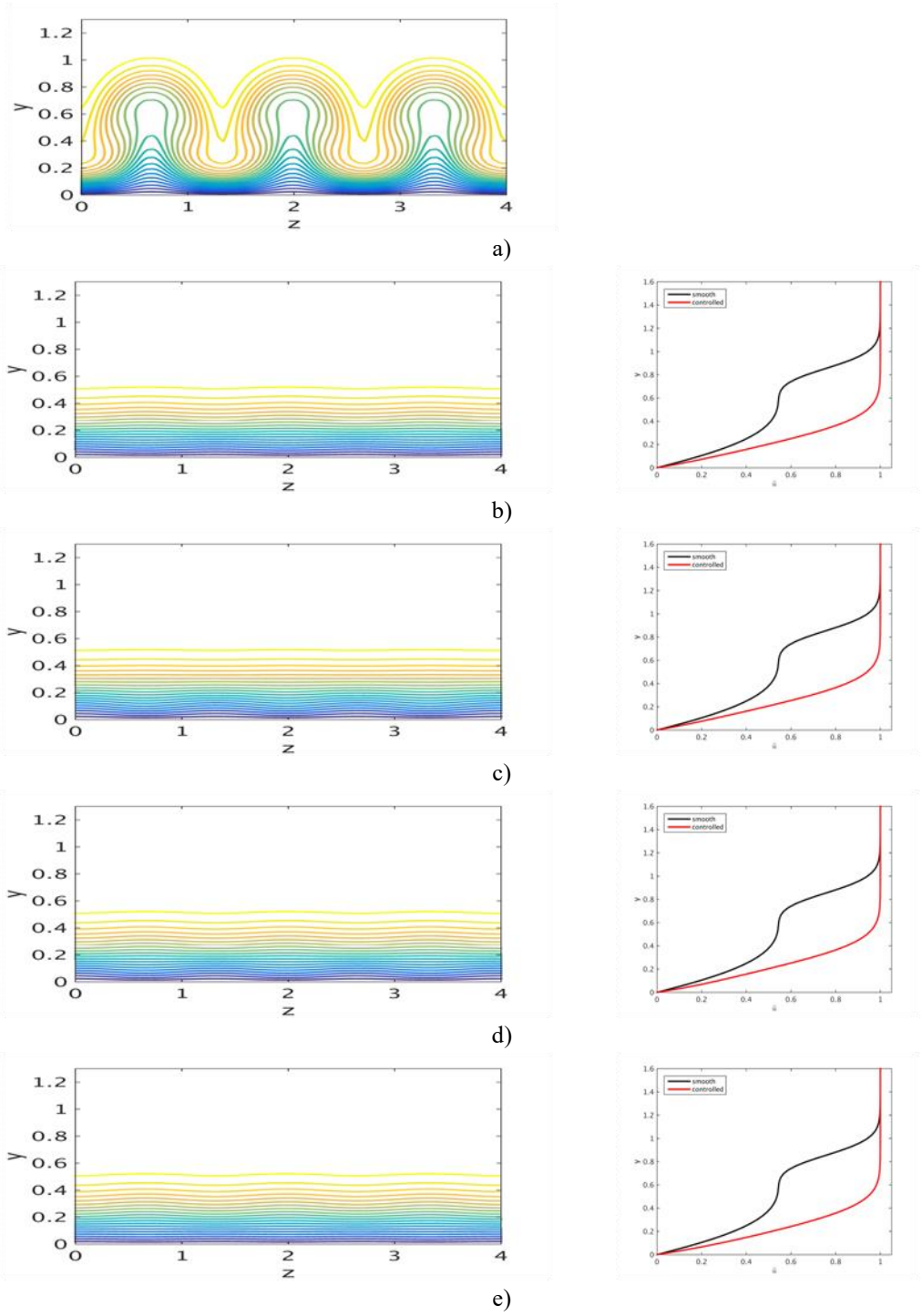

Figure 4.7 Stream wise velocity contours (left column) and profiles (right) for control based on blowing/suction for radius 0.5 m; spanwise separation is 1.8 cm.

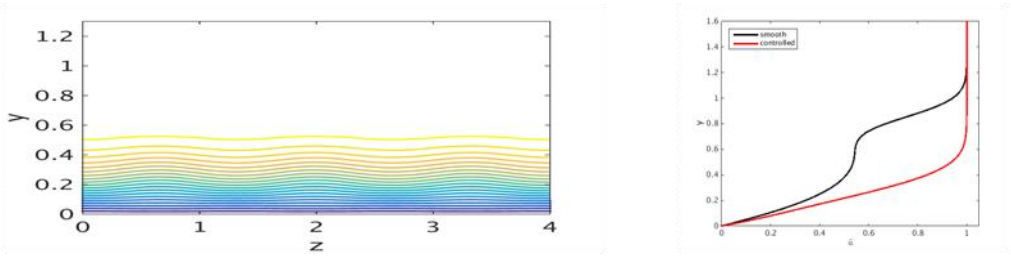

f)

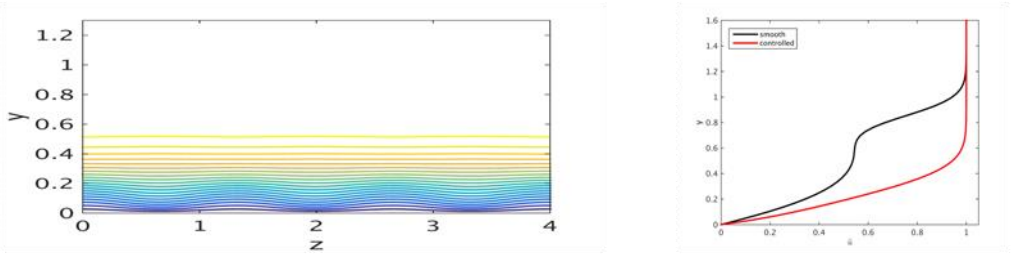

g)

Figure 4.7 (continued).

a) smooth surface; b) control based on u and control plane at y = 0.1; c) control based on v and control plane at y = 0.1; d) control based on u and control plane at y = 0.2; e) control based on v and control plane at y = 0.2; f) control based on u and control plane at y = 0.3; g) control based on v and control plane at y = 0.3.

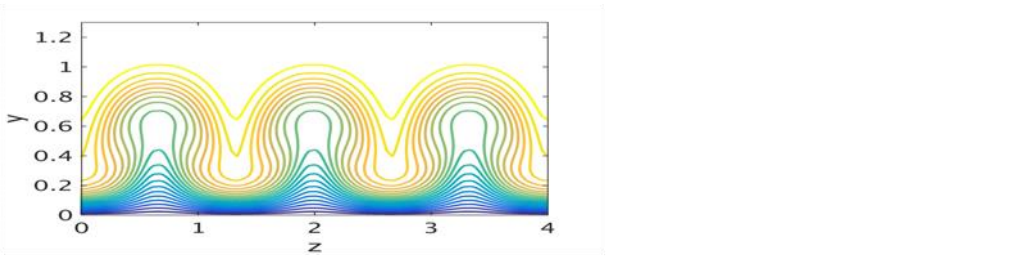

a)

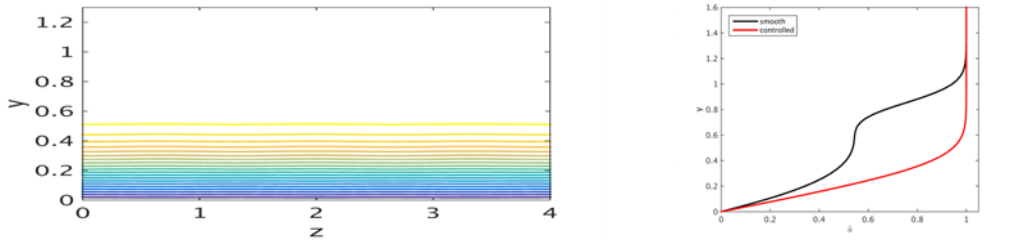

b)

Figure 4.8 Stream wise velocity contours (left column) and profiles (right) for control based on blowing/suction for radius 1 m; spanwise separation is 1.8 cm.

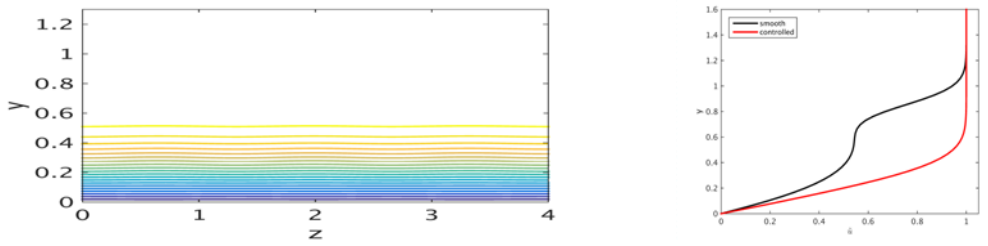

c)

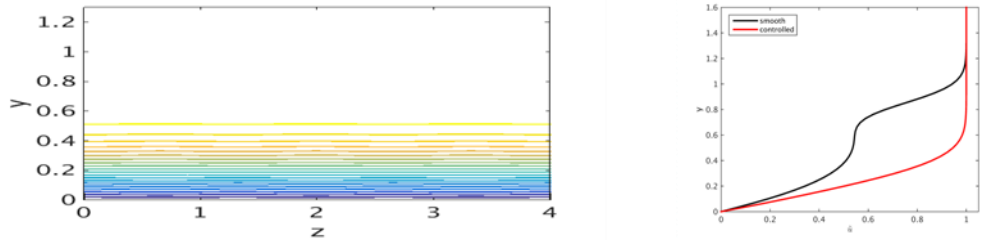

d)

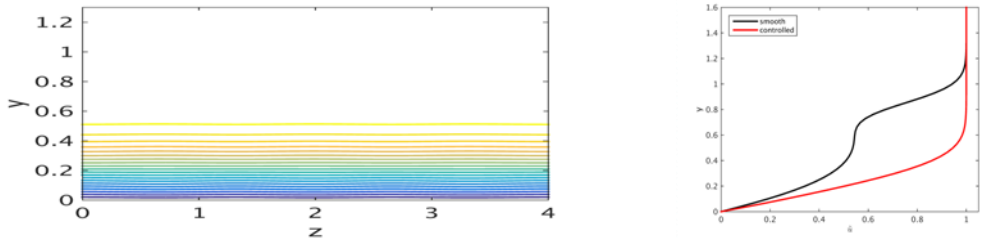

e)

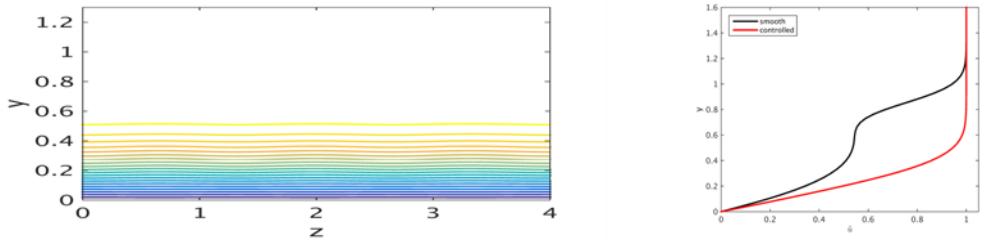

f)

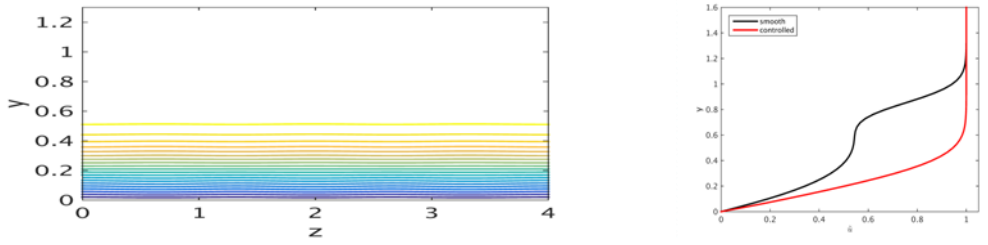

g)

Figure 4.8 (continued).

a) smooth surface; b) control based on u and control plane at y = 0.1; c) control based on v and control plane at y = 0.1; d) control based on u and control plane at y = 0.2; e) control based on v and control plane at y = 0.2; f) control based on u and control plane at y = 0.3; g) control based on v and control plane at y = 0.3.

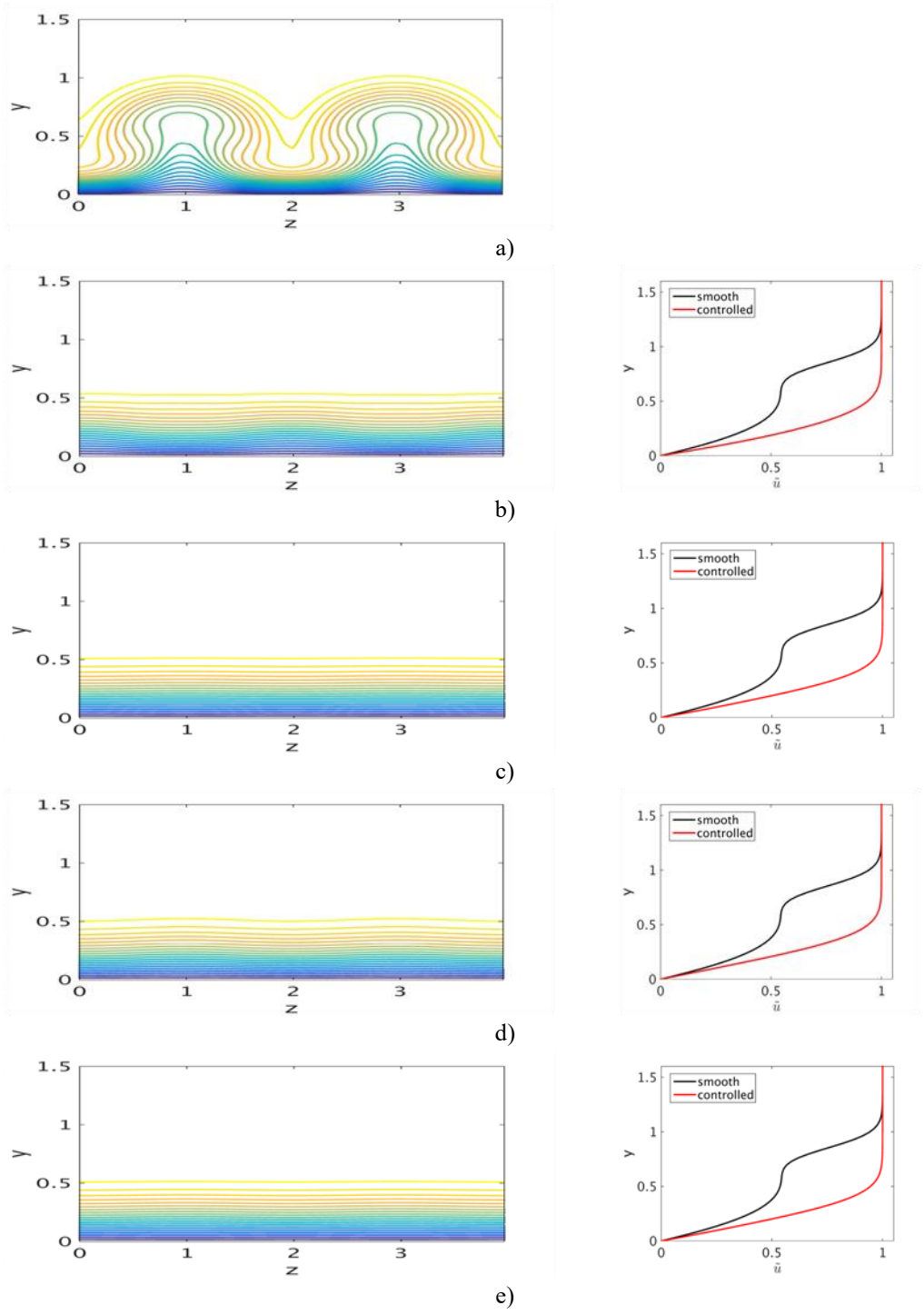

Figure 4.9 Stream wise velocity contours (left column) and profiles (right) for control based on wall deformation for radius 0.5 m; spanwise separation is 2.4 cm.

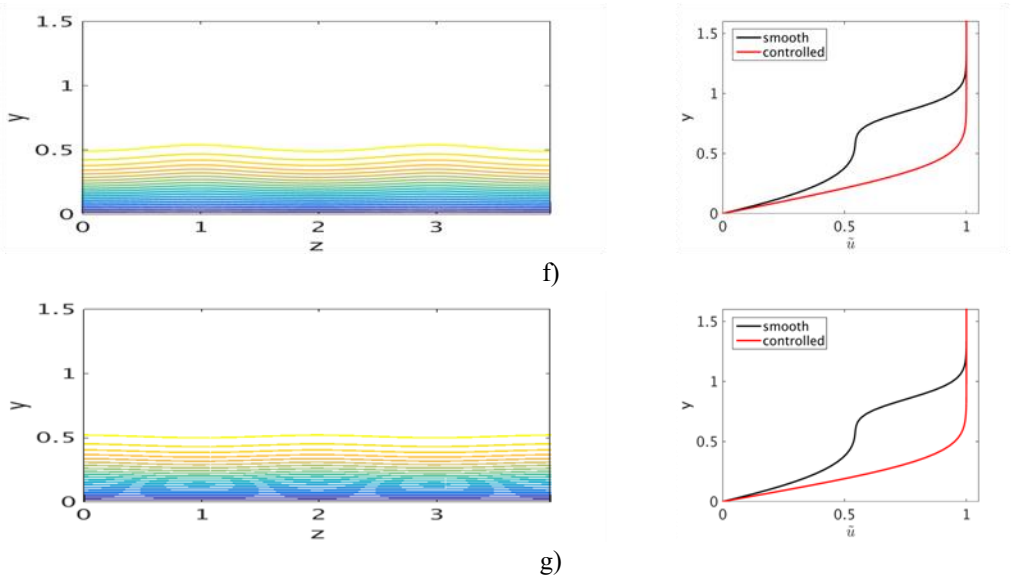

f)

g)

Figure 4.9 (continued).

a) smooth surface; b) control based on u and control plane at y = 0.1; c) control based on v and control plane at y = 0.1; d) control based on u and control plane at y = 0.2; e) control based on v and control plane at y = 0.2; f) control based on u and control plane at y = 0.3; g) control based on v and control plane at y = 0.3.

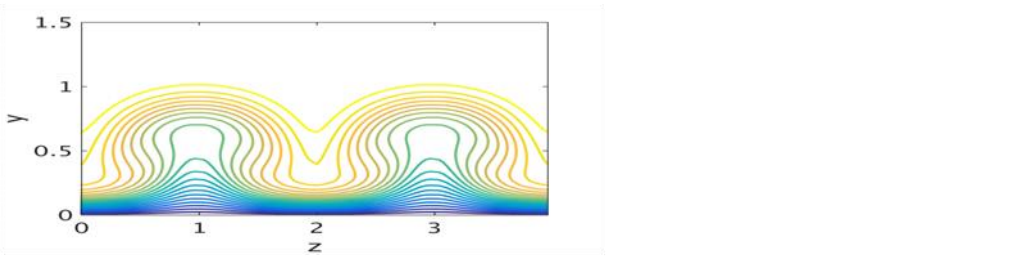

a)

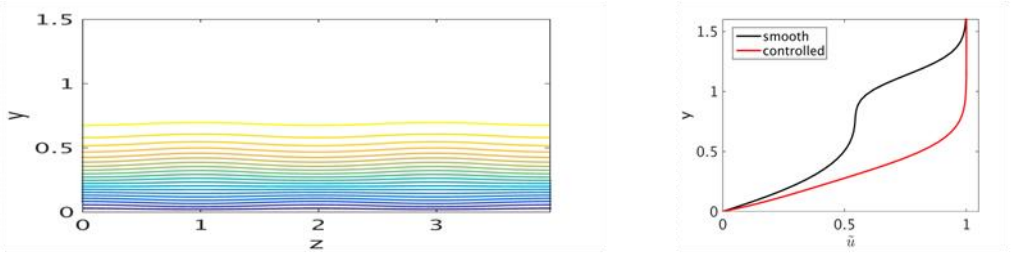

b)

Figure 4.10 Stream wise velocity contours (left column) and profiles (right) for control based on wall deformation for radius 1 m; spanwise separation is 2.4 cm.

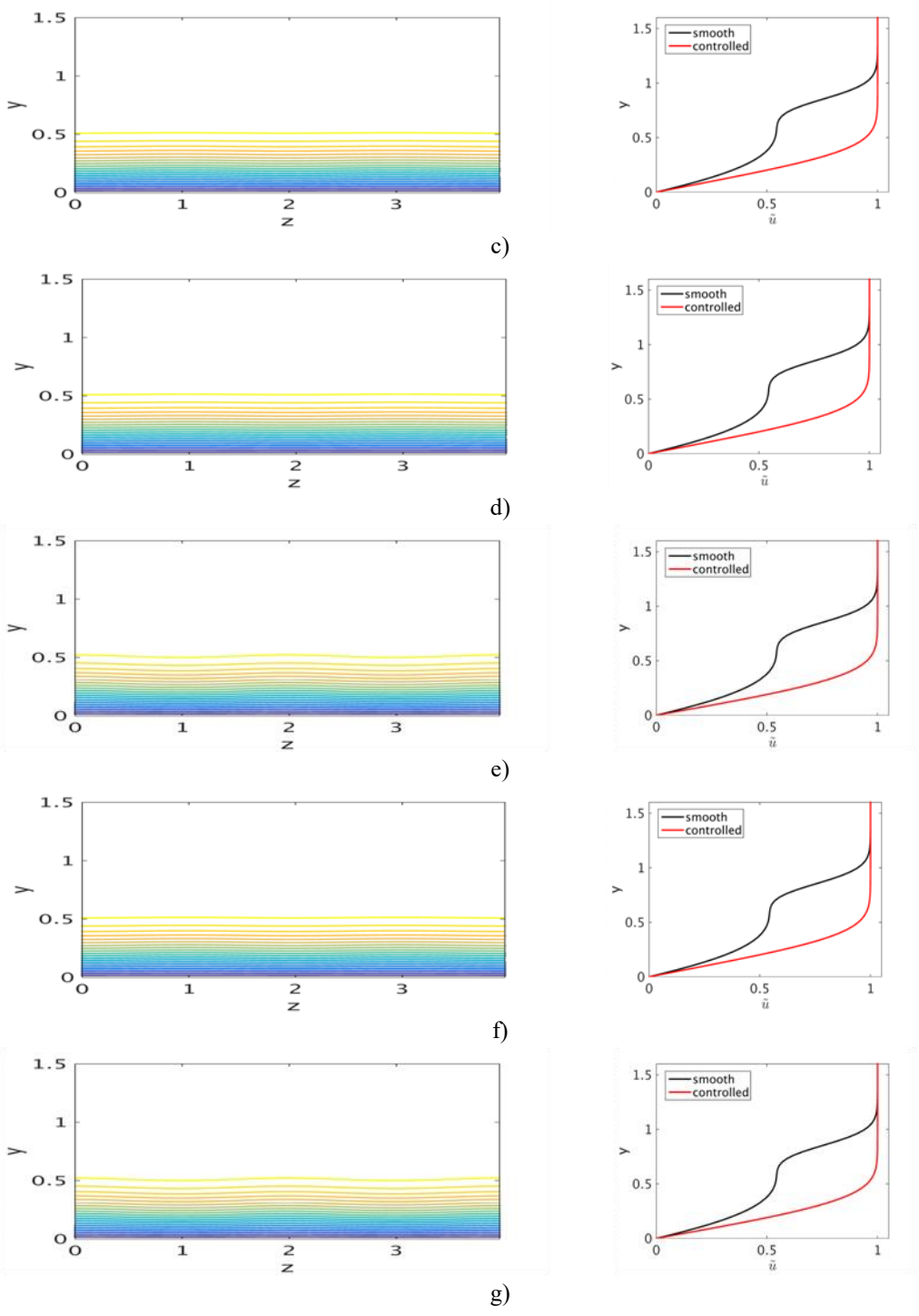

Figure 4.10 (continued).

a) smooth surface; b) control based on u and control plane at y = 0.1; c) control based on v and control plane at y = 0.1; d) control based on u and control plane at y = 0.2; e) control based on v and control plane at y = 0.2; f) control based on u and control plane at y = 0.3; g) control based on v and control plane at y = 0.3.

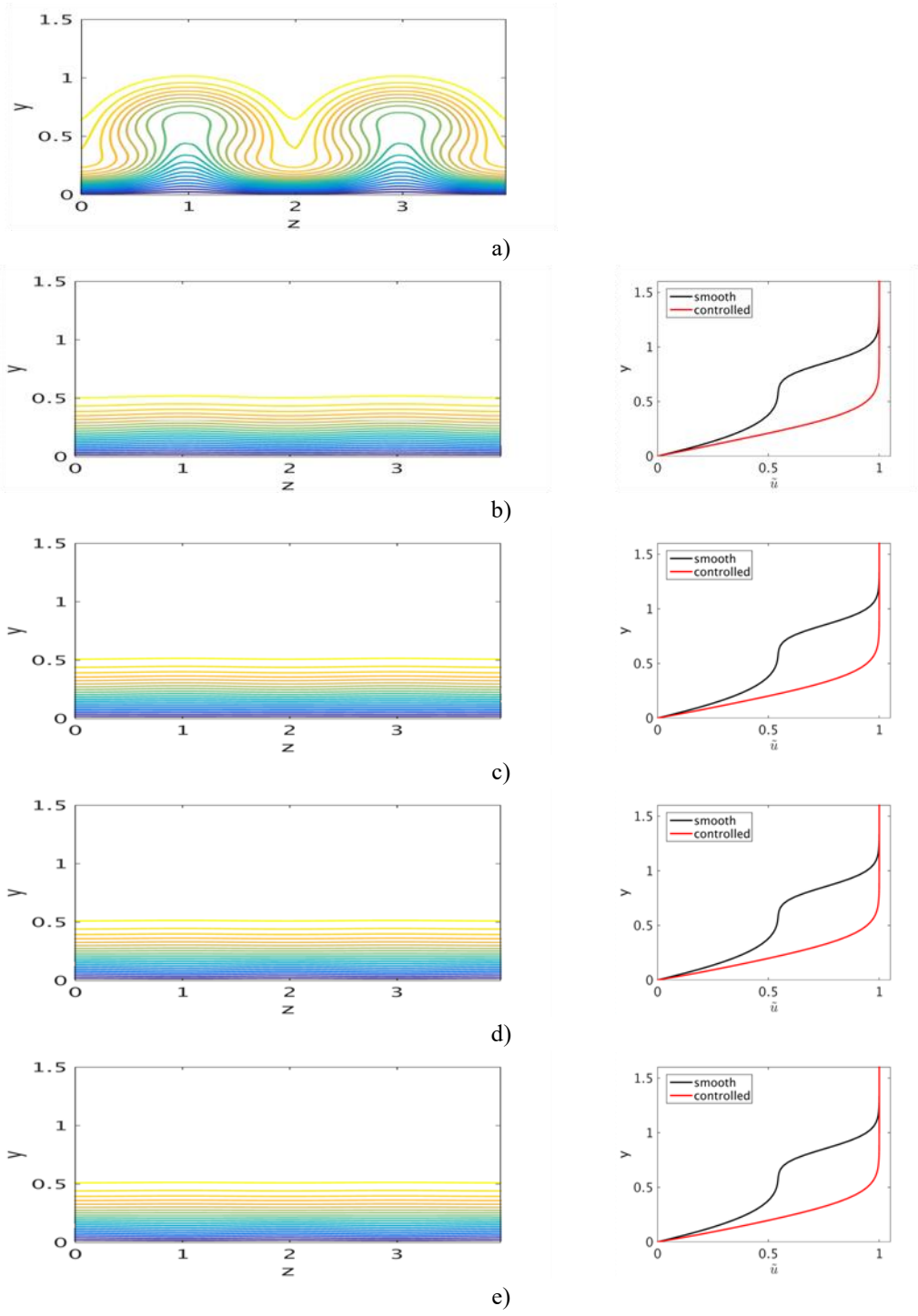

Figure 4.11 Stream wise velocity contours (left column) and profiles (right) for control based on blowing/suction for radius 0.5 m; spanwise separation is 2.4 cm.

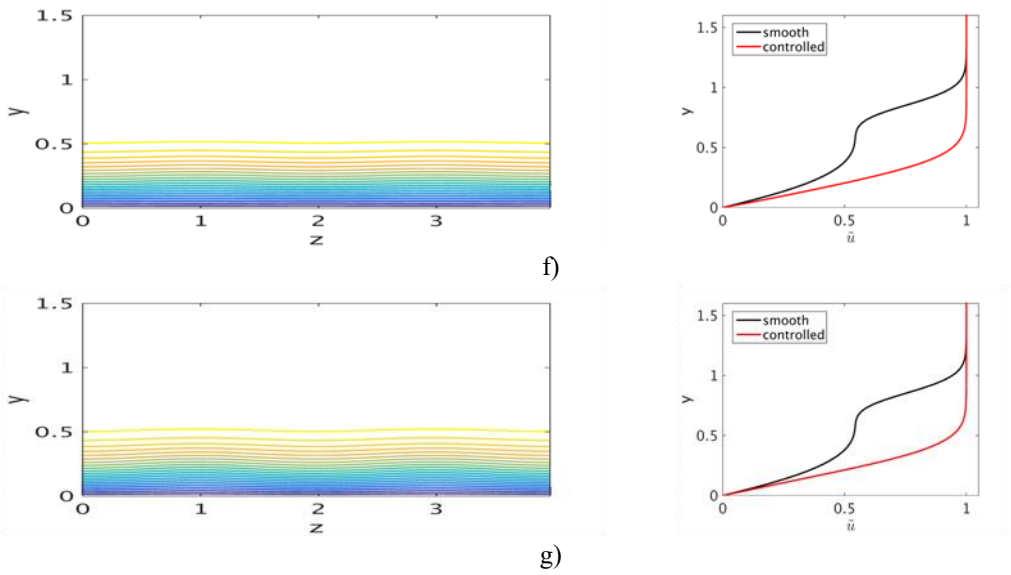

f)

g)

Figure 4.11 (continued).

a) smooth surface; b) control based on u and control plane at y = 0.1; c) control based on v and control plane at y = 0.1; d) control based on u and control plane at y = 0.2; e) control based on v and control plane at y = 0.2; f) control based on u and control plane at y = 0.3; g) control based on v and control plane at y = 0.3.

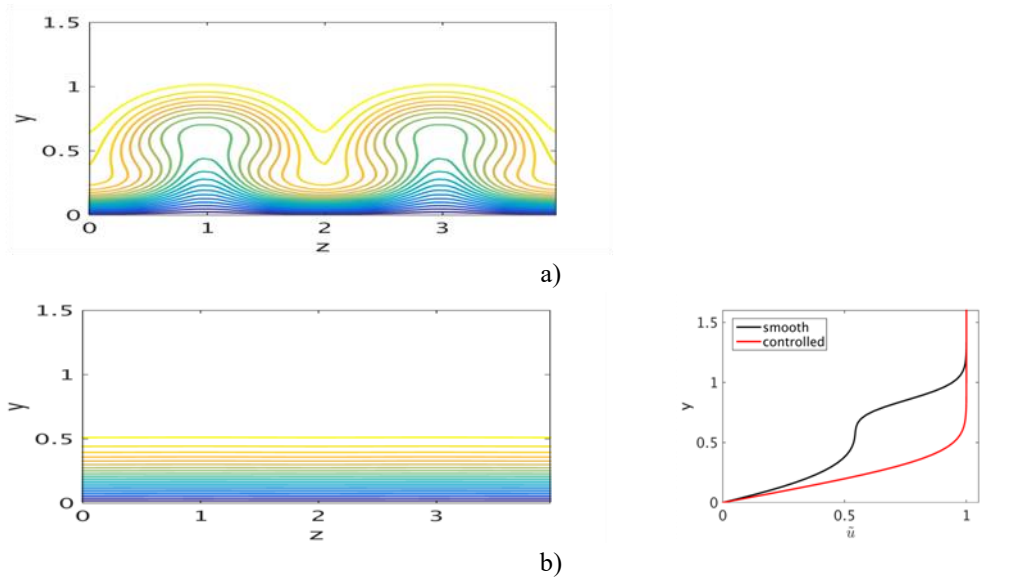

a)

b)

Figure 4.12 Stream wise velocity contours (left column) and profiles (right) for control based on blowing/suction for radius 1 m; spanwise separation is 2.4 cm.

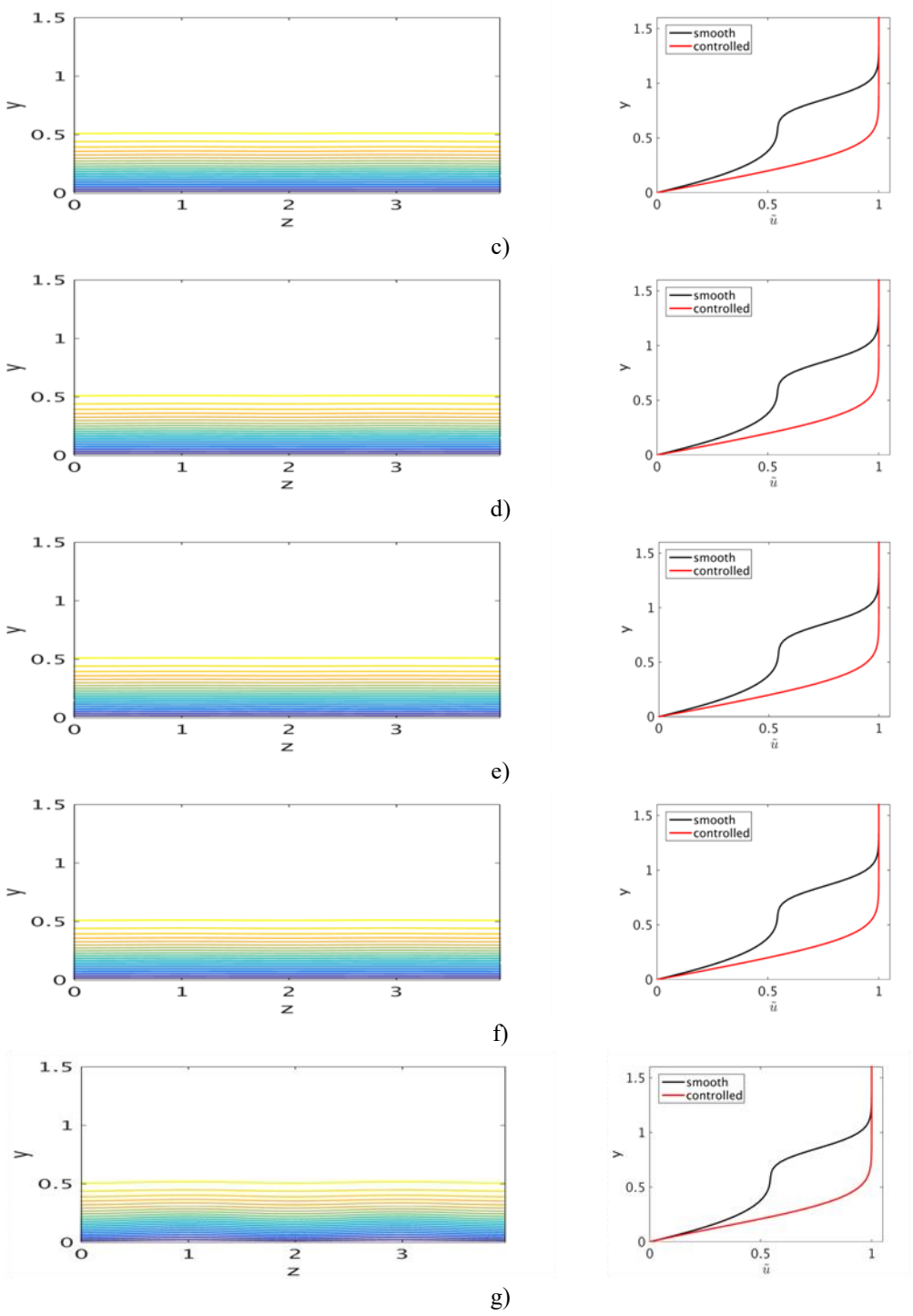

Figure 4.12 (continued).

a) smooth surface; b) control based on u and control plane at y = 0.1; c) control based on v and control plane at y = 0.1; d) control based on u and control plane at y = 0.2; e) control based on v and control plane at y = 0.2; f) control based on u and control plane at y = 0.3; g) control based on v and control plane at y = 0.3.

4.3 Energy growth rates

Figures 4.13, 4.14 and 4.15 show the kinetic energy of the disturbance, calculated according to

$$E(x) = \int_0^{2\pi l} \int_0^{\infty} [|u(x,y,z) - u_m(x,y)|^2 + |v(x,y,z) - v_m(x,y)|^2 + |w(x,y,z) - w_m(x,y)|^2] dz dy, \quad (4.2)$$

Where $u_m(x; y)$, $v_m(x; y)$, and $w_m(x; y)$ are the spanwise mean components of velocity. In the three figures below, the energy associated with the disturbances has been significantly reduced by almost one or two orders of magnitude.

The left figure of each energy plot is given for the entire domain and a zoomed-in version is shown on the right side and shows the energy reduction. For example, in figure 4.13, the control algorithm reduced the energy of the vortices significantly when *v'* was used as the control input for wall deformations. In the case of a spanwise separation of 1.8 cm, shown in figure 4.14, unexpectedly, the control based on blowing and suction with *v'* as the control input seems to provide the best results for the three control plane locations 0.1, 0.2 and 0.3. In contrast, figure 4.15, which corresponds to a spanwise separation of 2.4, for a curvature radius 0.5 m (left column), the wall deformation with *v'* as the control input gives more reduction than the blowing/suction method. For the case of a curvature radius of 1 m (right column), the energy of the disturbances is more reduced by the blowing/suction method for both *u'* and *v'* control than by the wall deformations.

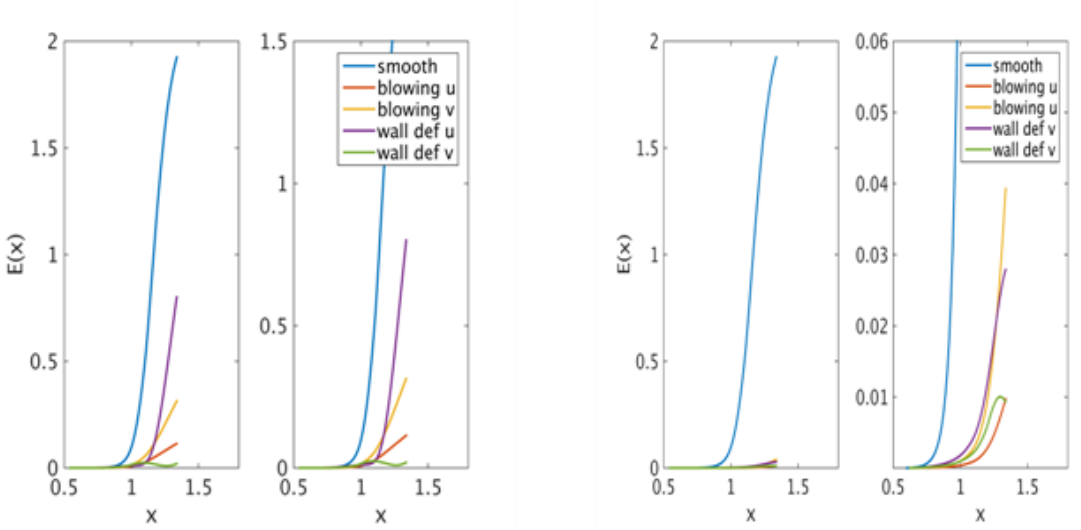

a)

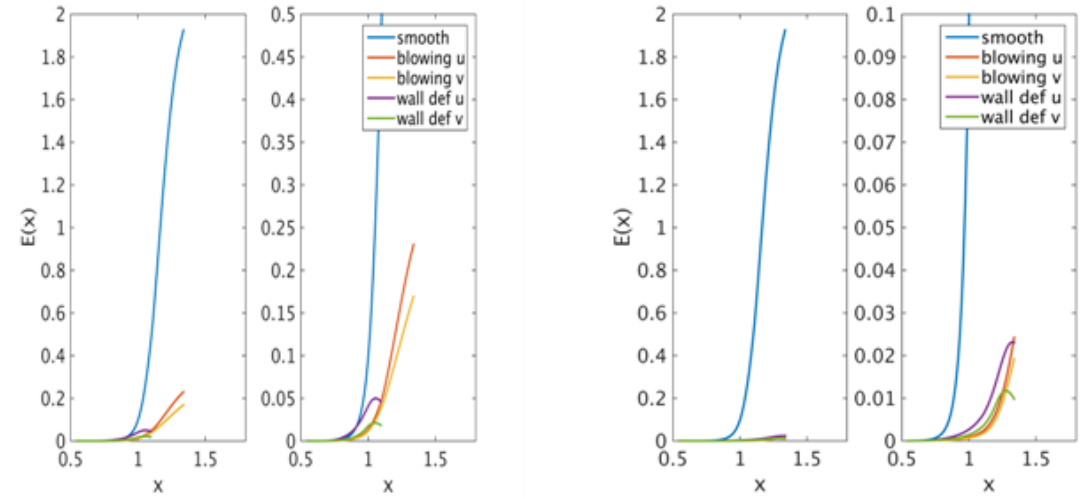

b)

Figure 4.13 Energy of disturbances for spanwise separation 1.2 cm; with curvature radius 0.5 m (left) and 1 m radius (right).

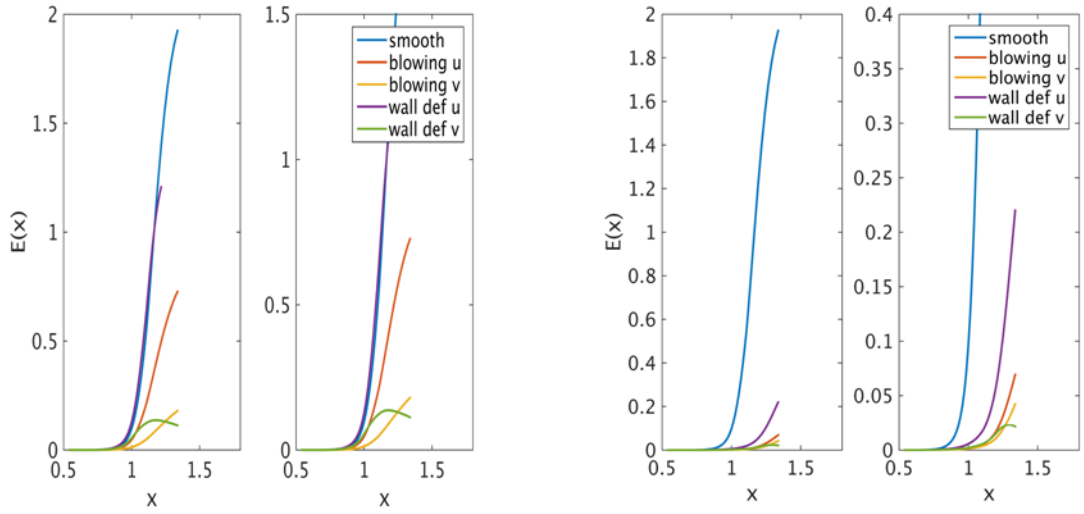

c)

Figure 4.13 (continued).

a) for control plane at y=0.1, b) for control plane at y=0.2 and c) for control plane at y=0.3.

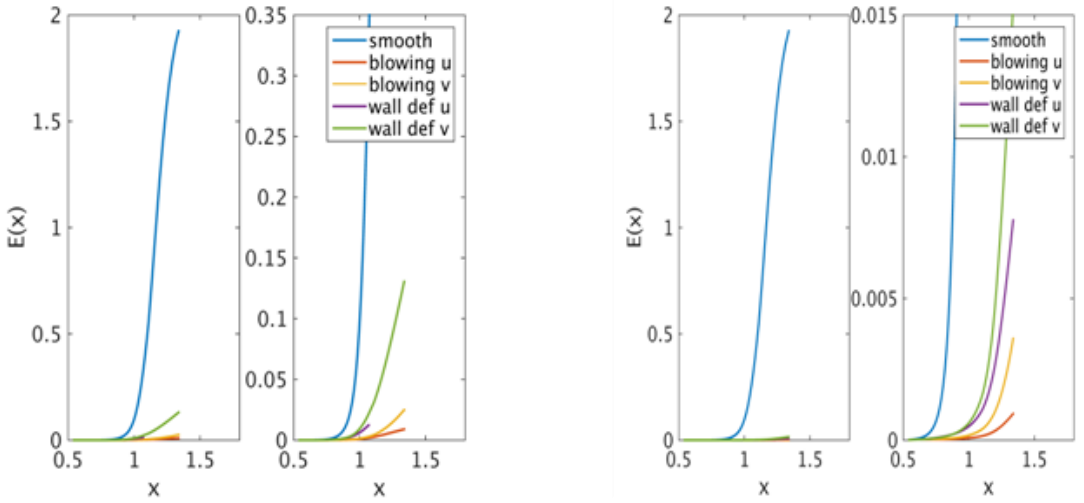

a)

Figure 4.14 Energy of disturbances for spanwise separation 1.8 cm; with curvature radius 0.5 m (left) and 1 m radius (right).

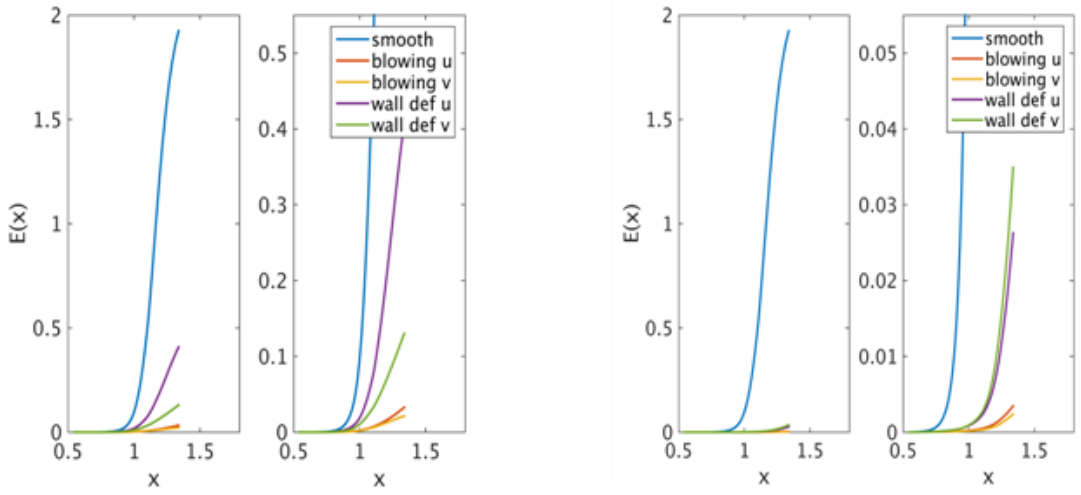

b)

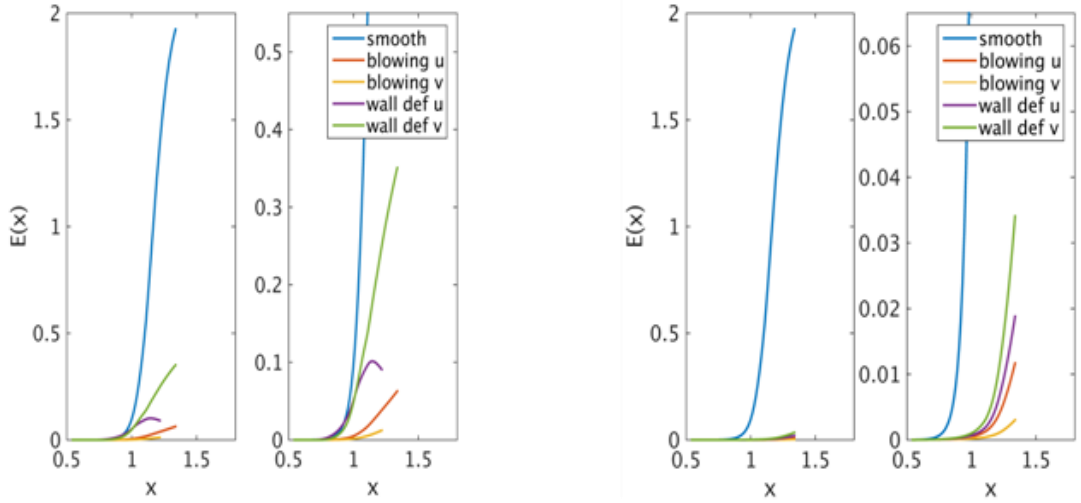

c)

Figure 4.14 (continued).

a) for control plane at y=0.1, b) for control plane at y=0.2 and c) for control plane at y=0.3.

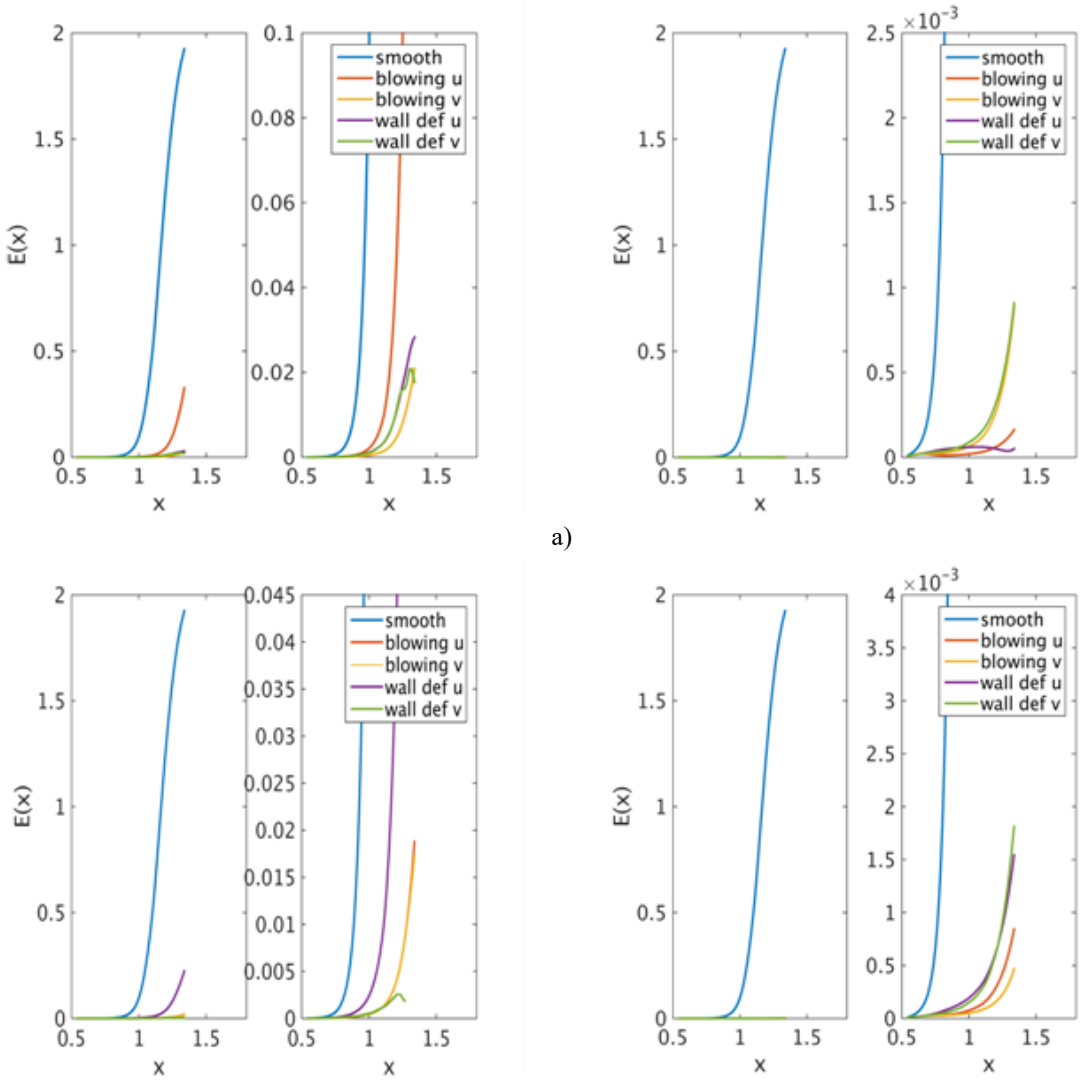

a)

b)

Figure 4.15 Energy of disturbances for spanwise separation 2,4cm; with curvature radius 0,5m (left) and 1 m radius (right).

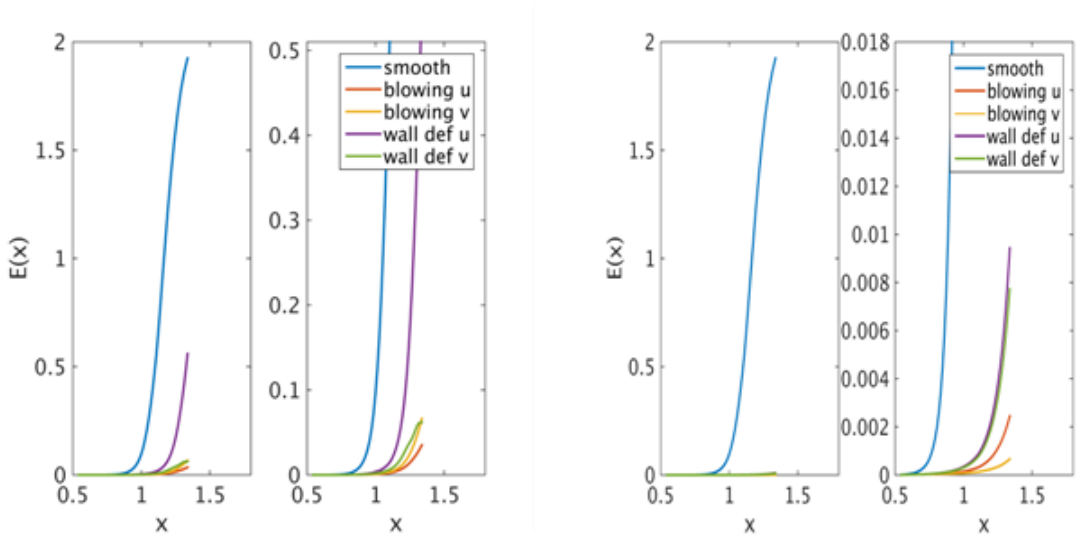

c)

Figure 4.15 (continued).

a) for control plane at y=0.1, b) for control plane at y=0.2 and c) for control plane at y=0.3.

4.4 Growth rates

The following figures show growth rates from the secondary instability analysis, in which a temporal stability problem is considered. The wavenumber α is considered real and the phase speed c is complex. The growth rate is then given by the imaginary part of the frequency $\omega = c\alpha$ as a function of α. In figures 4.16, 4.17 and 4.18, that the results are consistent with the energy distributions in section 4.3. Moreover, the wavenumber of the maximum growth rate is much smaller than the one corresponding to the undeformed surface about one-half of the value in some cases. The wavenumber for the maximum growth rates shifts to the left by 50%. This means that the wavelengths are smaller as the wall deformations and the blowing/suction methods are introduced. Also, comparing the left and right columns, it is clear that as the radius of the curvature increases, the wavenumber of the growth rates decreases.

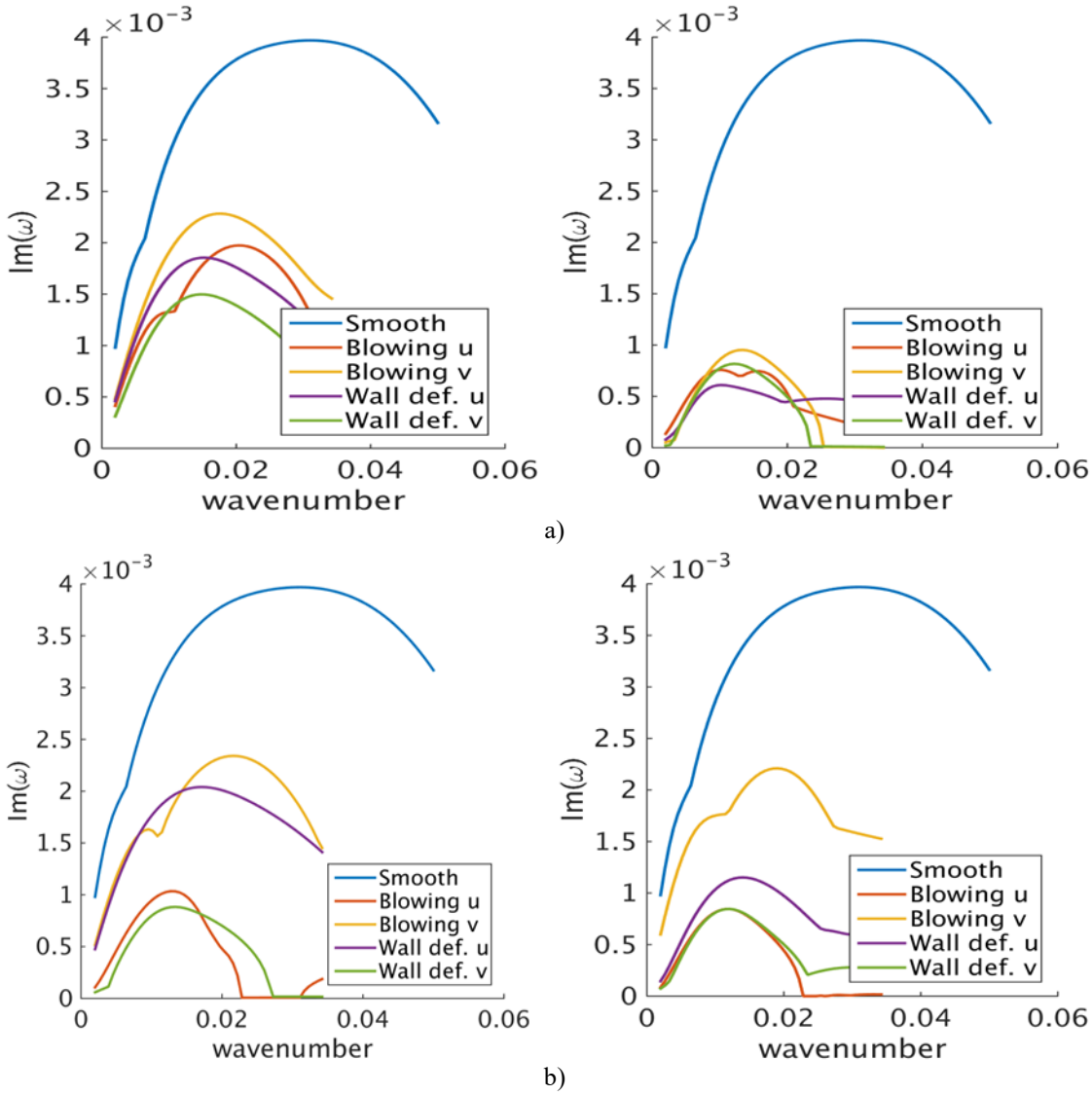

Figure 4.16 Growth rates for spanwise separation 1,2cm; with curvature radius 0,5m (left) and 1 m radius (right).

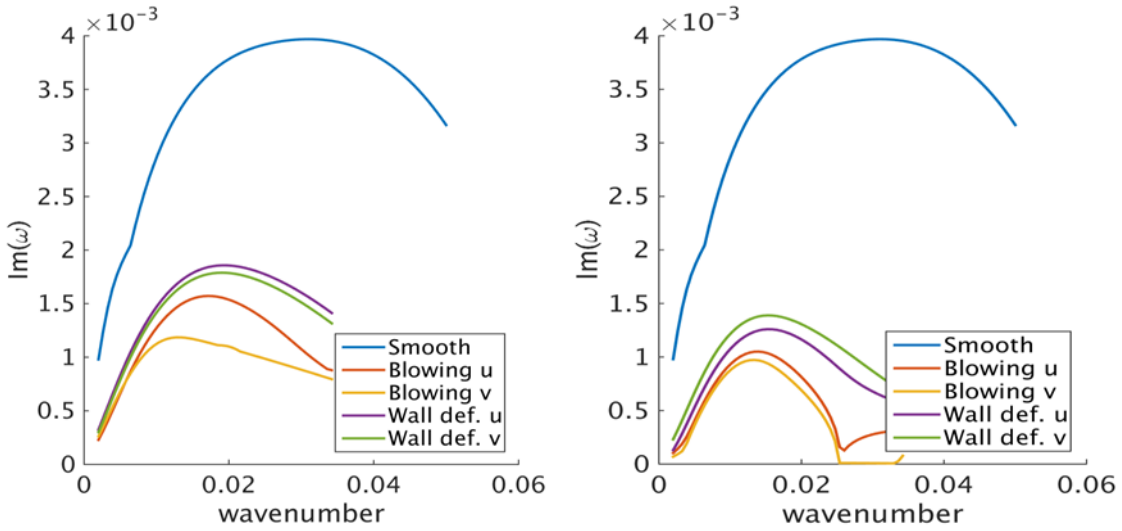

c)

Figure 4.16 (continued)

a) for control plane at y=0,1, b) for control plane at y=0,2 and c) for control plane at y=0,3.

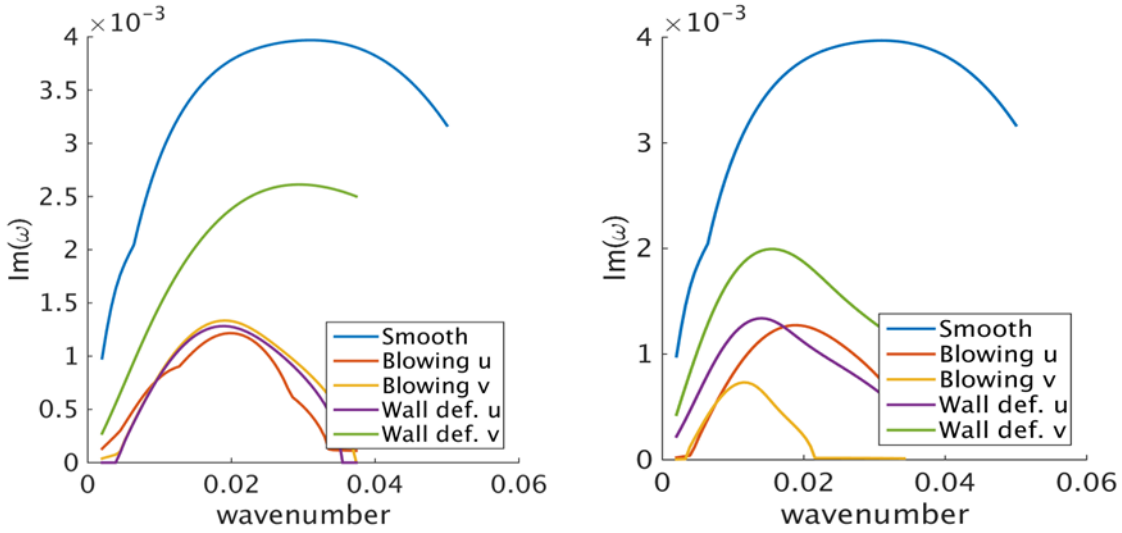

a)

Figure 4.17 Growth rates for spanwise separation 1,8cm; with curvature radius 0,5m (left) and 1 m radius (right).

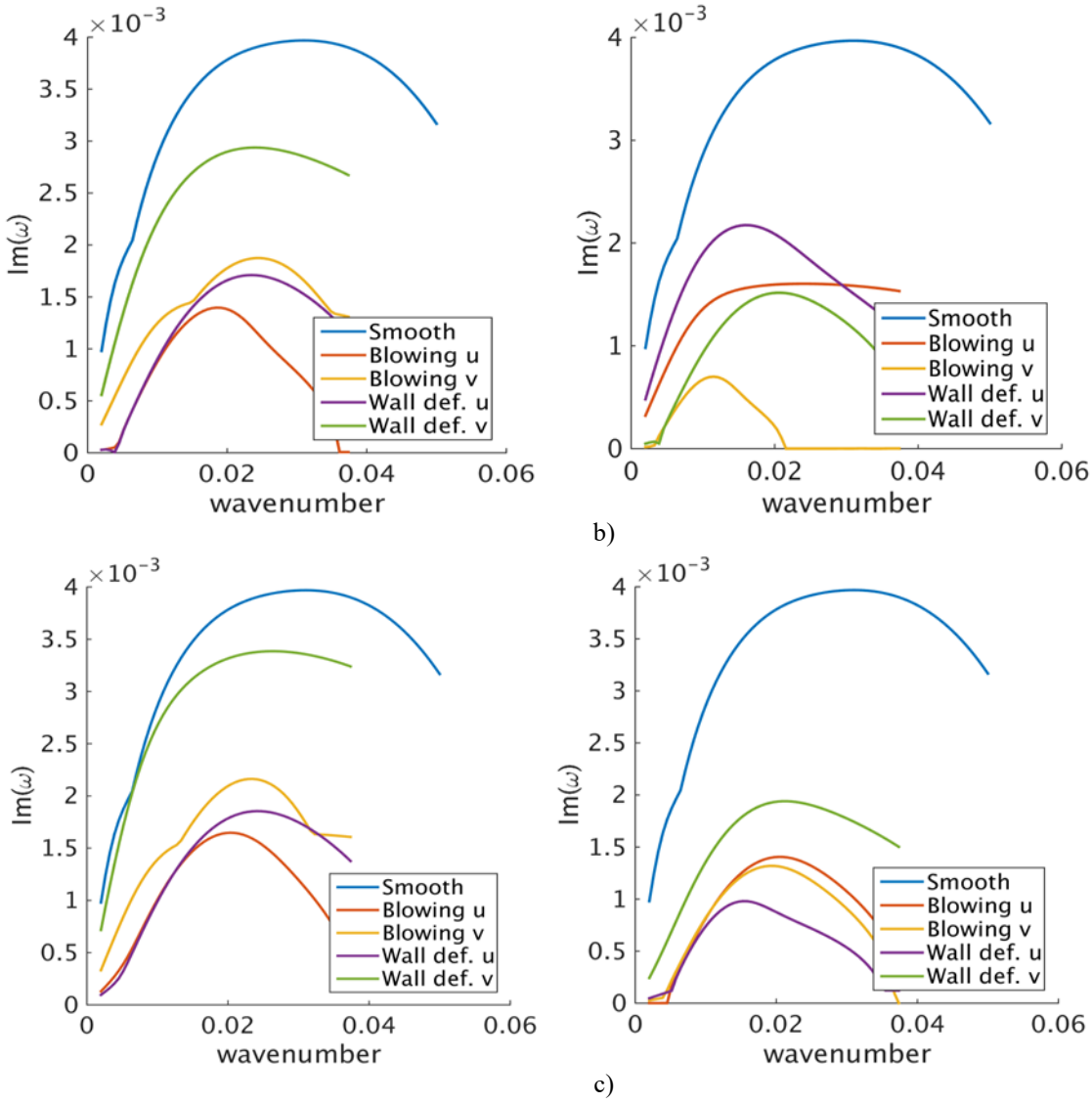

Figure 4.17 (continued)

a) for control plane at y=0,1, b) for control plane at y=0,2 and c) for control plane at y=0,3.

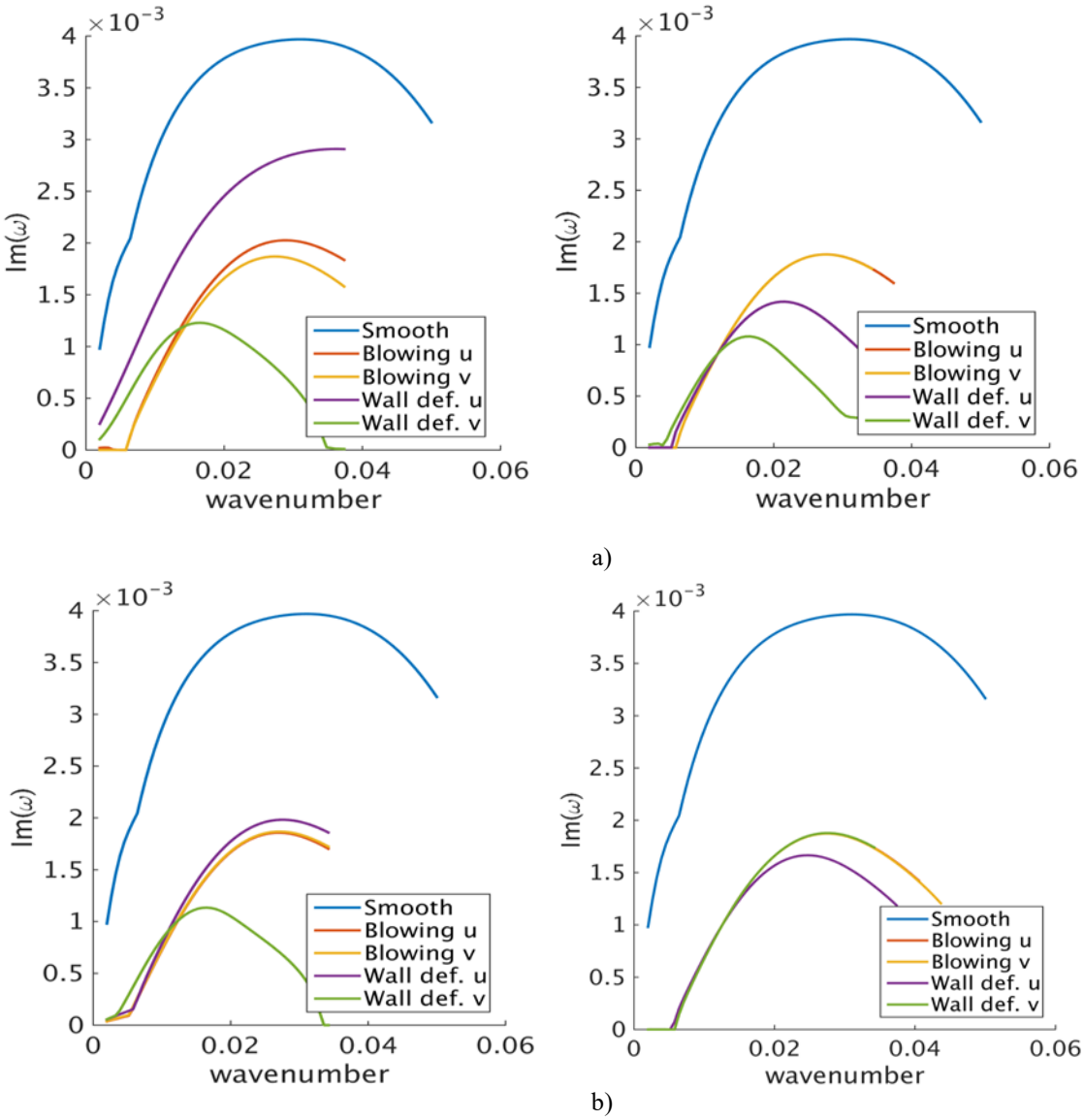

Figure 4.18 Growth rates for spanwise separation 2,4cm; with curvature radius 0,5m (left) and 1 m radius (right).

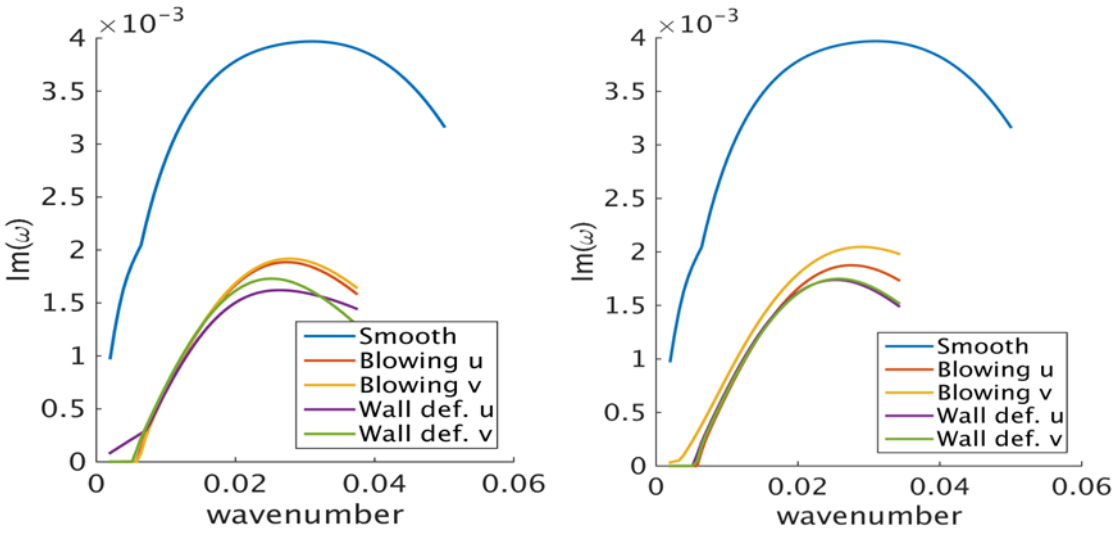

c)

Figure 4.18 (continued)

a) for control plane at y=0,1, b) for control plane at y=0,2 and c) for control plane at y=0,3.

The results from simulations show that for a spanwise separation of 1.2 cm a higher reduction of the vortices is achieved when wall deformations using v' as a feed back control input (case 3) is used (see Table 4.1). Similarly for spanwise separation of 2.4 cm, the results follow the same trend and wall deformations using surface streaks for a curvature radius of 0.5 cm and v' as the input for the control at a plane elevation of 0.2cm performed in case 52 (Table 4.3) reduces the energy associated with the disturbances by almost two orders of magnitudes. Unexpectedly, blowing/suction method is more effective for a spanwise separation of 1.8 cm especially for case 46 (Table 4.2) where a curvature radius of 1 m and the feedback control is performed using v' at a plane elevation of 0.2 cm.

Contour plots of velocity modescorresponding to all control schemes used in this work are shown in appendix B They all show that the regions of intense instability

revealed by patches of yellow or blue - are moved toward the wall as the control is applied.

CHAPTER V

CONCLUSIONS

The effect of controlled wall deformation and blowing/suction on the secondary instability of Görtler vortices in boundary layers developing on concave surfaces has been investigated. The problem was formulated in a high Reynolds asymptotic framework in which the streamwise vortex flow is determined by the boundary region equations (equations (3.3)-(3.6)) together with appropriate upstream boundary conditions. The upstream conditions were derived previously using an asymptotic analysis in the vicinity of the roughness element. The Rayleigh pressure equation was used to determine the growth rates associated with the secondary instability of the vortices. The effect of wall deformations was incorporated into the model using a Prandtl transformation applied to the boundary region equations. An arbitrary function G(X; z) representing the local surface deformation was included in the transformed equations (3.10)-(3.13). These equations were then used within a closed loop control strategy that attempted to minimize the vortex associated energy for a given G(X; z). A proportional integral (PI) controller was employed, with the input being the streamwise velocity disturbance distribution in a plane parallel to the wall. The input to the control algorithm was either the streamwise velocity disturbance u' or the wall-normal velocity disturbance v'.

The simulation results- streamwise velocity contours, disturbance energy and secondary instability growth rates - obtained in this study lead to the following conclusions:

- Both the surface deformations and the blowing/suction modify the streamwise development of the streaks for a given spanwise wavelength and control plane.
- The energy of the vortices was shown to decrease by one or even two orders of magnitude from the original amplitude, which corresponds to the undeformed surface.
- The growth rate of secondary instability is reduced corresponding to the minimization of the vortex energy.

Future efforts will focus on a more in depth investigation of the effect of a combination of wall deformation and blowing/suction methods on the secondary instability of Görtler vortices in developing the boundary layers on concave surfaces in order to achieve a higher reduction of skin friction drag.

REFERENCES

[1] Shlichting H., “Boundary Layer Theory”, Seventh edition (Mc Graw Hill 2014).

[2] Anderson J. D.2005, “Ludwig Prandtl’s boundary layer”, Physics Today, 42-48.

[3] http://sci-fix.blogspot.co.uk/2010/08/paragliding-aerodynamics.html, Accessed May 2016.

[4]WortmanF.X.,1969, “Visualization of transition”, J . Fluid Mech.vol. 38, part 3, pp. 473-480.

[5] Görtler, H., 1940, “Über eine dreidimensionale Instabilität laminarer Grenzschichte nan konkaven Wänden”, Ges. D. Wiss. Göttingen, Nachr. a. d., Math., Vol. 2 No. 1; translated as “On the three-dimensional instability of laminar boundary layers on concave walls”, NACA TM 1375.

[6] SaricW. S., ReedH. L., and KerschenE. J., 2002, “Boundary layer receptivity to freestream disturbances”,Annu. Rev. Fluid. Mech. 34:291-319

[7] Joslin R., 1998, “Overview of Laminar flow control”, Langley research center, Hampton, Virginia Nasa/TP-1998-2087705

[8] Hall, P., “The Linear Development of Görtler Vortices in Growing Boundary Layer”, Journal of Fluid Mechanics. Vol. 130, 1983, pp. 44-58.

[9] Floryan, J. M., Saric, W. S., 1982.“Stability of Görtler Vortices in Boundary Layers”, AIAA Journal. Vol. 20, No. 3, pp. 316-324.

[10] Peerhossaini, Wesfreid J. E., “Experimental study of the Taylor-Görtler Instability”, Vol 41 of the series Spring Series in Synergetics pp 399-412.

[11] Nayfeh A. H., 1981, “Effect of streamwise vortices on tollmien-shlishting waves”, J. Fluid Mech., 107:441-453.

[12] Malik M. R., 1986, “Wave interaction in three dimensional boundary layers”,AIAA Paper 86-1129.

[13] Ricco P. and Dilib F., 2010,“The influence of wall suction and blowing on boundary layer laminar streaks generated by free-stream votical disturbances” Physics of Fluids 22, 044101.

[14] Bhattacharyya K. and Layek G.C. “Effects of suction/blowing on steady boundary layer stagnation-point flow and heat transfer towards a shrinking sheet with thermal radiation”, International Journal of Heat and Mass Transfer 54 302-307.

[15] Kerho M., 2002, “Active reduction of skin friction drag using low speed streak control”, American Institute of Aeronautics and Astronautics.

[16] Sescu A., Afsar M., 2016, “Can surface streaks counteract boundary layer streaks ?”, AIAA paper

[17] Endo T., Kasagi N. and Suzuki Y., 2002, “Feedback control of wall turbulence with wall deformation” published in the International Journal of Heat and Fluid Flow 21 (2000) 568-575.

[18] Sescu A., Taoudi L., Afsar M., Thompson D., 2016, “Control of Görtler vortices by means of staggered surface streaks”, AIAA paper.

[19]Goldstein, M., Sescu, A., Duck, P. and Chaudhari, M., 2010, “The Long Range Persistence of Wakes behind a Row of Roughness Elements”, Journal of Fluid Mechanics, Vol. 644, pp. 123-163.

[20] Hall, P. and Horseman. N., 1991, “The linear inviscid secondary instability of longitudinal vortex structures in boundary layers”, Journal of Fluid Mechanics, Vol. 232, pp. 357-375.

[21] Braslow A., 1966, “A review of factors affecting boundary-layer transition” NASA Technical Note TN D-3384.

[22] Saric, W., Reed H., 2003, “Crossflow instabilities - Theory and technology” AIAA paper 0771.

[23]Dagenhart JR, SaricWS., 1999,“Crossflow stability and transition experiments in swept-wing flow”. NASA TP 1999-209344.

[24] Kohama Y, Saric WS, Hoos JA. ,1991,“A highfrequency, secondary instability of crossflow vortices that leads to transition”. In Proc. Royal Aero. Soc. Conf. on Boundary-Layer Transition and Control.

[25] Kawakami M, Kohama Y, Okutsu M,1999,“Stability characteristics of stationary crossflow vortices in three-dimensional boundary layer”, AIAA Pap. No. 99-0811.

[26] Malik MR, Li F, Chang CL.,1994,“Crossflow disturbances in three-dimensional boundary layers: Nonlinear development, wave interaction and secondary instability”, J. Fluid Mech. 268:1-36.[27] Janke E, Balakumar P., 2000, “On the secondary instability of three-dimensional boundary layers”, Theoret. Comput. Fluid Dyn. 14:167–94.

[28] Lu P., Thapa M., Liu C., 2012."Surface friction and boundary layer thickening in transitional flow". Advances in modeling of fluid dynamics, chapter1. Ping Lu, ManojThapa and Chaoqun Liu (2012). Surface Friction and Boundary Layer Thickening in Transitional Flow, Advances in Modeling of Fluid Dynamics, Dr. Chaoqun Liu (Ed.), InTech, DOI: 10.5772/53581. Available from: http://www.intechopen.com/books/advances-in-modeling-of-fluid-dynamics/surface-friction-and-boundary-layer-thickening-in-transitional-flow. Accessed in May 2016.

[29]Kendall, J. M., 1985, "Experimental study of disturbances produced in a pre-transitional laminar boundary layer by weak free-stream turbulence", in AIAA Paper 85-1695 .

[30] Kendall, J. M., 1991, "Studies on laminar boundary-layer receptivity to freestream turbulence near a leading edge in Boundary Layer Stability and Transition to Turbulence", (ed. D. C. Reda, H. L. Reed & R. Kobayashi), pp. 2330. ASME.

[31] Morkovin, M. V., 1969, "The many faces of transition", Viscous Drag Reduction Plenum Press.

[32] Souza, L. F., Mendonça, M. T., Medeiros, M. A. F., &Kloker M., 2004, "Seeding of Görtler vortices through a suction and blowing strip". Journal of the Brazilian Society of Mechanical Sciences and Engineering, 26(3), 269-279.

[33] Taylor, G. I., "Stability of a Viscous Liquid Contained Between Two RotatingCylinders," Phil. Trans. Roy. Soc. A223, pp. 289-343.

[34] Liepmann, H. W., 1945, "Investigation of the Boundary Layer Transition on ConcaveWalls," NASA Wartime Report ARC No. 4J28.

[35] Smith, A. M. O., 1955, "On the Growth of Taylor-Görtler Vortices Along Highly Concave Walls," Quarterly Journal of Mathematics, Vol. 13, pp. 233-262.

[36] Herert, T.,1976, "On the Stability of the Boundary Layer Along a Concave Wall," MechanikiStosowanei, Vol. 28, pp. 1039-1055.

[37] Ragab, S. A. and Nayfeh, A. H., 1980, "Effect of Pressure Gradients on GörtlerInstability",AIAA Paper No. 80-1377.

[38]Hall, P.,1982, "Taylor-Görtler Vortices in Fully Developed or Boundary-Layer Flows:Linear Theory," Journal of Fluid Mechanics. Vol. 124, pp. 475-494.

[39] Gregory, N. and Walker, B. S., 1956, "The Effect of Transition of Isolated SurfaceExcrescences in the Boundary Layer", ARC R&M 2779.

[40] Tani, I. And Sakagami, J., 1962, “Boundary Layer Instability at Subsonic Speeds,” Proc.ICAS, Third Congress, Stockholm, Sweden, pp. 391-403.

[41] Bippes, M., 1978, “Experimental Study of the Laminar Turbulent Transition on a Concave Wall in a Parallel Flow,” NASA TM-75243.

[42] Mangalam, S. M., Dagenhart, J. R., Hepner, T. and Meyers, J. F., 1985, “The Görtler Instability on an Airfoil,” AIAA Paper No. 85-0491.

[43] Dagenhart, J. H., and Mangalam, S. M., 1986,“Disturbances Functions of the Görtler Instability on an Airfoil”, ICAS-86-1.8.11, 15th Congress of the ICAS.

[44]Day, H. P., Herbert, T., and Saric, W. S., 1990, “Comparing Local and Marching Analyses of Görtler Instability”, AIAA Journal, Vol. 28, No. 6.

[45] Mack, L. M., 1984, “Boundary-layer linear stability theory”, AGARD Rep. No. 709.

[46] Sabry, A.S., Yu, X., and Liu, J.T.C., 1989, “Secondary Instabilities of Three-DimensionalInflectional Velocity Profiles Resulting from Longitudinal Vorticity Elements inBoundary Layers”, Laminar-Turbulent Transition, IUTAM Symposium, Toulouse/France.

[47]Tani I., 1969,“Boundary-Layer Transition”Annual Review of Fluid Mechanics Vol. 1, pp. 169-196.

[48]Hack, M.J.P. and Zaki, T.A.,2012,“The continuous spectrum of time-harmonic shear layers”, Phys. Fluids, Vol. 24, pp. 03410.

[49]Galionis, I. and Hall, P., 2005, “On the stabilization of the most amplified Görtler vortex on a concave surface by spanwise oscillations”, J. Fluid Mech., Vol. 527, pp. 265-283.

[50]Laadhari, F., Skandaji, L. and Morel, R.,1994, “Turbulence reduction in a boundary layer by a local spanwiseoscillatingsurface”, Phys. Fluids, Vol. 6, pp. 3218-3220.

[51]Quadrio, M. and Ricco, P., 2003, “Initial response of a turbulent channel flow to spanwise oscillation of the walls”, J. Turbul., Vol. 4, pp. N7.

[52]Jung, W. J., Mangiavachchi, N. and Akhavan, R. , 1992, “Suppression of turbulence in wall-bounded flows by high-frequencyspanwise oscillations”, Phys. Fluids A, Vol. 4, pp. 1605-1607.

[53]Kramer, M. O., 1961, “The Dolphinos Secret”. J. Am. Soc. Nav. Engrs, Vol. 73, pp. 103-107.

[54]Bushnell, D. M., Hefner, J. N. and Ash, R. L., 1977, “Effect of compliant wall motion on turbulent boundary layers”, Phys. Fluids, Vol. A 20, pp. S31

[55] Carpenter, P. W. and Morris, P. J., 1990, 'The effect of anisotropic wall compliance on boundary-layer stability andtransition", J. Fluid Mech. Vol. 218, pp. 171-223.

[56] Davies, C. and Carpenter, P. W., 1997, "Numerical simulations of the evolution of Tollmien-Schlichting waves over finitecompliant panels", J. Fluid Mech. Vol. 335, pp. 361-392.

[57] Seddougui S. O., Bowles R. I., Smith F. T., 1990, "Surface cooling effects on compressible boundary layer instability", NASA Contractor Report 182003, ICASE Report No 90-19.

[58] Choi, H., Moin, P. and Kim, J., 1994,"Active turbulence control for drag reduction in wall-bounded flows", J. Fluid Mech., Vol. 262, pp. 75-110.

[59] Koumoutsakos P., 1999, "Vorticity flux control for a turbulent channel flow", Phys. Fluids, Vol. 11, pp. 248.

[60 Kang, S. and Choi, H., 2000, "Active wall motions for skin-friction drag reduction", Phys. Fluids, Vol. 12, pp. 3301-3304.

[61] Koberg, H., 2007, "Turbulence control for drag reduction with active wall deformation", PhD Thesis, Imperial College London.

[62] Goldstein, M., Sescu, A., Duck, P. and Choudhari, M., 2011, "Algebraic/transcendental Disturbance Growth behind aRow of Roughness Elements", Journal of Fluid Mechanics, Vol. 668, pp. 236-266.

[63] Sescu, A. and Thompson, D., 2015, "On the Excitation of Görtler Vortices by Distributed Roughness Elements", Theoreticaland Computational Fluids Dynamics, Vol. 29, pp. 67-92.

[64] Ziegler, M. and Nichols, N.B., 1942, "Optimal settings for automatic controllers", Trans. ASME, Vol. 65, pp. 433-444

APPENDIX A

GSDC

The spanwise-mean component is determined as:

$$\tilde{\mathrm{u}}(\hat{X},\bar{\mathrm{y}}) = U'_B(\bar{\mathrm{y}})A(\hat{X}), \tilde{\bar{v}}(\hat{X},\bar{\mathrm{y}}) = -U'_B(\bar{\mathrm{y}})\frac{dA(\hat{X})}{dX}, \tilde{\bar{p}}(\hat{X}) \to \frac{\tilde{\bar{p}}_0}{X^{\beta_0}} \tag{A.1}$$

$$\hat{X} \equiv (x^* - x_0^*)/x_0^*\delta^{3/4}, \tag{A.2}$$

$$A(\hat{X}) \to a_0\lambda^{\frac{2}{3}}\hat{F}_0(0) + \frac{\tilde{\bar{p}}_0}{i(\beta_0-1)X^{\beta_0-1}}\ as\hat{X} \to 0, \tag{A.3}$$

$$a_0 = -3(-3Ai'(0)/4)^{3/4}\cos(\pi/8) \tag{A.4}$$

$$\tilde{\bar{p}}_0 = \frac{\sqrt{3}\Gamma(2/3)}{\Gamma(1/3)}9^{1/3}\lambda^{5/3}\hat{F}_0(0) \tag{A.5}$$

where $\beta_0 = 2/3$, and $\hat{F}_0$ is determined from the Fourier expansion

$$\sum_{n=-\infty}^{n=\infty}\int_{-\infty}^{\infty}\hat{F}_n(k)e^{i\left(\frac{nz}{l}+kx\right)}dk, \tag{A.6}$$

The initial conditions for the linear BRE are given by

$$\tilde{\mathrm{u}} \to \frac{1}{(\bar{X})-1)^{2/3}}\left[\tilde{\mathrm{u}}_0^{(0)}(\bar{\mathrm{y}},\bar{z}) + \frac{\widetilde{U}_0(\eta,\bar{z})}{(\bar{X})-1)^{1/3}} - \frac{9}{10\bar{\mathrm{y}}\lambda}\frac{\delta^2\tilde{p}_0^{(0)}(0,\bar{z})}{\partial\bar{z}^2}\right] + \frac{1}{(\bar{X})-1)^{1/3}}\left[\tilde{\mathrm{u}}_0^{(1)}(\bar{\mathrm{y}},\bar{z}) + \frac{\widetilde{U}_1(\eta,\bar{z})}{(\bar{X})-1)^{1/3}} - \frac{9}{4\bar{\mathrm{y}}\lambda}\frac{\delta^2\tilde{p}_0^{(1)}(0,\bar{z})}{\partial\bar{z}^2} + \frac{3\Gamma\left(\frac{2}{3}\right)(3\lambda)^{1/3}}{4\bar{\mathrm{y}}(\bar{X})-1)^{1/3}}\frac{\delta^2\tilde{p}_0^{(1)}(0,\bar{z})}{\partial\bar{z}^2}\right], \tag{A.7}$$

$$\tilde{v} \to \frac{1}{(\bar{X})-1)^{5/3}}\left[\tilde{v}_0^{(0)}(\bar{\mathrm{y}},\bar{z}) + \lambda^{-1/3}\tilde{V}_0(\eta,\bar{z}) - \frac{3}{5\lambda}\frac{\delta^2\tilde{p}_0^{(0)}(0,\bar{z})}{\partial\bar{z}^2}\right] + \frac{1}{(\bar{X})-1)^{4/3}}\left[\tilde{v}_0^{(1)}(\bar{\mathrm{y}},\bar{z}) + \lambda^{-1/3}\tilde{V}_1(\eta,\bar{z}) - \frac{3}{5\lambda}\frac{\delta^2\tilde{p}_1^{(0)}(0,\bar{z})}{\partial\bar{z}^2} + \frac{\Gamma\left(\frac{2}{3}\right)(3\lambda)^{1/3}}{2\bar{\mathrm{y}}(\bar{X})-1)^{1/3}}\frac{\delta^2\tilde{p}_0^{(1)}(0,\bar{z})}{\partial\bar{z}^2}\right], \tag{A.8}$$

$$\tilde{w} \to \frac{1}{(\bar{X})-1)^{5/3}}\left[\tilde{w}_0^{(0)}(\bar{\mathrm{y}},\bar{z}) + \frac{\widetilde{W}_0(\eta,\bar{z})}{(\bar{X})-1)^{1/3}} - \frac{3}{5\bar{\mathrm{y}}\lambda}\frac{\delta^2\tilde{p}_0^{(0)}(0,\bar{z})}{\partial\bar{z}^2}\right] + \frac{1}{(\bar{X})-1)^{1/3}}\left[\tilde{w}_0^{(1)}(\bar{\mathrm{y}},\bar{z}) + \frac{\widetilde{W}_1(\eta,\bar{z})}{(\bar{X})-1)^{1/3}} - \frac{3}{4\bar{\mathrm{y}}\lambda}\frac{\delta^2\tilde{p}_0^{(1)}(0,\bar{z})}{\partial\bar{z}^2}\right], \tag{A.9}$$

$$p \to \frac{\tilde{p}_0^{(0)}(\bar{\mathrm{y}},\bar{z})}{(\bar{X})-1)^{8/3}} + \frac{\tilde{p}_0^{(1)}(\bar{\mathrm{y}},\bar{z})}{(\bar{X})-1)^{7/3}} \tag{A.10}$$

where

$$\tilde{p}_0^{(0)}(\bar{y},\bar{z}) = \frac{5.2\sqrt{3}\Gamma\left(\frac{2}{3}\right)}{9\Gamma\left(\frac{1}{3}\right)} 9^{\frac{1}{3}}\lambda^{\frac{5}{3}} \sum_{n=-\infty,n\neq 0}^{\infty} \pi_n(\bar{y},0)\frac{l^2\hat{F}_n(0)}{n^2} e^{in\bar{z}/l} \tag{A.11}$$

$$\tilde{p}_0^{(1)}(\bar{y},\bar{z}) = \frac{2\sqrt{3}9^{\frac{2}{3}}\lambda^{\frac{4}{3}}}{9\Gamma\left(\frac{1}{3}\right)} \sum_{n=-\infty,n\neq 0}^{\infty} \pi_n(\bar{y},0)\frac{l^4\hat{F}_n(0)\pi_n'''(0,0)}{n^4} e^{in\bar{z}/l} \tag{A.12}$$

With $\pi_n(\bar{y},0)$ determined from the boundary value problem

$$U^2{}_B(\bar{y})\frac{d}{d\bar{y}}\left[\frac{1}{U^2{}_B(\bar{y})}\frac{d\pi_n(\bar{y},0)}{d\bar{y}}\right] - (\frac{n}{l})^2\pi_n(\bar{y},0) \tag{A.13}$$

which is the result of Fourier transforming the Poisson equation for pressure, satisfying the boundary conditions

$$\pi_n(0,0) = 1, \pi_n(\bar{y},0) \to 0, \bar{y} \to \infty \tag{A.14}$$

In the above equations,

$$\tilde{v}_0^{(j)} = \frac{3}{(5-j)U_n(\bar{y})}\tilde{p}_{0,\bar{y}}^{(j)} \tag{A.15}$$

$$\tilde{w}_0^{(j)} = \frac{3}{(5-j)U_n(\bar{y})}\tilde{p}_{0,\bar{z}}^{(j)} \tag{A.16}$$

$$\tilde{u}_0^{(j)} = \frac{3U_B{}'(\bar{y})}{(2-j)U_n(\bar{y})}\tilde{v}_0^{(j)} \tag{A.17}$$

$$\widetilde{W_j} = \frac{-\pi}{\lambda^{\frac{2}{3}}\sqrt{3}\Gamma\left(\frac{8-j}{3}\right)}\frac{\delta^2\tilde{p}_0^{(0)}(0,\bar{z})}{\partial\bar{z}^2}\widehat{W}_j(\eta) \tag{A.18}$$

$$\widetilde{U_j} = \frac{\pi}{\lambda^{\frac{2}{3}}\sqrt{3}\Gamma\left(\frac{8-j}{3}\right)}\frac{\delta^2\tilde{p}_0^{(0)}(0,\bar{z})}{\partial\bar{z}^2}\widehat{U}_j(\eta) \tag{A.19}$$

Where $\widehat{V}_j$ is determined from

$$\frac{\partial^2\widetilde{U_j}}{\partial\eta^2} + \eta[\frac{\eta}{3}\frac{\partial\widetilde{U_j}}{\partial\eta} + (\alpha_j - \frac{5}{3})\widetilde{U_j}] = \widehat{V}_j \tag{A.20}$$

Also, j=1,2, and

$$\widetilde{U_0} = \frac{1}{\pi\sqrt{3}}\eta e^{-\eta^3/9}\left[\Gamma\left(\frac{2}{3}\right)\int_0^{\eta} e^{\tilde{\eta}^{\frac{3}{9}}}\partial\tilde{\eta} - \frac{2\pi}{3^{\frac{1}{3}}\sqrt{3}}\right] - \frac{3^{\frac{1}{3}}}{\pi}\Gamma\left(\frac{1}{3}\right)\widetilde{U}_{H,0} \tag{A.21}$$

$$\widetilde{U_1} = \frac{\sqrt{3}}{\pi}\Gamma\left(\frac{4}{3}\right)e^{-\eta^3/9}\int_0^{\eta}\tilde{\eta}e^{\tilde{\eta}^{\frac{3}{9}}}\partial\tilde{\eta} - \frac{3^{\frac{1}{3}}}{\pi}\Gamma\left(\frac{1}{3}\right)\widetilde{U}_{H,1} \quad \text{(A.22)}$$

$$\widetilde{U}_{H,0} = \frac{\eta}{3^{\frac{2}{3}}\sqrt{3}}\left[\frac{3^{\frac{1}{3}}\Gamma\left(\frac{2}{3}\right)}{\Gamma\left(\frac{1}{3}\right)}\eta M\left(\frac{2}{3},\frac{4}{3};-\frac{\eta^3}{9}\right) - \frac{\Gamma\left(\frac{1}{3}\right)}{\Gamma\left(\frac{2}{3}\right)}\eta M\left(\frac{1}{3},\frac{2}{3};-\frac{\eta^3}{9}\right)\right] \quad \text{(A.23)}$$

Where $\Gamma(a)$ is the well-known gamma function, and $M(a,b;z)$ is the confluent hypergeometric function.

$$\widetilde{U}_{1,H} = \frac{\sqrt{3}}{3.3^{\frac{1}{3}}}\int_0^{\eta}\tilde{\eta}e^{\tilde{\eta}^{\frac{3}{9}}}\partial\tilde{\eta} \quad \text{(A.24)}$$

$$\widetilde{W_j} = \frac{-1}{\pi^3\sqrt{3}}\eta\left\{\left[2(2-j) - \frac{\eta^3}{3}\right]e^{-\frac{\eta^3}{9}}\left[\Gamma\left(\frac{2-j}{3}\right)\eta^{-j}\int_0^{\eta}\tilde{\eta}e^{\tilde{\eta}^{\frac{3}{9}}}\partial\tilde{\eta} - \delta_{j,0}\frac{2\pi}{3^{\frac{1}{3}}\sqrt{3}}\right] + \Gamma\left(\frac{2-j}{3}\right)\eta\right\} \text{(A.25)}$$

It should be mentioned that the asymptotic solution given by (A.7) - (A.10) is only valid around$\mathrm{X} = 1$, and itbreaks down for $\mathrm{X} - 1 \gg 0$.

APPENDIX B

VELOCITY MODES

The following figures show the contour plots of the first stability modes for *u* velocity (on the left) and *v* velocity (on the right) at a certain streamwise position for both wall deformation and blowing/suction methods using three different spanwise seperations1.2, 1.8 and 2.4 cm for two different curvature radii 0.5 m and 1 m where a feedback control using *u* and *v* is considered. These figures show the stability of the flow and describe how and where the instabilities are generated for both *u* and *v* velocities.

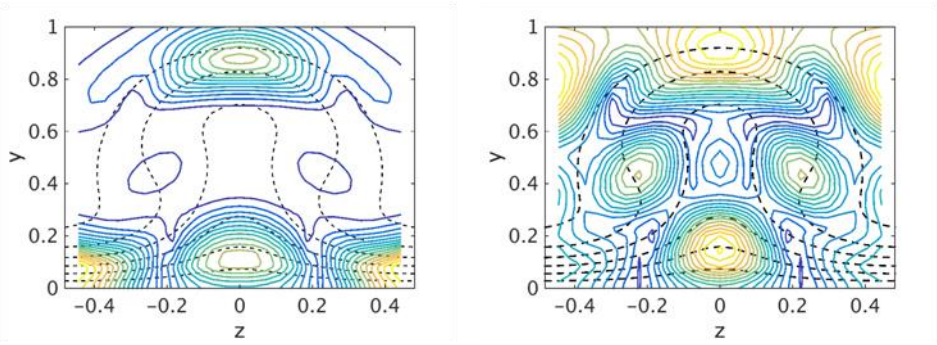

a)

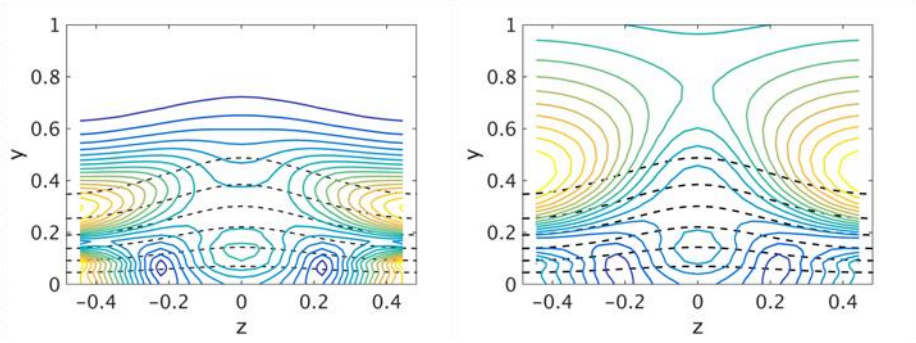

b)

Figure B.1 First stability modes of the streamwise velocity for control based on wall deformation for radius 0.5 m and spanwise separation is 1.2 cm; U modes (left column) and V modes(right).

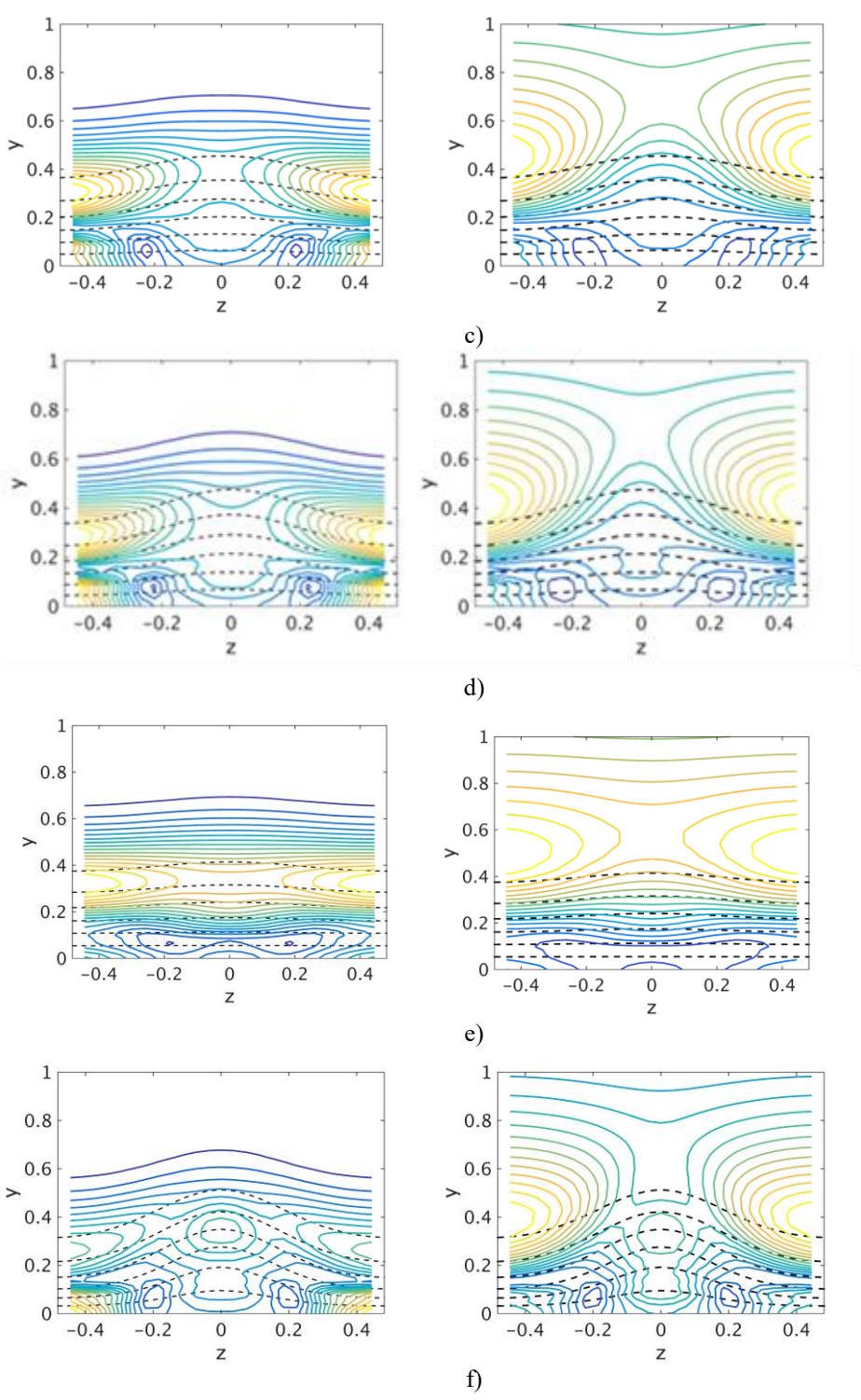

Figure B.1 (continued).

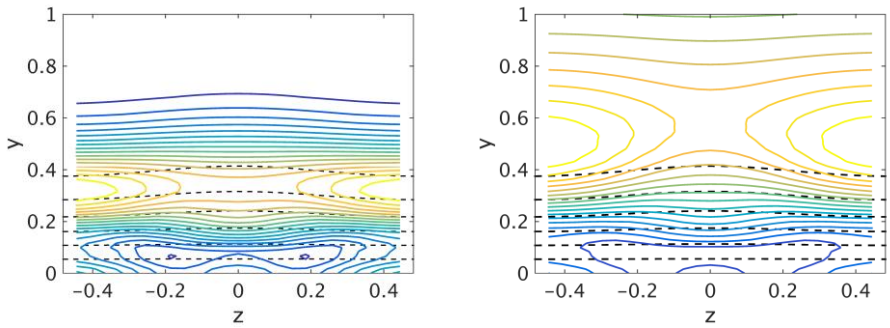

g)

Figure B.1 (continued).

a) smooth surface; b) control based on u and control plane at y = 0.1; c) control based on v and control plane at y = 0.1; d) control based on u and control plane at y = 0.2; e) control based on v and control plane at y = 0.2; f) control based on u and control plane at y = 0.3; g) control based on v and control plane at y =0.3.

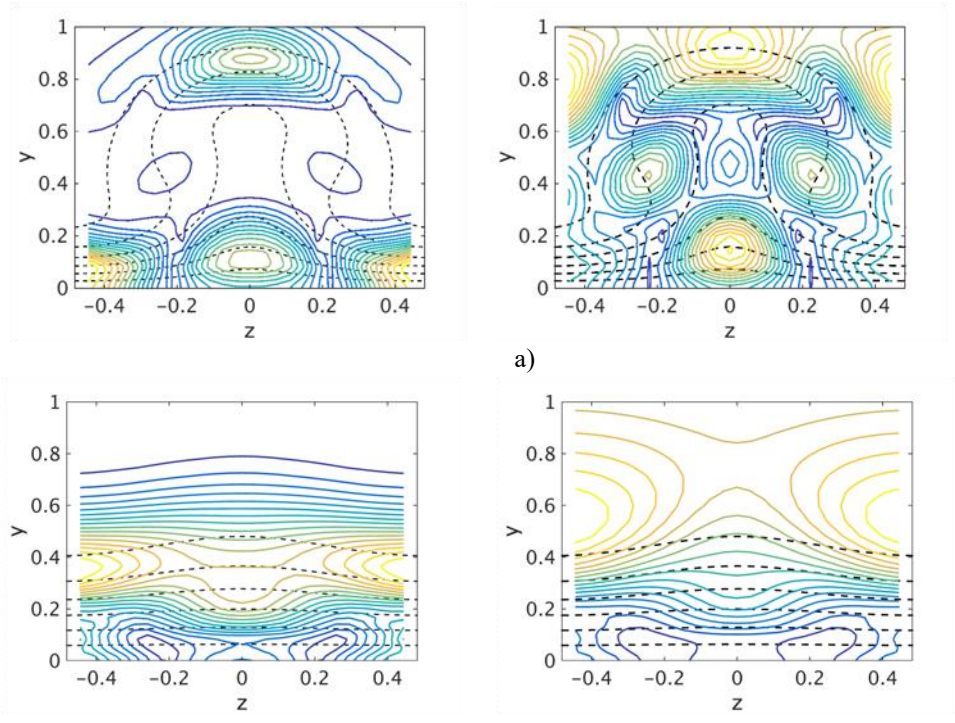

a)

b)

Figure B.2 First stability modes of the streamwise velocity for control based on wall deformation for radius 1 m and spanwise separation is 1.2 cm; U modes (left column) and V modes(right).

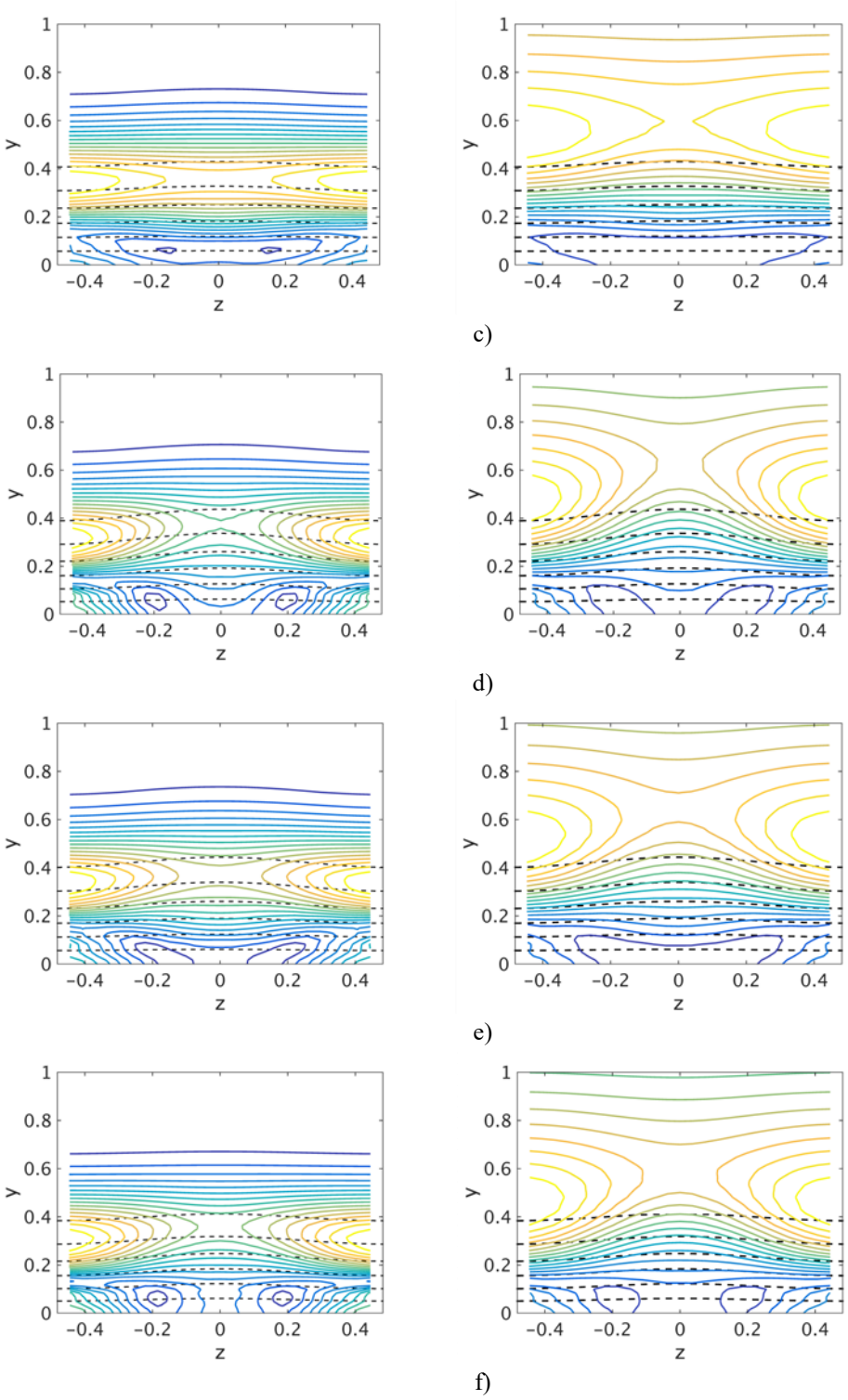

c)

d)

e)

f)

Figure B.2 (continued).

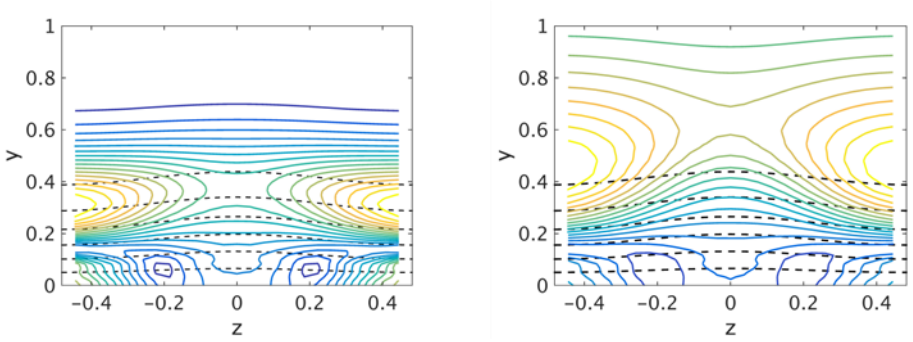

g)

Figure B.2 (continued).

a) smooth surface; b) control based on u and control plane at y = 0.1; c) control based on v and control plane at y = 0.1; d) control based on u and control plane at y = 0.2; e) control based on v and control plane at y = 0.2; f) control based on u and control plane at y = 0.3; g) control based on v and control plane at y =0.3.

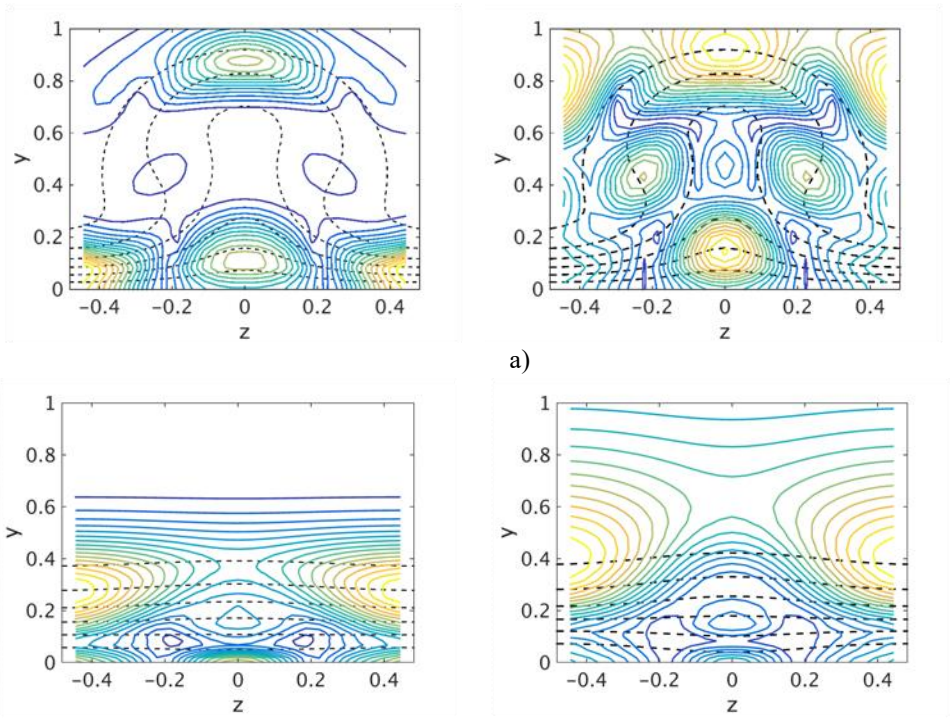

a)

b)

Figure B.3 First stability modes of the streamwise velocity for control based on blowing/suction for radius 0.5 m and spanwise separation is 1.2 cm; U modes (left column) and V modes(right).

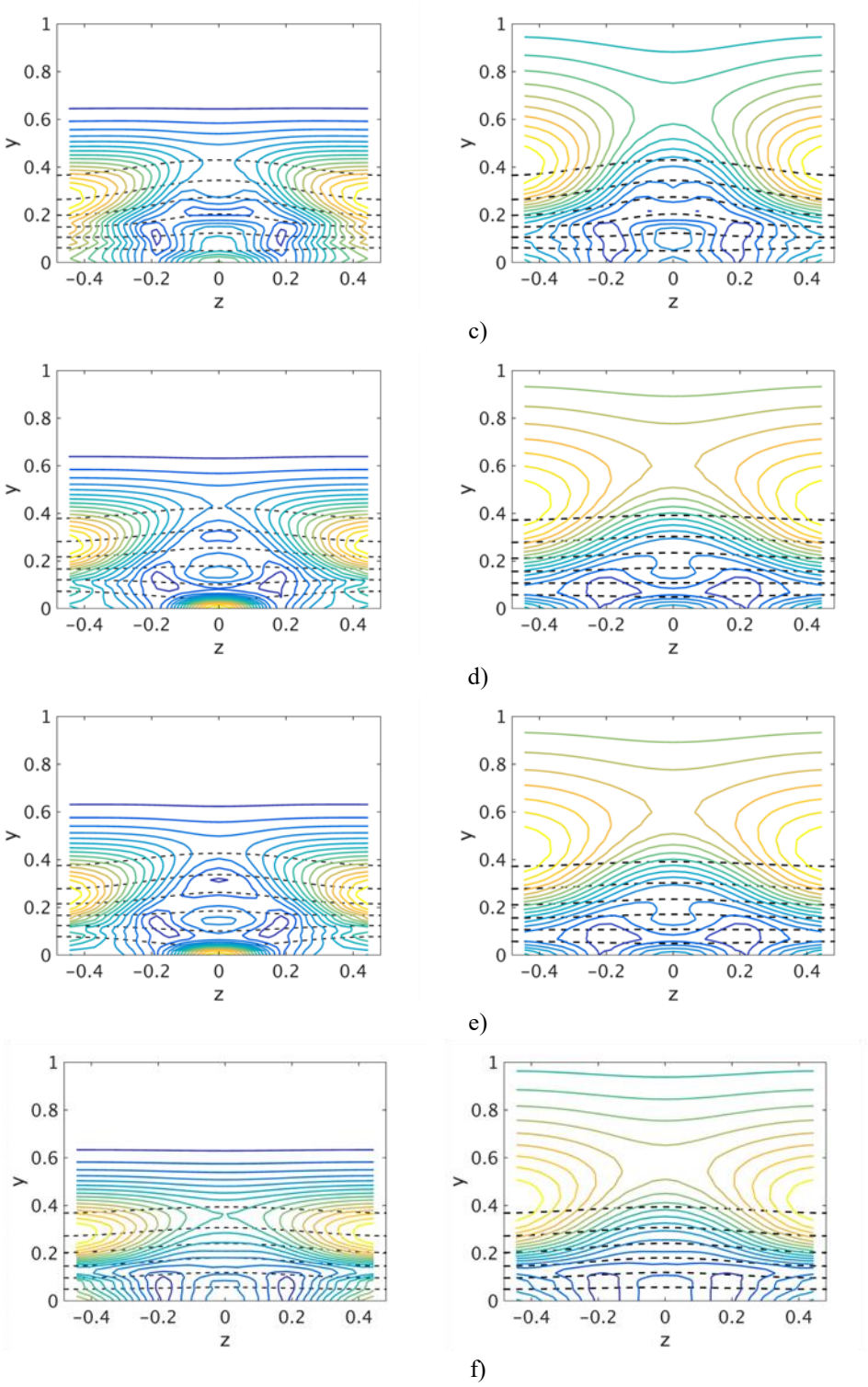

Figure B.3 (continued).

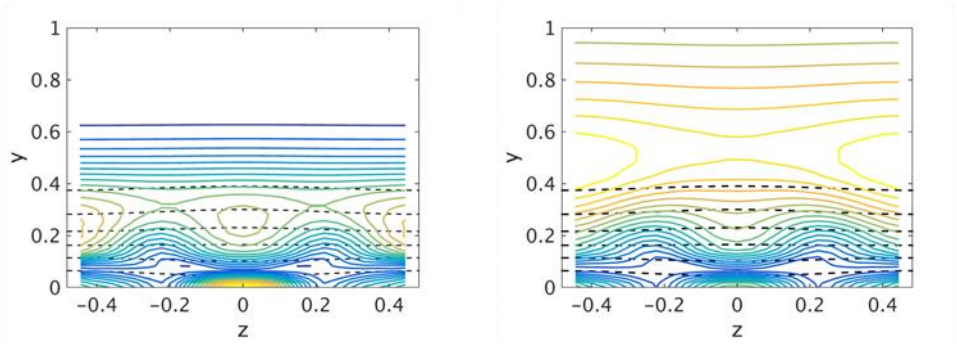

g)

Figure B.3 (continued).

a) smooth surface; b) control based on u and control plane at y = 0.1; c) control based on v and control plane at y = 0.1; d) control based on u and control plane at y = 0.2; e) control based on v and control plane at y = 0.2; f) control based on u and control plane at y = 0.3; g) control based on v and control plane at y =0.3.

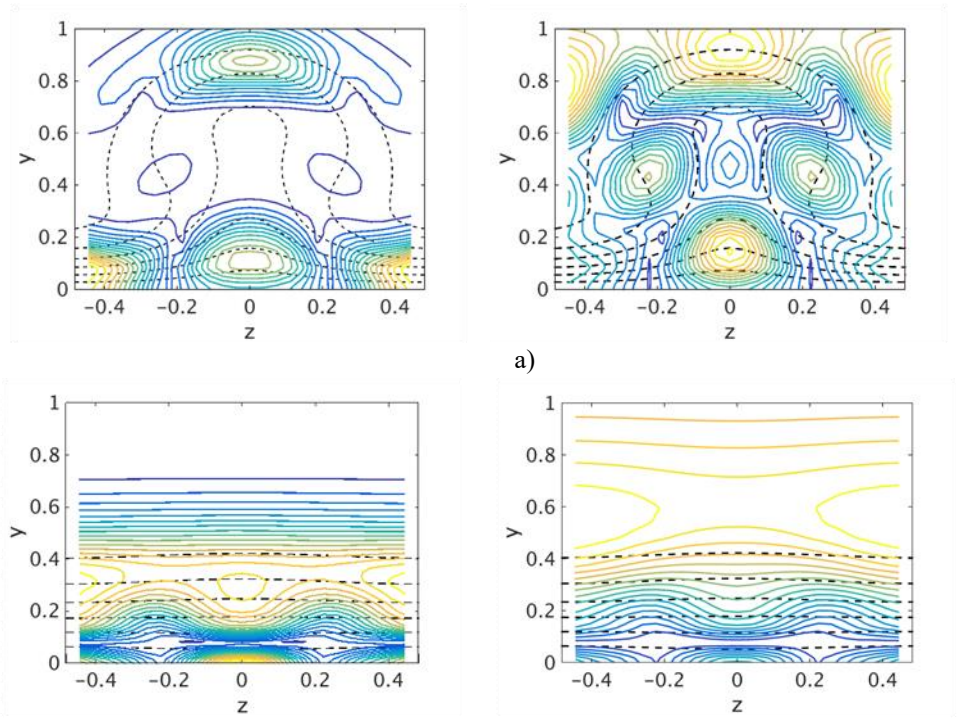

a)

b)

Figure B.4 First stability modes of the streamwise velocity for control based on blowing/suction for radius 1 m and spanwise separation is 1.2 cm; U modes (left column) and V modes(right).

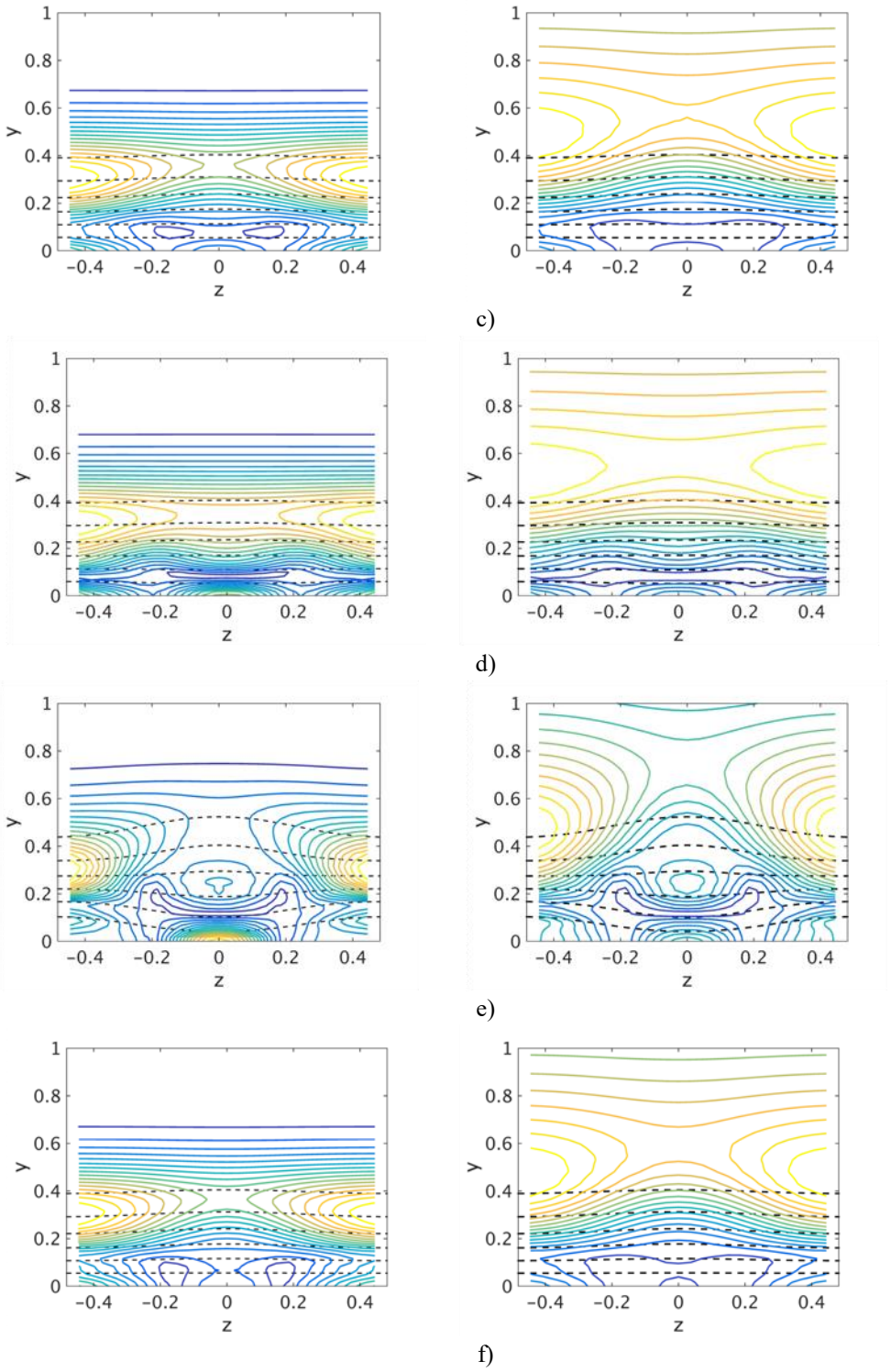

Figure B.4 (continued).

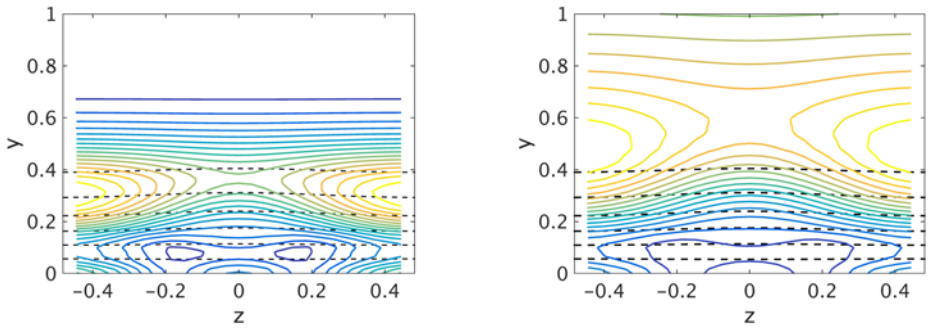

g)

Figure B.4 (continued).

a) smooth surface; b) control based on u and control plane at y = 0.1; c) control based on v and control plane at y = 0.1; d) control based on u and control plane at y = 0.2; e) control based on v and control plane at y = 0.2; f) control based on u and control plane at y = 0.3; g) control based on v and control plane at y =0.3.

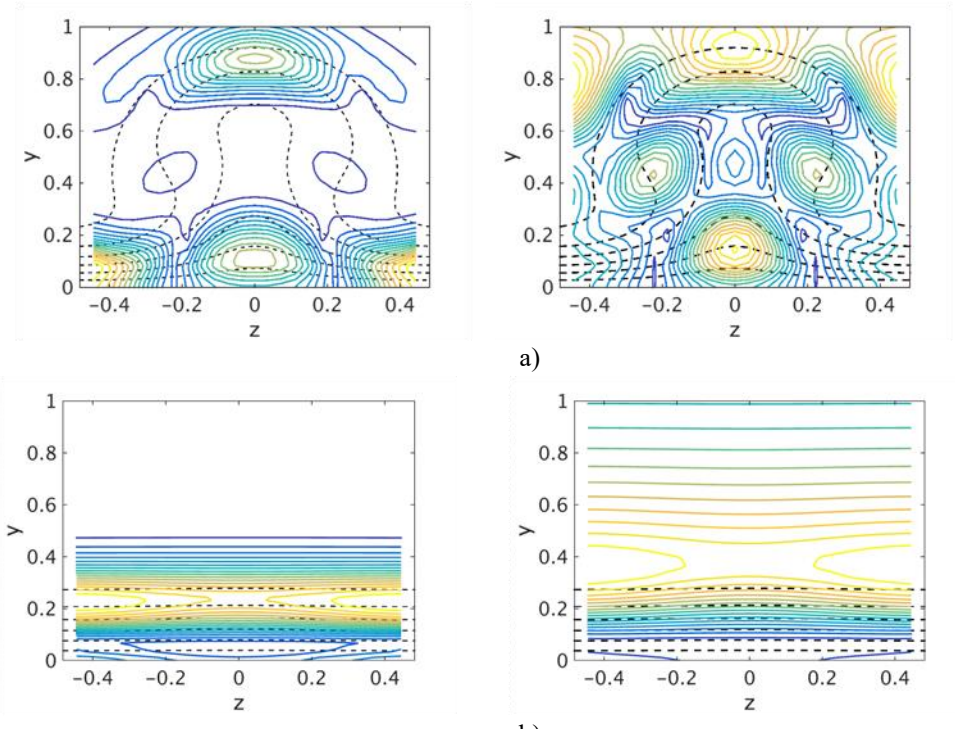

a)

b)

Figure B.5 First stability modes of the streamwise velocity for control based on wall deformation for radius 0.5 m and spanwise separation is 1.8 cm; U modes (left column) and V modes(right).

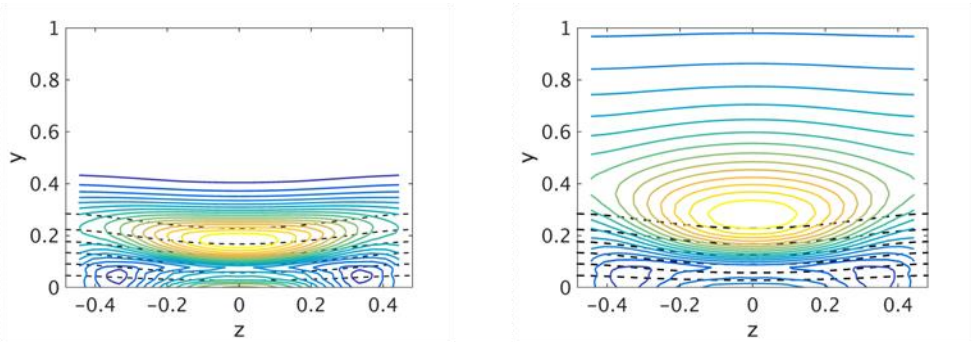

c)

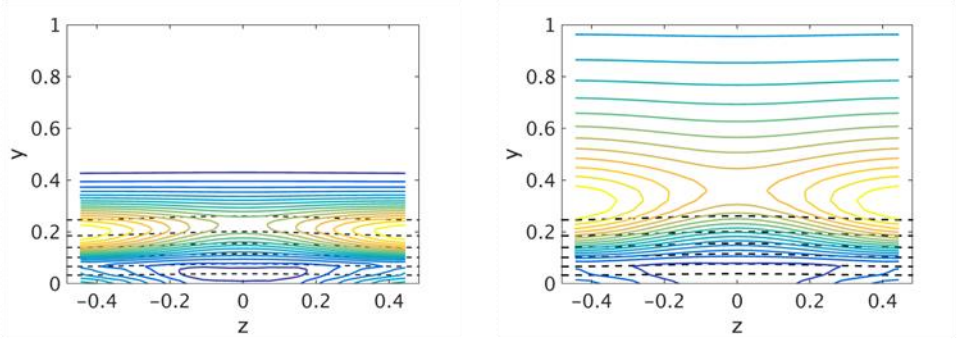

d)

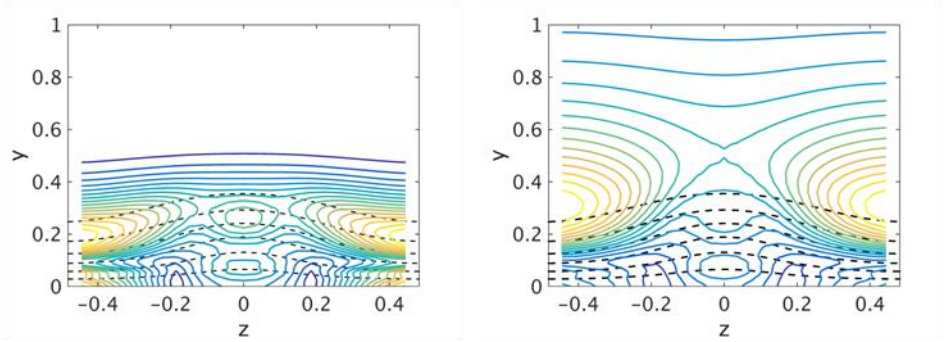

e)

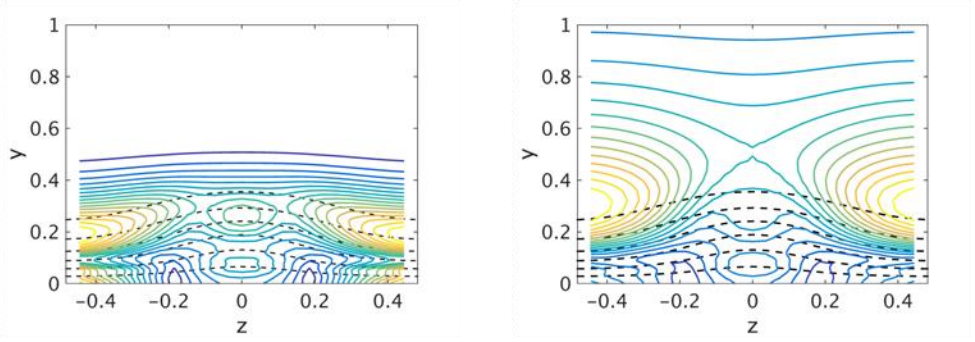

f)

Figure B.5 (continued).

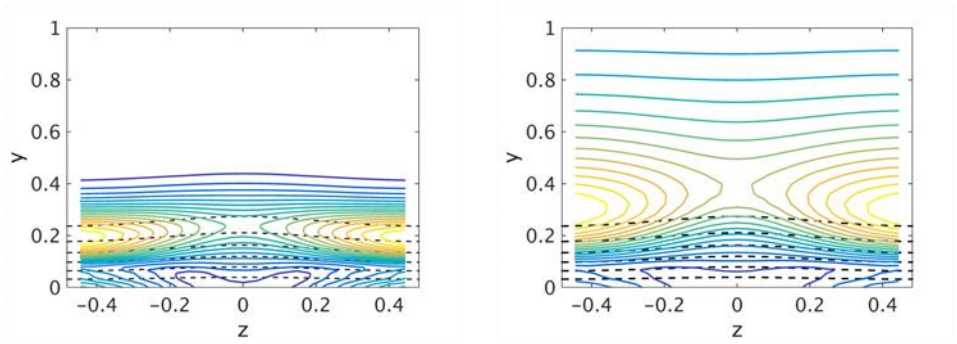

g)

Figure B.5 (continued).

a) smooth surface; b) control based on u and control plane at y = 0.1; c) control based on v and control plane at y = 0.1; d) control based on u and control plane at y = 0.2; e) control based on v and control plane at y = 0.2; f) control based on u and control plane at y = 0.3; g) control based on v and control plane at y =0.3.

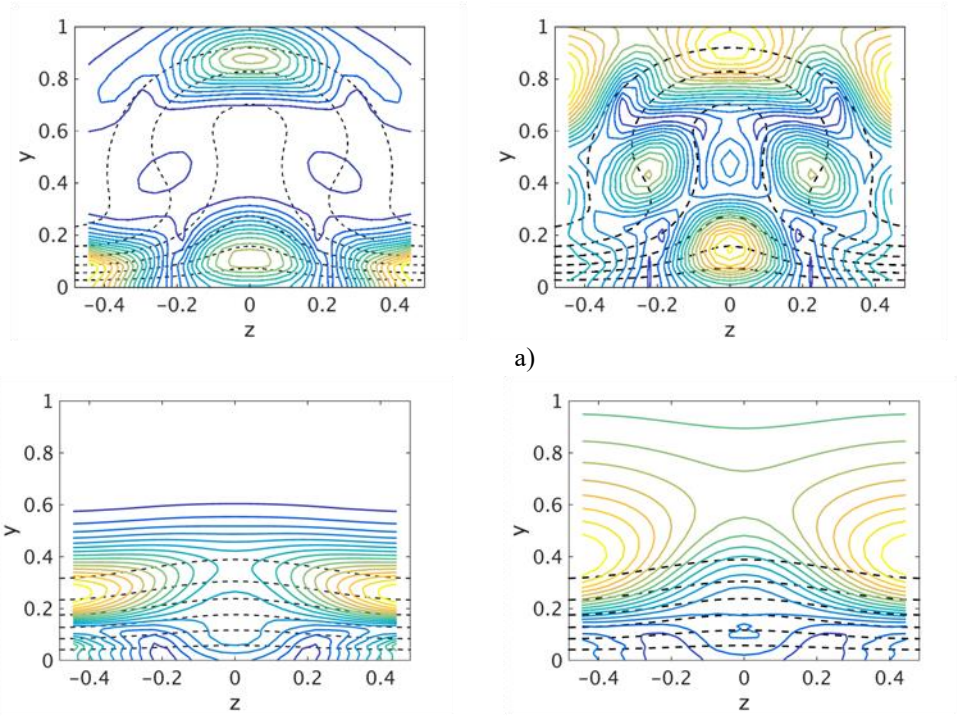

a)

b)

Figure B.6 First stability modes of the streamwisevelocityfor control based on wall deformation for radius1 m and spanwise separation is 1.8 cm; U modes (left column) and V modes(right)

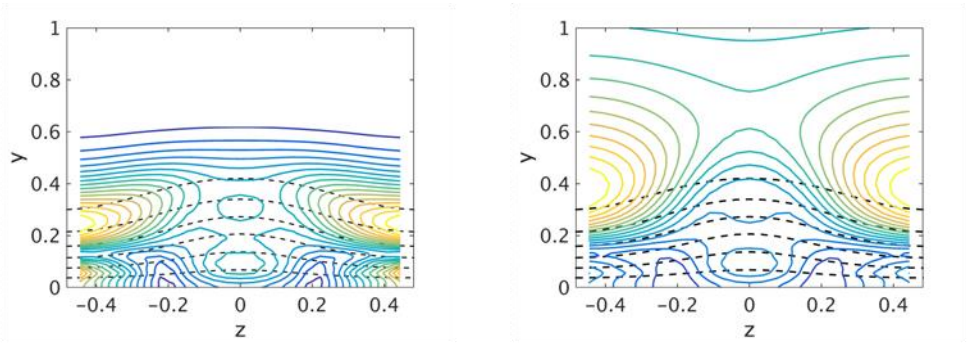

c)

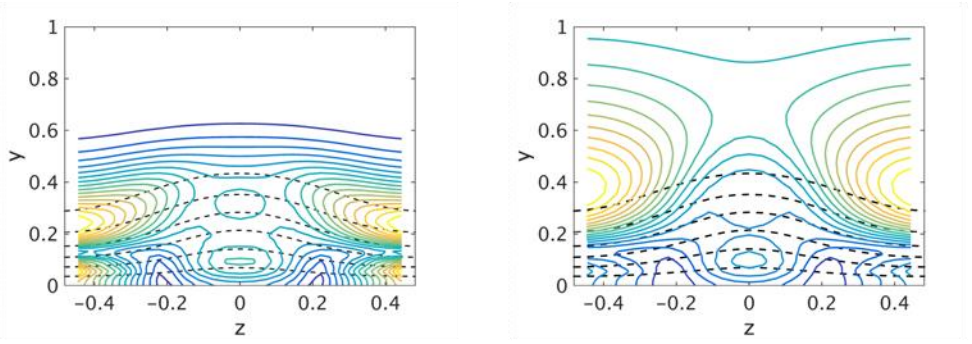

d)

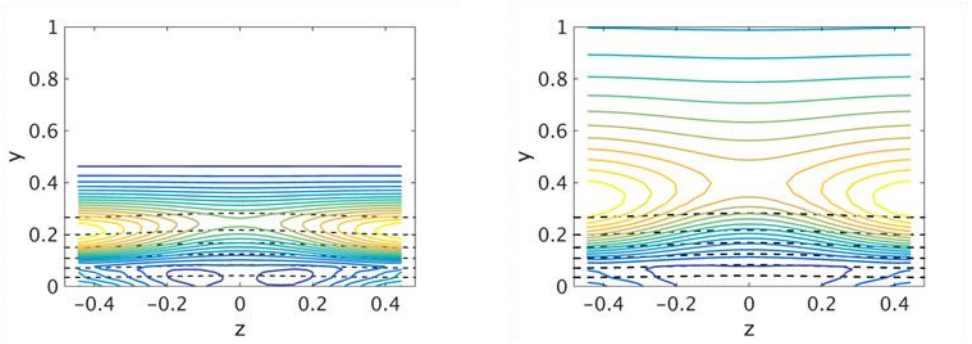

e)

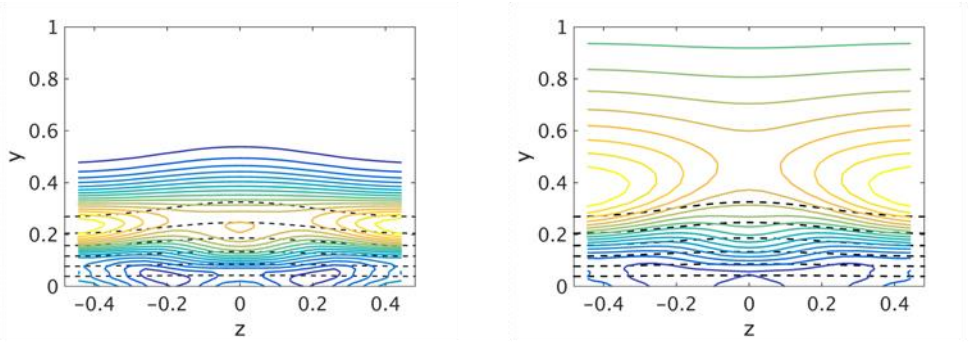

f)

Figure B.6 (continued).

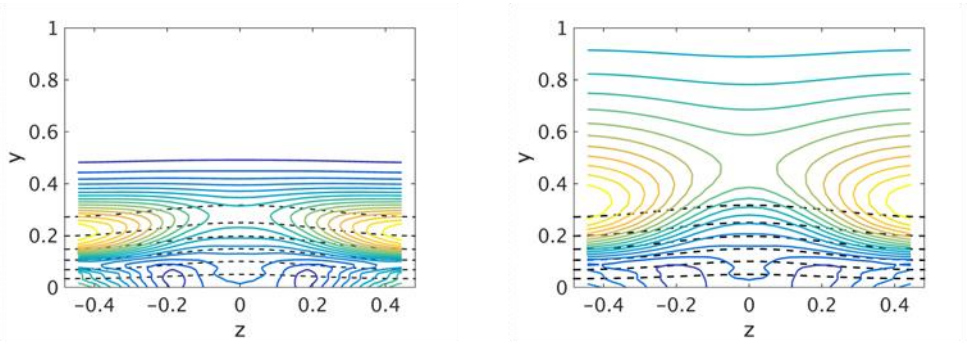

g)

Figure B.6 (continued).

a) smooth surface; b) control based on u and control plane at y = 0.1; c) control based on v and control plane at y = 0.1; d) control based on u and control plane at y = 0.2; e) control based on v and control plane at y = 0.2; f) control based on u and control plane at y = 0.3; g) control based on v and control plane at y =0.3.

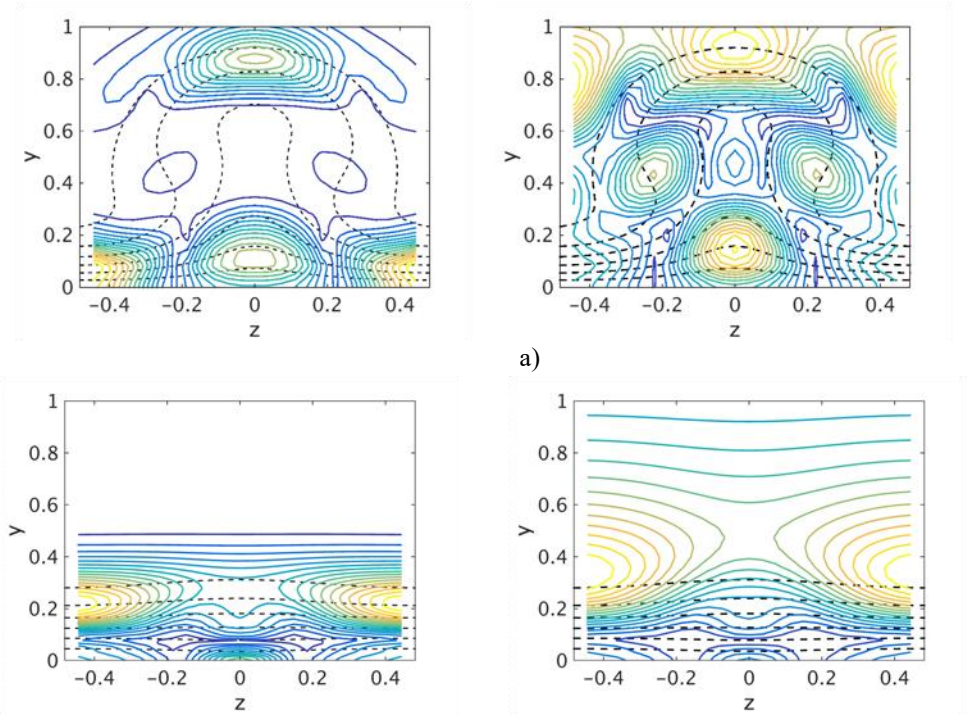

a)

b)

Figure B.7 First stability modes of the streamwise velocity for control based on blowing/suction for radius 0.5 m and spanwise separation is 1.8 cm; U modes (left column) and V modes(right).

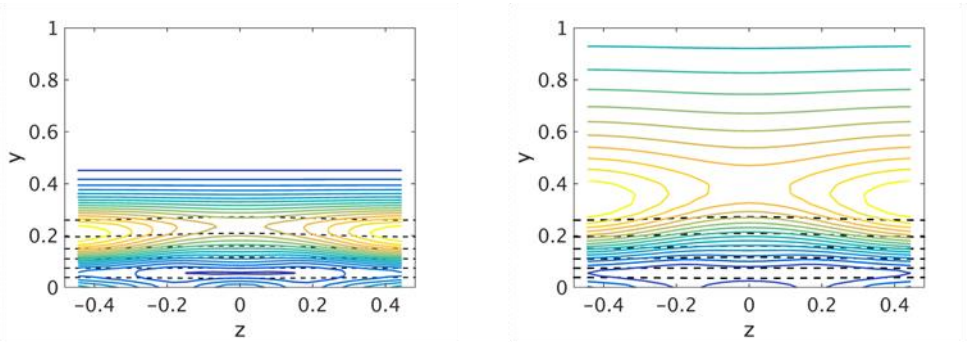

c)

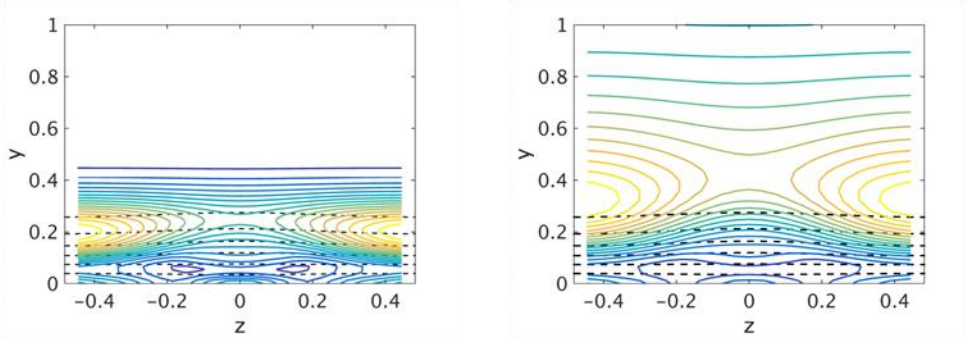

d)

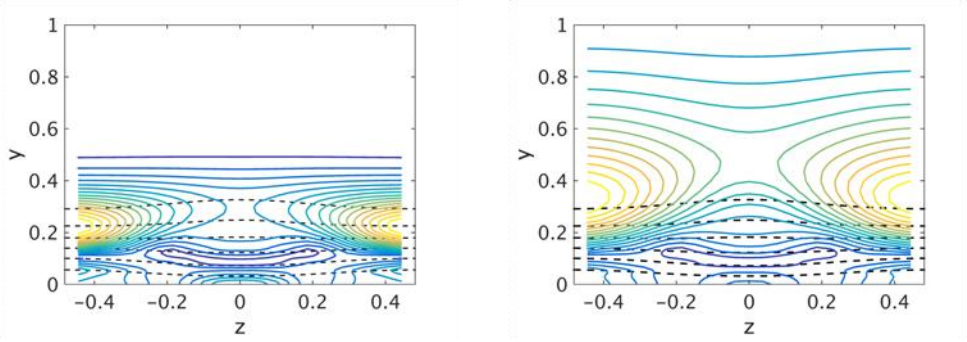

e)

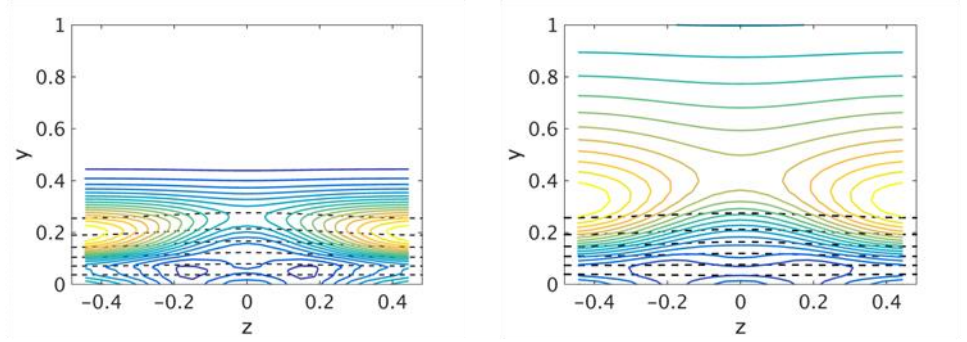

f)

Figure B.7 (continued).

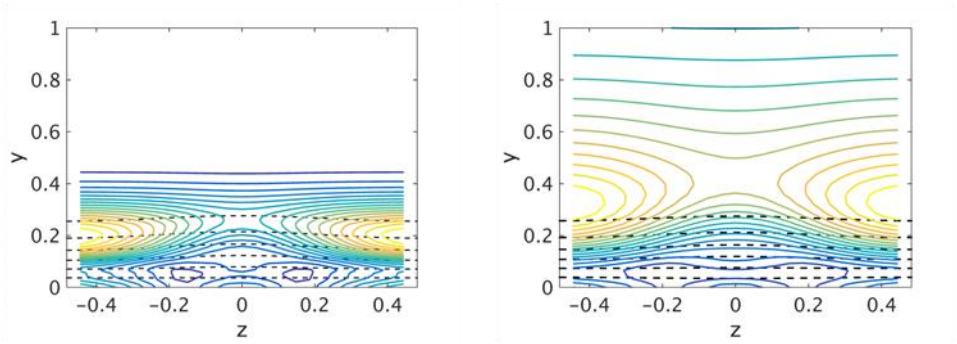

g)

Figure B.7 (continued).

a) smooth surface; b) control based on u and control plane at y = 0.1; c) control based on v and control plane at y = 0.1; d) control based on u and control plane at y = 0.2; e) control based on v and control plane at y = 0.2; f) control based on u and control plane at y = 0.3; g) control based on v and control plane at y =0.3.

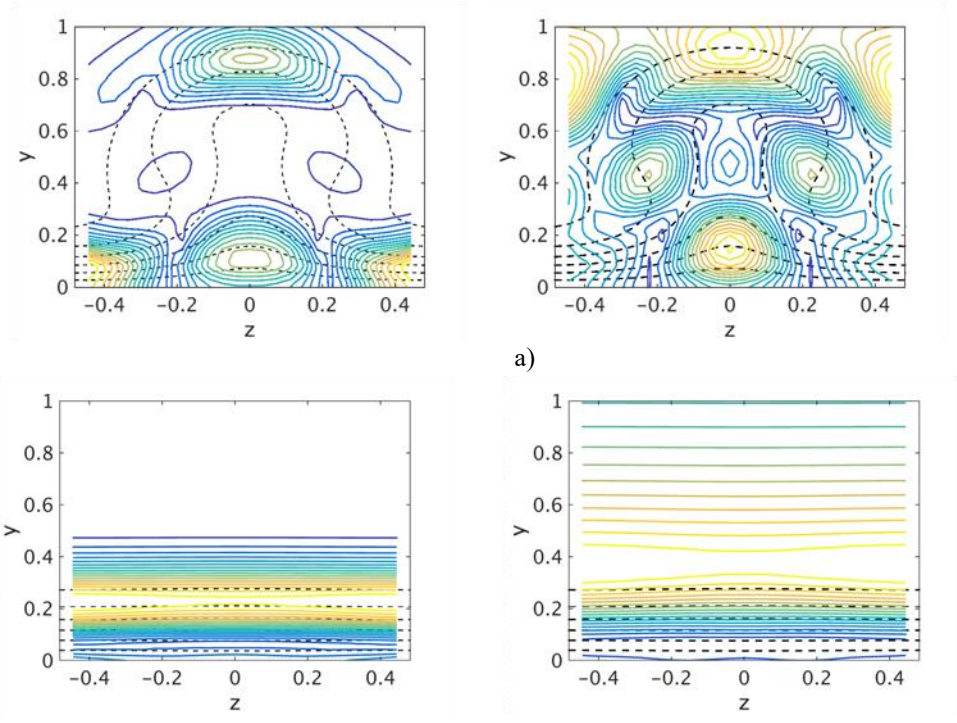

a)

b)

Figure B.8 First stability modes of the streamwise velocity for control based on blowing/suction for radius1 m and spanwise separation is 1.8 cm; U modes (left column) and V modes(right).

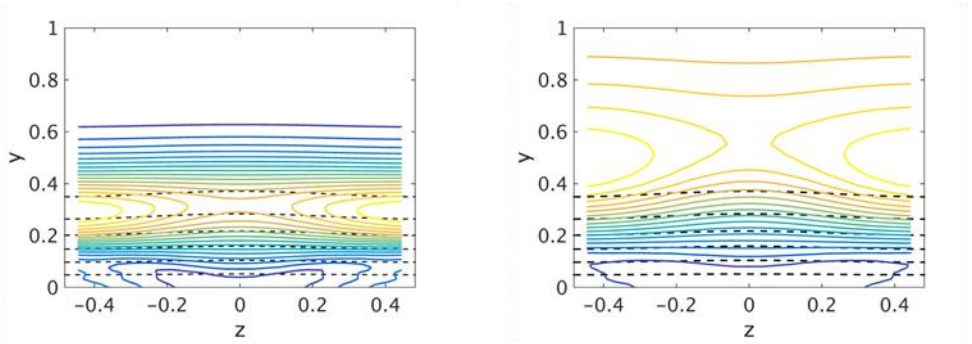

c)

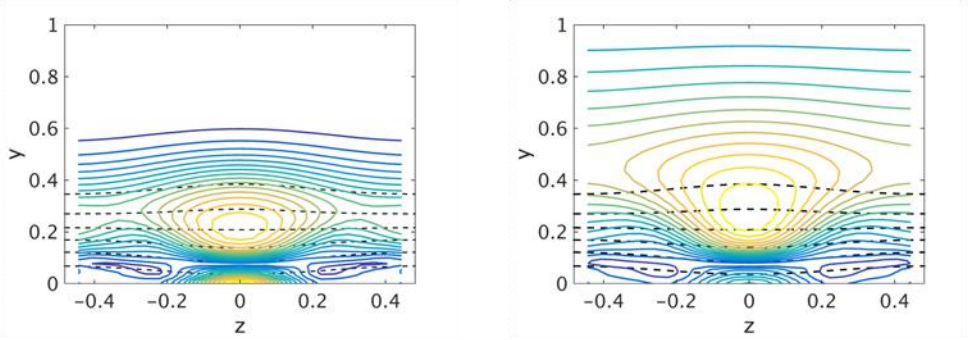

d)

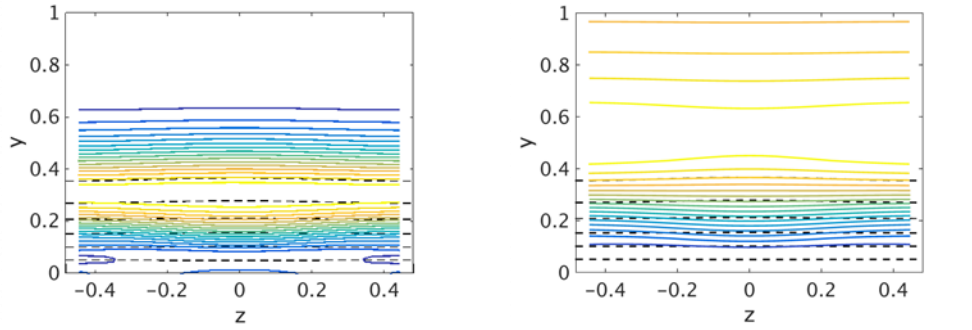

e)

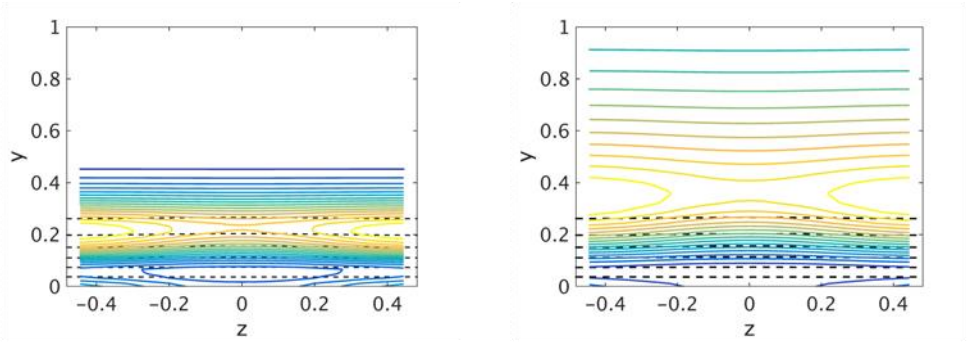

f)

Figure B.8 (continued).

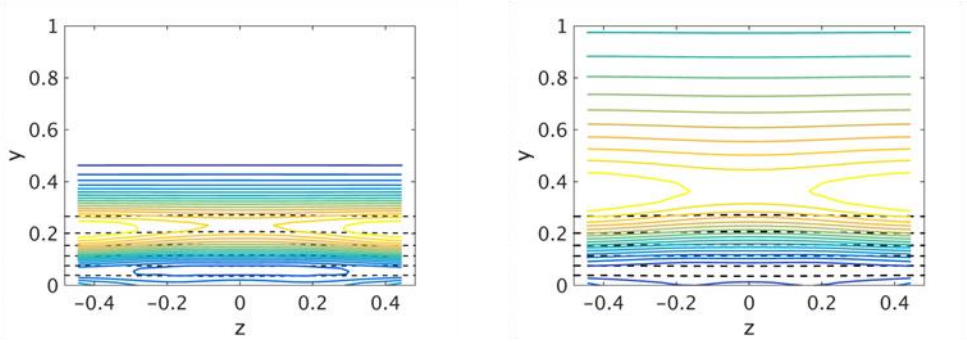

g)

Figure B.8 (continued).

a) smooth surface; b) control based on u and control plane at y = 0.1; c) control based on v and control plane at y = 0.1; d) control based on u and control plane at y = 0.2; e) control based on v and control plane at y = 0.2; f) control based on u and control plane at y = 0.3; g) control based on v and control plane at y =0.3.

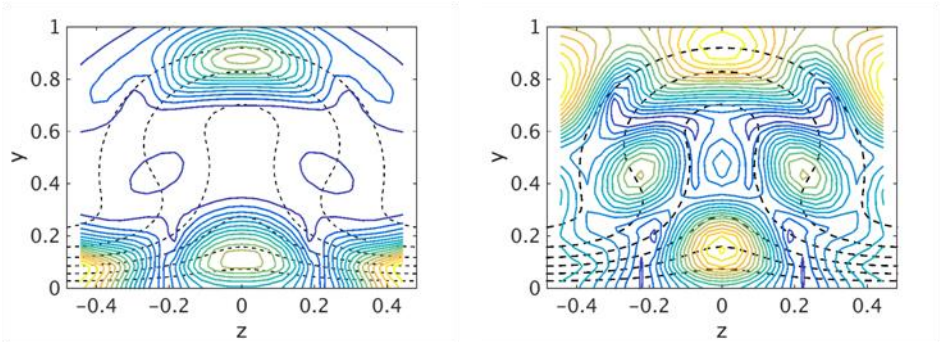

a)

Figure B.9 First stability modes of the streamwise velocity for control based on wall deformation for radius 0.5 m and spanwise separation is 2.4 cm; U modes (left column) and V modes(right).

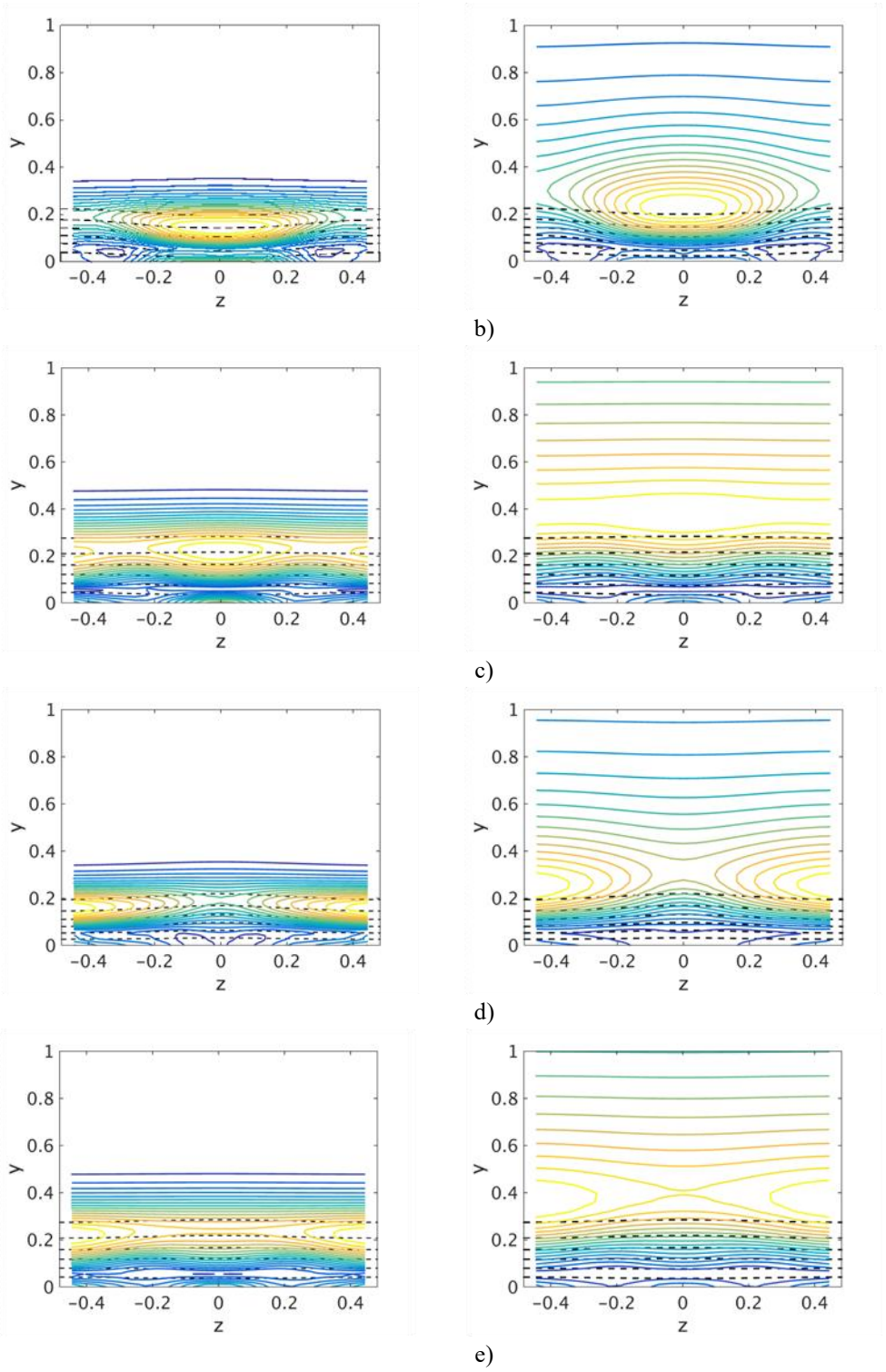

Figure B.9 (continued).

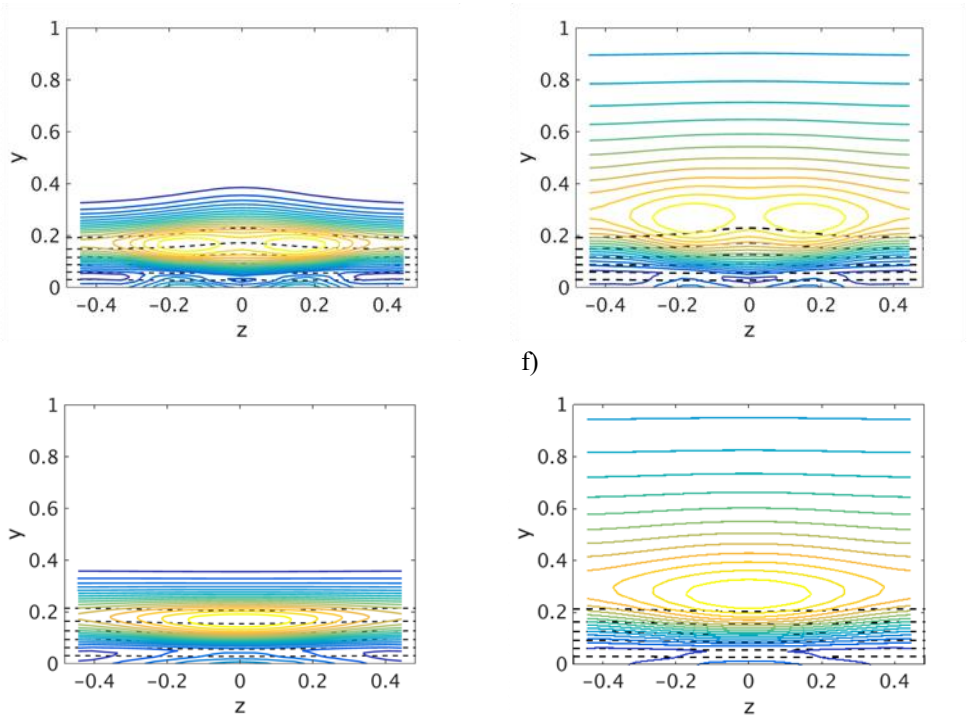

f)

g)

Figure B.9 (continued).

a) smooth surface; b) control based on u and control plane at y = 0.1; c) control based on v and control plane at y = 0.1; d) control based on u and control plane at y = 0.2; e) control based on v and control plane at y = 0.2; f) control based on u and control plane at y = 0.3; g) control based on v and control plane at y =0.3.

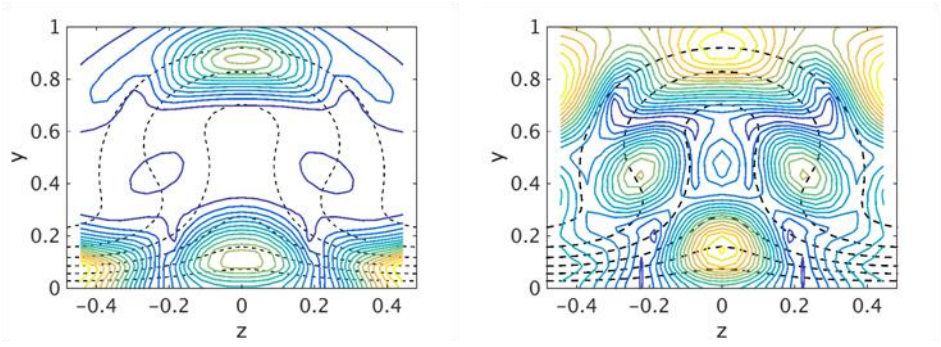

a)

Figure B.10 First stability modes of the streamwise velocity for control based on wall deformation for radius 1 m and spanwise separation is 2.4 cm; U modes (left column) and V modes(right).

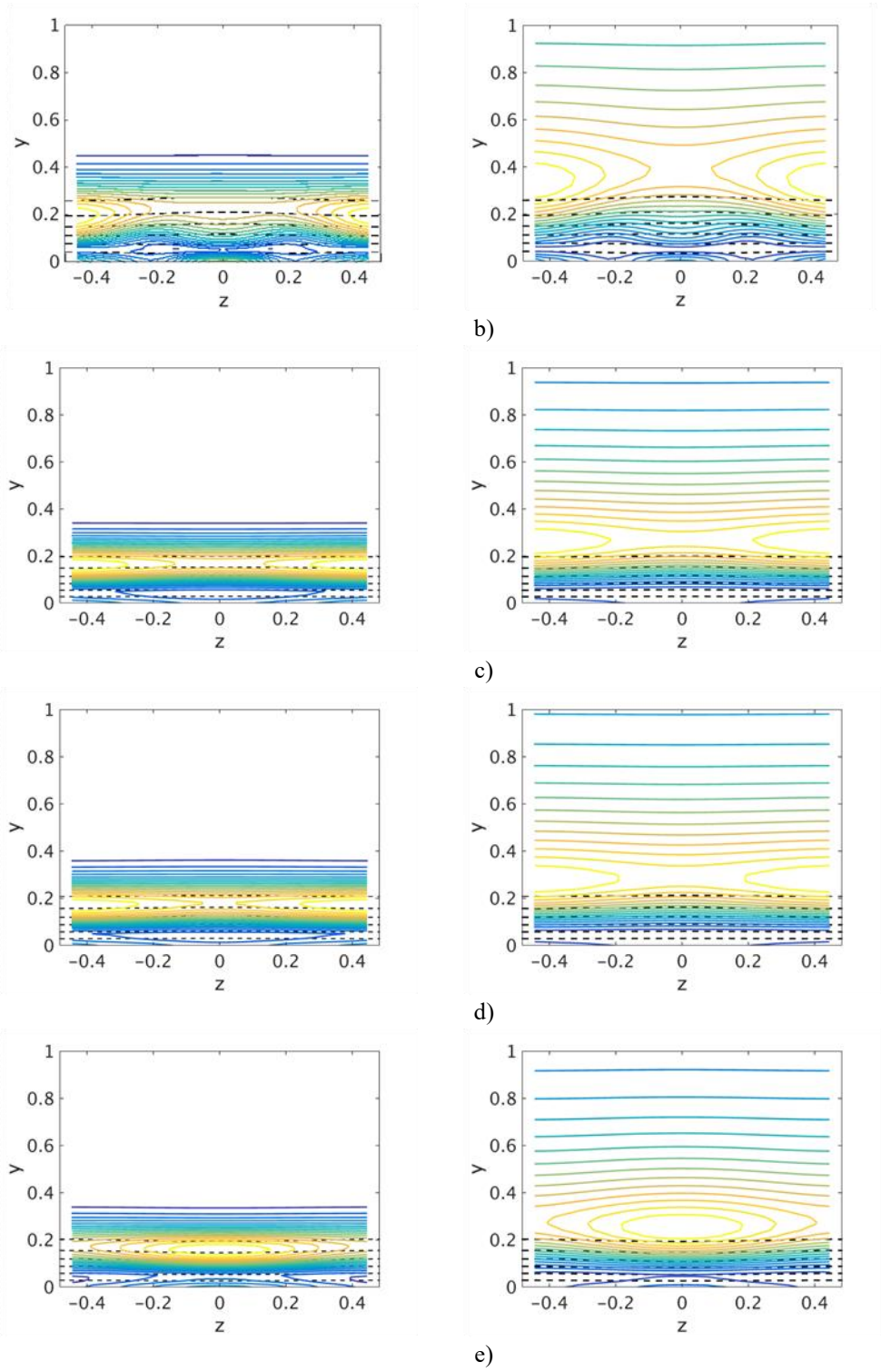

b)

c)

d)

e)

Figure B.10 (continued).

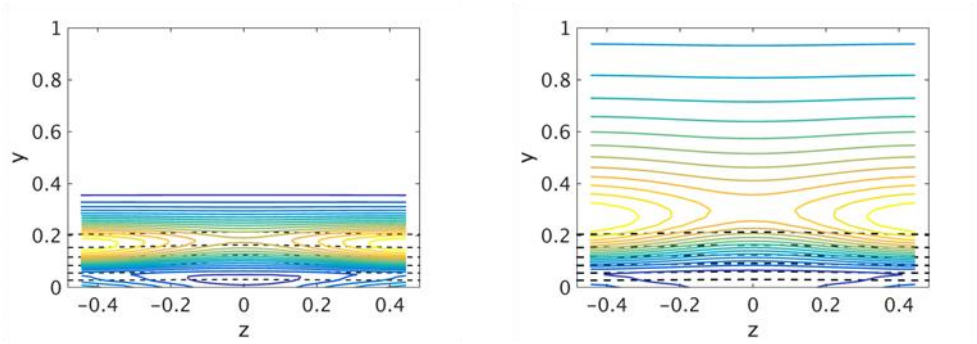

f)

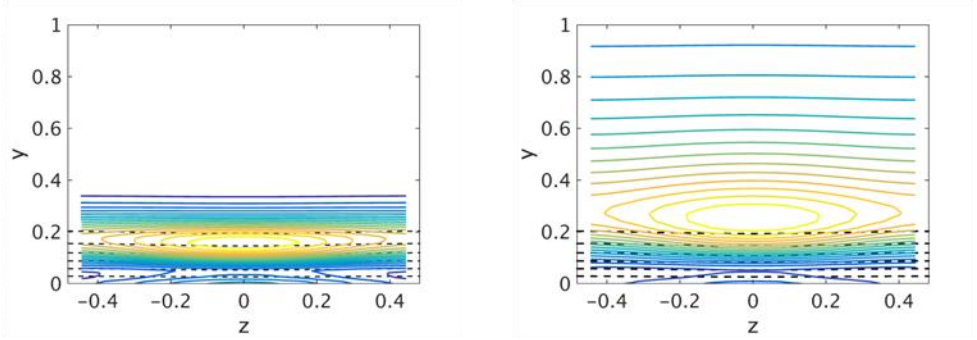

g)

Figure B.10 (continued).

a) smooth surface; b) control based on u and control plane at y = 0.1; c) control based on v and control plane at y = 0.1; d) control based on u and control plane at y = 0.2; e) control based on v and control plane at y = 0.2; f) control based on u and control plane at y = 0.3; g) control based on v and control plane at y =0.3.

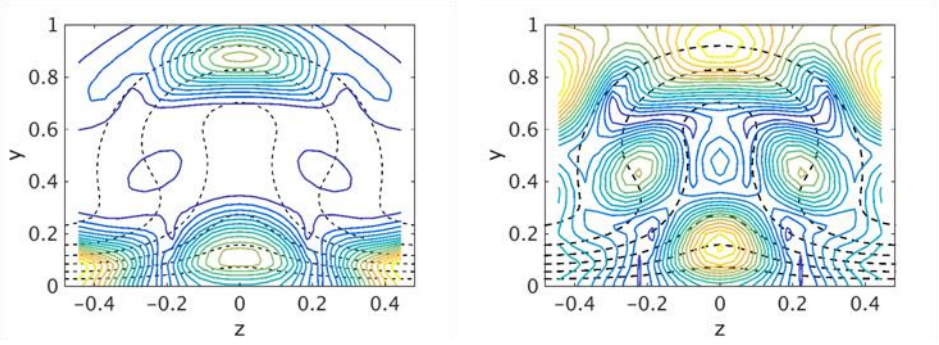

a)

Figure B.11 First stability modes of the streamwise velocity for control based on blowing/suction for radius 0.5 m and spanwise separation is 2.4 cm; U modes (left column) and V modes(right).

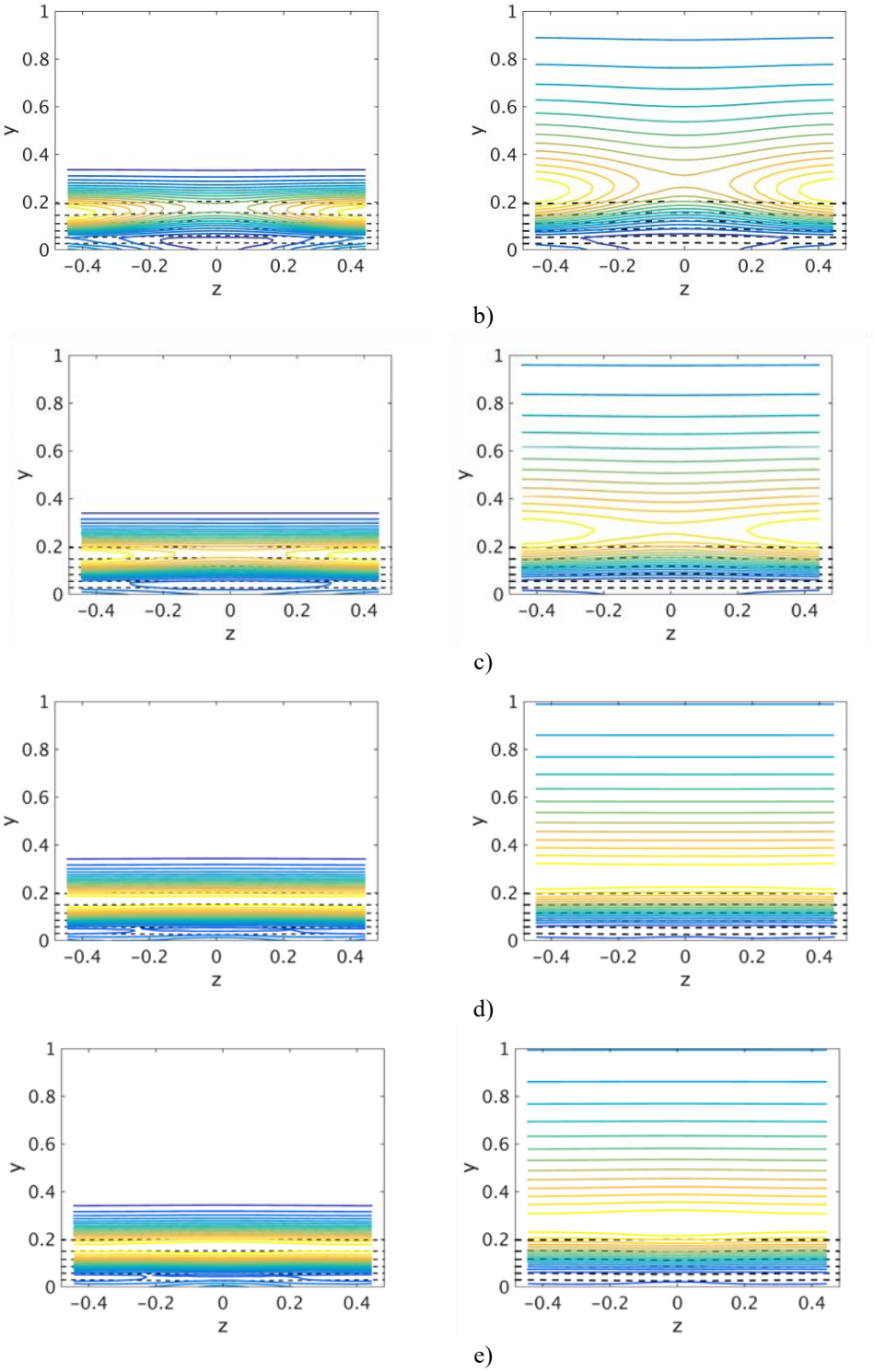

Figure B.11 (continued).

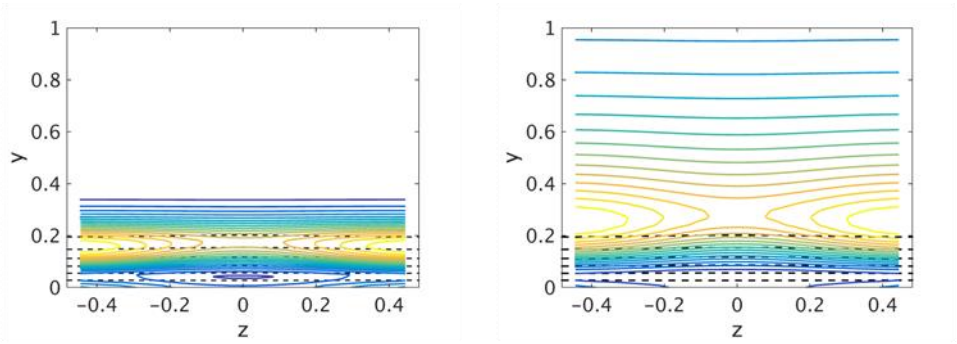

f)

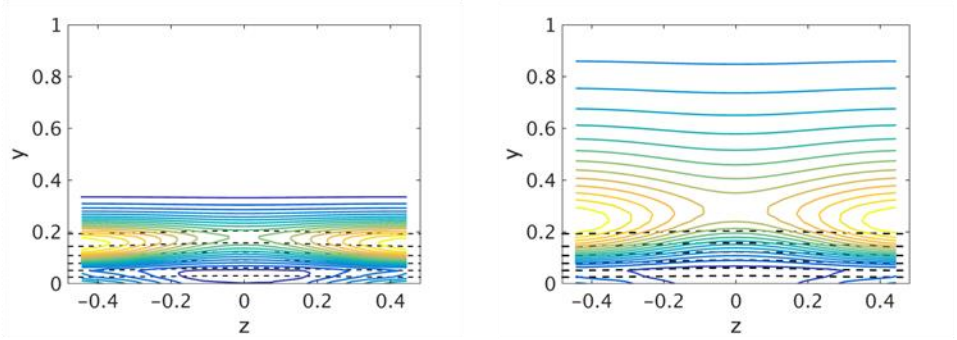

g)

Figure B.11 (continued).

a) smooth surface; b) control based on u and control plane at y = 0.1; c) control based on v and control plane at y = 0.1; d) control based on u and control plane at y = 0.2; e) control based on v and control plane at y = 0.2; f) control based on u and control plane at y = 0.3; g) control based on v and control plane at y =0.3.

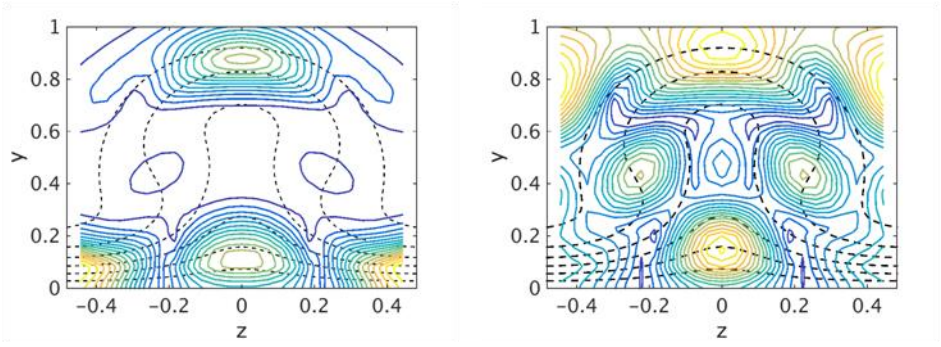

a)

Figure B.12 First stability modes of the streamwise velocity for control based on blowing/suction for radius 1 m and spanwise separation is 2.4 cm; U modes (left column) and V modes(right).

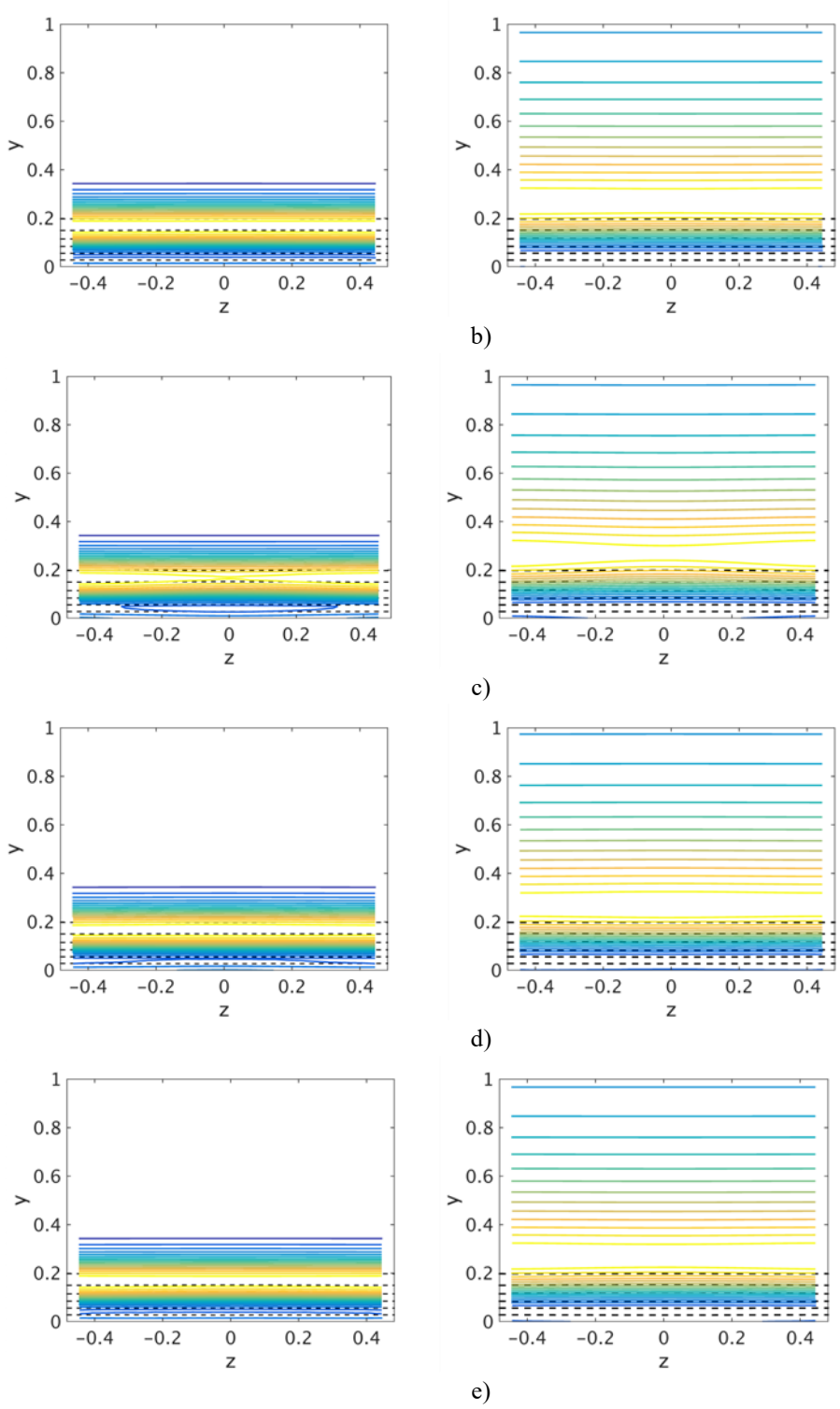

Figure B.12 (continued).

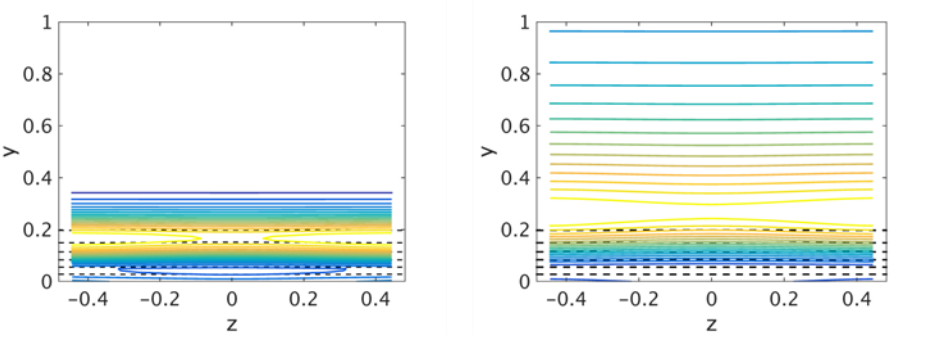

f)

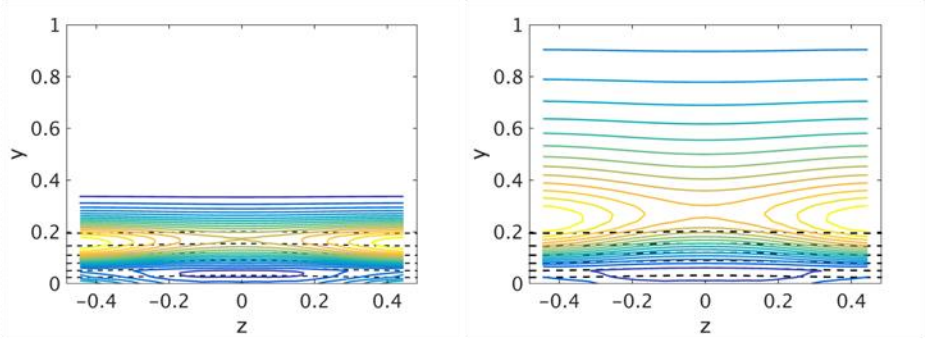

g)

Figure B.12 (continued).

a) smooth surface; b) control based on u and control plane at y = 0.1; c) control based on v and control plane at y = 0.1; d) control based on u and control plane at y = 0.2; e) control based on v and control plane at y = 0.2; f) control based on u and control plane at y = 0.3; g) control based on v and control plane at y =0.3.